



MARMARA UNIVERSITY
FACULTY OF ENGINEERING



AN EXAMINATION of IMPACT
PROPERTIES of AUTOMOTIVE WHEELS
UNDER DIFFERENT CLIMATE
CONDITIONS

Müdekkilik Final Project Commission		
The essential features of an acceptable design Project		
	Satisfied	Unsatisfied
1 Mechanical or Thermal Design		<input checked="" type="checkbox"/>
2 Report writing technique	<input checked="" type="checkbox"/>	
3 Development of student creativity		<input checked="" type="checkbox"/>
4 Use of open-ended problems		<input checked="" type="checkbox"/>
5 Formation of design	<input checked="" type="checkbox"/>	
6 Problem statement and specification	<input checked="" type="checkbox"/>	
7 Synthesis of alternative solutions		<input checked="" type="checkbox"/>
8 Feasibility	<input checked="" type="checkbox"/>	
9 Detailed system description	<input checked="" type="checkbox"/>	
10 Consideration of constraints (e.g. economic, safety, reliability, etc.)		<input checked="" type="checkbox"/>
11 Utilization of engineering and scientific principle	<input checked="" type="checkbox"/>	
Decision	Signature	
Accepted but not approved	13.07.2021	
Prof. Dr. Bülent Ekici,		
Dr. Öğr. Üyesi Uğur Tümerdem		
Ar. Gör Serkan Öğüt		

Ümit ELMAHTİ, Emirhan KURTUL

GRADUATION PROJECT REPORT
Department of Mechanical Engineering

Supervisor

Prof. Dr. Paşa YAYLA

ISTANBUL, 2021



MARMARA UNIVERSITY
FACULTY OF ENGINEERING



**Examination Impact Properties of Automotive Wheels Under
Different Climate Conditions**

by

Ümit ELMAHTİ, Emirhan KURTUL

May 2021, Istanbul

**SUBMITTED TO THE DEPARTMENT OF MECHANICAL ENGINEERING IN PARTIAL
FULFILLMENT OF THE REQUIREMENTS FOR THE DEGREE**

OF

BACHELOR OF SCIENCE

AT

MARMARA UNIVERSITY

The author(s) hereby grant(s) to Marmara University permission to reproduce and to distribute publicly paper and electronic copies of this document in whole or in part and declare that the prepared document does not in any way include copying of previous work on the subject or the use of ideas, concepts, words, or structures regarding the subject without appropriate acknowledgment of the source material.

Signature of Author(s).....

A handwritten signature in black ink, appearing to read 'Elmahtı'.

Department of Mechanical Engineering

Certified By.....

Prof.Dr. Paşa YAYLA

A handwritten signature in blue ink, appearing to read 'Paşa YAYLA'.

Project Supervisor, Department of Mechanical Engineering

Accepted By.....

Prof. Dr. Bülent EKİCİ

Head of the Department of Mechanical Engineering

A handwritten signature in blue ink, appearing to read 'Bülent EKİCİ'.

ACKNOWLEDGEMENT

First of all, we would like to thank our supervisor Prof. Dr. Paşa YAYLA, for the valuable guidance and advice on preparing this thesis and for giving us moral and material support.

Also, we would like to thank the CEVHER Wheel Industry A.Ş. family for their moral, material and financial supports for this work. Special thanks should go to Onur ÖZAYDIN and YİĞİT KAYA for their support throughout the project.

We would like to thank Marmara University – Engineering Faculty – Mechanical Engineering Department - Materials Engineering Laboratory officer and manager for their support.

We would like to thank our whole family, especially our mothers and fathers, who have not spared their efforts throughout our education life.

July 2021

Ümit Elmahti, Emirhan Kurtul

CONTENTS

ACKNOWLEDGEMENT	i
CONTENTS	ii
ÖZET	iv
ABSTRACT	v
SYMBOLS	vi
ABBREVIATIONS	vii
LIST OF FIGURES	viii
LIST OF TABLES	xii
1.INTRODUCTION	1
1.1 Aim of the Thesis	2
1.2 Literature Survey	2
1.2.1 Classification of Cast Aluminium Alloy	2
1.2.2 Automotive Wheel Production	10
1.2.3 Wheel Test Methods.....	13
1.3 Charpy Impact Testing	13
1.4 Instrumented Charpy Impact Testing	14
2. MATERIAL AND METHOD	15
2.1 Sample Production.....	15
2.1 Sample Preparation.....	15
2.2 Sample conditioning.....	16
3. TESTING AND DATA INTERPRETATION	17
3.1 Instrumented Charpy Impact Testing	17
3.2 Tests at Different Temperatures	17
3.2.1 Tests at 175 °C.....	17
3.2.2 Tests at 95 °C.....	19
3.2.3 Tests at 60 °C.....	21
3.2.4 Tests at 20 °C.....	24
3.2.5 Tests at 0 °C.....	26

3.2.6 Tests at -40 °C	29
3.2.7 Tests at -75 °C	32
3.3 Charpy Impact Resistance Variation with Temperature	34
4. MACROSCOPIC and MICROSCOPIC EXAMINATION	36
4.1 Microscopic Examination of Sample	36
4.1.1 Sample Preparation.....	36
4.1.2 Optical Microscope Results.....	41
4.2 Optical Examination of Fracture Surface	44
4.2.1 Sampling.....	44
4.2.2 Optical Results.....	44
4.3 SEM and EDS Examination of Fracture Surface	49
4.3.1 SEM and EDS Results.....	51
5. RESULTS and DISCUSSION	74
6. CONCLUSIONS	75
6.1 Main Conclusions	75
6.2 Recommendations for Further Work.....	75
6.3 Evaluation of the Work from MUDEK Perspective.....	76
6.3.1 Economic Analysis	76
6.3.2 Real Life Conditions.....	76
6.3.3 Producibility	76
6.3.4 Constraints	76
REFERENCES	77

ÖZET

Farklı İklim Koşullarında Otomotiv Jantlarının Darbe Özelliklerinin İncelenmesi

Ümit ELMAHTI, Emirhan KURTUL

Bu tez araştırmasında, AlSi7Mg3 alaşımından Alçak Basınç Döküm metodu ile üretilen jantların farklı iklim koşullarında Instrumented Charpy V-çentik darbe deneyi analizi çalışılmıştır. Dünya üzerindeki farklı sıcaklıklara sahip bölgelerde kullanılabilecek A356 alaşımı jant mukavemetinin simülasyonunu elde etmek için, ISO 148-3 standartlarına uygun, LPDC yöntemiyle üretilen jantlardan numuneler alındı. Bu numuneler -75°C, -40°C, 0°C, 20°C, 60°C, 95°C ve 175°C sıcaklıklarda iklimlendirildi ve aletli Charpy V-çentik darbe testine tabi tutuldu. Uyguladığımız bu testler, numunelerin farklı koşullar altındaki darbe enerjisini belirler.

Daha sonra kırılan numunelerin kırık yüzeyleri sünek-kırılınca geçiş sıcaklığı tespiti için incelendi. İlk olarak gözle ve optik mikroskopla numuneler birbirleri ile karşılaştırılmak sureti ile incelendi. Jantın üretim kalitesi ve Charpy numunesinin darbe enerjisi arasında bağlantı kurabilmek için numunenin iki farklı yüzeyinin mikro yapısı incelendi.

Taramalı elektron mikroskopu ile -75°C, 20°C ve 175°C sıcaklıklarında kırılan numunelerin kırık yüzeyleri incelendi.

Yapılan bütün incelemelerin sonucunda düşük sıcaklıkta kırılan numunelerin kırık yüzeyinde kırılınca yapı örnekleri gözlemlense de numunelerin geneline sünek kırılma yapısı örnekleri hakimdi.

Sonuç olarak, A356 alaşımından alçak basınç döküm yöntemi ile üretilen jantlardan aldığımız numunelerde -75°C ve 175°C sıcaklıklarları arasında sünek-kırılınca geçiş gözlemlenmedi. Toplam darbe enerjileri yakın değer gösterdiler. Bu sıcaklıkların ürünün kırılma yapısına ve darbe enerjisine fazla etkisi olmadığı gözlemlendi.

ABSTRACT

Examination Impact Properties of Automotive Wheels Under Different Climate Conditions

Ümit ELMAHTI, Emirhan KURTUL

In this thesis research, Instrumented Charpy V-notch impact test analysis of AlSi7Mg3 alloy wheels produced by Low Pressure Casting method under different climatic conditions has been studied. In order to simulate the strength of A356 alloy wheels that can be used in regions with different temperatures around the world, samples were taken from the wheels produced by the LPDC method in accordance with ISO 148-3 standards. These specimens were conditioned at -75°C, -40°C, 0°C, 20°C, 60°C, 95°C and 175°C temperatures and subjected to the instrumented Charpy V-notch impact test. These tests we apply determine the impact energy of the samples under different conditions.

Then, the fractured surfaces of the fractured samples were examined for the determination of the ductile-brittle transition temperature. Firstly, the samples were examined visually and with an optical microscope by comparing them with each other. In order to establish a connection between the production quality of the wheel and the impact energy of the Charpy sample, the microstructure of two different surfaces of the sample was examined.

The fractured surfaces of the samples, which were fractured at -75°C, 20°C and 175°C temperatures, were examined with a scanning electron microscope.

As a result of all the examinations, although brittle structure samples were observed on the fracture surface of the samples that were broken at low temperature, ductile fracture structure samples were dominant in the samples in general.

As a result, no ductile-brittle transition was observed between -75°C and 175°C temperatures in the samples we took from the rims produced by the low-pressure die casting method from A356 alloy. Total impact energies showed close values. It was observed that these temperatures did not have much effect on the fracture structure and impact energy of the product.

SYMBOLS

μ : Micro

π : Pi number

α : Primary alloying element shown in the phase diagram

ABBREVIATIONS

A356	: AlSi7Mg0.3 alloy
Al10Ti	: Aluminium Titanium alloy
Al5TiB	: Aluminium Titanium Boron alloy
AlSi11Mg	: Aluminium Silicon Magnesium alloy
AlSi7Mg0.3	: Aluminium Silicon Magnesium alloy
ASTM	: American Society for Testing and Materials
EAA	: European Aluminium Association
FCC	: Face Centered Cubic
Fe	: Iron
ISO	: International Organization for Standardization
LPDC	: Low Pressure Die Casting
Mg	: Magnesium
Ppm	: Parts per million
SEM	: Scanning Electron Microscope
Si	: Silicon
Sr	: Strontium

LIST OF FIGURES

Figure 1. 1. Section of the binary Al-Si phase diagram that covers the most common Al-Si compositions for the 3xx.x series of alloys.....	5
Figure 1.2. Al-Si cast alloy, Thin-walled transmission casing	6
Figure 1.3. Microstructure of Alloy 357 with π phase	7
Figure 1.4. Main particles forming the Al-Si structure	8
Figure 1.5. T6 heat treatment process	9
Figure 1.6. Wheel Production by Forging Method	11
Figure 1.7. Charpy impact testing machine	13
Figure 2.1. Display of samples taken from the wheel	16
Figure 3.1. NÜVE EV 018 model vacuum oven	17
Figure 3.2. Load-time and Energy-Time graphs of 3 specimens at 175 °C temperature.	18
Figure 3.3. Load-time and Energy-Time graphs of 3 specimens at 95 °C temperature. 20	20
Figure 3.4. Setting the samples to 60°C	22
Figure 3.5 Force-time and Energy-Time graphs of 3 specimens at 60 °C temperature. 23	23
Figure 3.6. Force-time and Energy-Time graphs of 3 specimens at 20 °C temperature.	25
Figure 3.7. Setting the samples to 0°C	27
Figure 3.8. Force-time and Energy-Time graphs of 3 specimens at 0 °C temperature. 28	28
Figure 3.9. Setting the samples to -40°C	30
Figure 3.10. Force-time and Energy-Time graphs of 3 specimens at -40 °C temperature.	31
Figure 3.11. Force-time and Energy-Time graphs of 4 specimens at -75 °C temperature.	33
Figure 3.12. Crack Initiation and Total Energy to Temperature graph	35
Figure 4.1. Abrasive Cutter.	37
Figure 4.2. Hot Moulding Machine.	38
Figure 4.3. Specimen after moulding.	38
Figure 4.4. Grinding and specimen after grinding.....	39
Figure 4.5. Polishing device.	40

Figure 4.6. After etching.....	40
Figure 4.7. The regions of samples.....	41
Figure 4.8. Optic results of transverse surface by (a)5x (b)10x and (c)20x	42
Figure 4.9. Optic results of longitudinal surface by(a)5x (b)10x and (c)20x	43
Figure 4.10. Fracture image of sample at +175 °C.(a) 20x and (b) 70x magnification images of the first sample. (c) 20x and (b) 70x magnification images of the second sample.....	45
Figure 4.11. Fracture image of sample at +20 °C.(a) 20x and (b) 70x magnification images of the first sample. (c) 20x and (b) 70x magnification images of the second sample.....	46
Figure 4.12. Fracture image of sample at -75 °C.(a) 20x and (b) 70x magnification images of the first sample. (c) 20x and (b) 70x magnification images of the second sample.....	47
Figure 4.13. Fractured surface images of Charpy impact test specimen fractured at different temperatures.....	48
Figure 4.14. Samples inside the red circle for SEM+EDS	49
Figure 4.15. Sputter coater	50
Figure 4.16. ZEISS model SEM device	50
Figure 4.17. SEM micrographs of fracture surface after impact tests; (a) -75°C, 50X magnification, (b) -75°C, 150X magnification, (c) 20°C, 50X magnification, (d) 20°C, 150X magnification, (e) 175°C, 50X magnification, (f) 175°C, 150X magnification ...	51
Figure 4.18. SEM micrographs of fracture surface after impact tests; (a) -75°C, 250X magnification, (b) -75°C, 2.5KX magnification, (c) -75°C, 5KX magnification, (d) 20°C, 250X magnification, (e) 20°C, 2,5KX magnification, (f) 20°C, 5KX magnification, (g) 175°C, 250X magnification, (h) 175°C, 2,5KX magnification, (k) 175°C, 5KX magnification.....	52
Figure 4.19. Detail of Fig.18. (d). (20°C). Morphology of the fracture surface around the deep secondary crack in the biphasic region. Well-protected conformation zones can be seen at the interfaces between α -aluminium and silicon.	52
Figure 4.20. Detail of in Fig. 18(d). (20°C). Fracture of mixed morphology. Oval shear dimples are situated near the cleavage facet.....	53
Figure 4.21. Detail of Fig. 20. (20°C). The secondary brittle crack took place on the interface between α -Aluminium and silicon.....	53
Figure 4.22. Detail of Fig. 17(d). (20°C). 500X.....	54
Figure 4.23. Detail of Fig. 22. (20°C). 1500X.....	54

Figure 4.24. Morphology of the fracture surface in the deformed α -Aluminium solid solution. The shelves of the oval dimples are shown. (20°C). 2500X	55
Figure 4.25. (20°C). 500X	55
Figure 4.26. (20°C). 2500X	56
Figure 4.27. Detail in Fig. (20°C). 18(e)	56
Figure 4.28. (20°C), 2500X	57
Figure 4.29. (20°C), 2500X	57
Figure 4.30. Transcrysalline fracture with the greatly developed surface. The main crack crossed the silicon precipitate in the cleavage planes of different orientations in relation to the average fracture plane. The rectilinear secondary cracks, the branched cleavage steps, and the tear ridges have formed in the α - Aluminium solid solution. (-75°C), 500X	58
Figure 4.31. Surface of the silicon plate cracked several times. The crack front crossed the numerous cleavage planes of different orientations. (-75°C), 1500X	58
Figure 4.32. Detail of Fig.30, numerous secondary cracks are visible.(-75°C).1500X	59
Figure 4.33. Cleavage steps formed in the branched particles. The cleavage step system is a result of the crack front propagation on the successive cleavage planes. (-75°C), 1500X	59
Figure 4.34. (-75°C), 1500X.....	60
Figure 4.35. Detail of Fig.34 (-75°C), 5000X	60
Figure 4.36. Detail of Fig.35 (-75°C), 10000X	61
Figure 4.37. Transcrysalline fracture of medium-developed surface. The areas of fracture of both cleavage and cellular features are visible (175°C), 1500X	61
Figure 4.38. (175°C), 2500X	62
Figure 4.39. (175°C), 1500X	62
Figure 4.40. (175°C), 2500X	63
Figure 4.41. (175°C), 1500X	63
Figure 4.42. Fracture in two-phase region. The cell is formed from a deformed matrix band around the cracked silicon particles. The zone of the interface cohesion is present on the interface between α -Aluminium and silicon. In the silicon particle, the numerous cleavage cracks are visible. In the microregion of the solid solution the oval and open shear dimples are revealed. Detail of Fig.41, (175°C), 2500X	64
Figure 4.43. Detail of Fig.42, (175°C), 5000X.....	64
Figure 4.44. (175°C), 7000X	65

Figure 4.45. (175°C), 10000X	65
Figure 4.46. (175°C), 2500X	66
Figure 4.47. (175°C), 1500X	66
Figure 4.48. (175°C), 1500X	67
Figure 4.49. (175°C), 2500X	67
Figure 4.50. (175°C), 2500X	68
Figure 4.51. (175°C), 500X	68
Figure 4.52. Area 1 of sample at 20°C, (a) SEM view of fracture surface, (b) EDS analyses.....	69
Figure 4.53. Area 2 of sample at 20°C, (a) SEM view of fracture surface, (b) EDS analyses.....	70
Figure 4.54. Area 3 of sample at 20°C, (a) SEM view of fracture surface, (b) EDS analyses.....	71
Figure 4.55. Area 4 of sample at 20°C, (a) SEM view of fracture surface, (b) EDS analyses.....	72
Figure 4.56. Area 5 of sample at 20°C, (a) SEM view of fracture surface, (b) EDS analyses.....	73

LIST OF TABLES

Table 1.1. Aluminum alloy designation system – Aluminum Association	3
Table 1.2. Temper Serial Numbers Definitions for Aluminium Alloys	3
Table 1.3. Solid Solubility of Elements in Aluminium	4
Table 2.1. Chemical composition of A356 alloy	15
Table 3.1. Charpy test results of samples at 175° C	19
Table 3.2. Charpy test results of samples at 95° C	21
Table 3.3. Charpy test results of samples at 60° C	24
Table 3.4. Charpy test results of samples at 20° C	26
Table 3.5. Charpy test results of samples at 0° C	29
Table 3.6. Charpy test results of samples at -40° C	32
Table 3.7. Charpy test results of samples at -75° C	34

1. INTRODUCTION

Aluminium is one of the most extensively employed light metals owing to castability ease as well as good corrosion properties, and sufficient strength. These features of aluminium provide widely used in automotive industry products such as wheels. The wheels are used in many geographies from the coldest areas to deserts. This means that the maximum service temperature of the wheels can reach around 150°C [1]. The alloy that is used to produce wheels should be selected considering its behaviour in extreme climatic conditions. Today, many wheels are produced from A356 alloy by using the low-pressure casting (LPDC) technique. A356 is hardening with sedimentation. Therefore, the impact energy, which is vital for the wheels, can be increased by applying heat treatments [2]. For instance, dissolving at 540°C in less than 6 hours gives optimal impact energy value. In addition, impact energy drops significantly after 16 hours of aging, [3]. However, Alexopoulos et al. (2011) observed that there are also sharp drops in impact energy due to over-aging [4].

Impact fracture is generally unexpected, influenced by many known factors. Not only the heat treatment is a critical parameter, but also the amount of Sr, Fe, Mg, grain size, and microstructure are a few of the key factors of fracture toughness [5] [6] [7] [8] [9] [10]. Samuel et al. (2014) obtained in some results like impact energy decreases because of Sr-B interactions in the microstructure studies. Morphology of interdendritic phases also impresses the impact toughness. The best toughness value was observed in Al5TiB grain-refining samples with 200 ppm Sr addition with T6 heat treatment compared to the addition of 30 ppm Sr, and Al10Ti master alloy [11]. Also, Tilová et al. (2016) studied that the Sr addition of AlSi11Mg alloy had a positive effect on impact energy. 0.05%, 0.1% and 0.15% Sr were added to the samples, respectively. In the sample with 0.05% Sr added, the best fracture toughness was observed [12]. Another study has been done by Amne Elahi et al. (2016). They obtained that grain refinement and modification cause an increase in impact energy separately, in addition, grain refinement did not cause that much increase in impact energy compared to the modification in the as cast condition (without heat treatment) [2].

On the other hand, it should not be forgotten that even if all factors are at the optimum level, porosities around the notch can affect the impact energy test result [13]. As well as all these parameters affecting fracture toughness, the effect of service temperatures is currently being studied as in the past [5]. According to Lalpoor et al. (2014) that all samples below 200°C showed relatively fragile properties. It showed more ductile behaviour at 400°C. As the temperature dropped, brittleness was observed [14]. The general view is that in face-centered cubic (FCC) lattice structured metals (e.g., aluminum), the rising of the ambient temperature slightly increases the impact energy. However, this increase is not in the ductile brittle transition temperature type seen like in low strength body-centered cubic lattice structured steels. This behaviour contradiction is thought to be related to the nature of dislocation motion with the separate crystal lattices [15] [16].

In this research, worked on aluminum alloy wheel casting with the method of Low Pressure Die Casting. That aluminum alloy has %7 Si, %0.1 Fe, %0.3 Mg, %0.15 Sr and after casting, applied heat treatment processes. In the end of the manufacturing process, aluminum alloy wheel begins to take tests and investigations for the determination of mechanical behaviour such as fracture mechanics and impact properties. Some of these tests and investigations are Charpy V-notch test, macro and micro fracture surface examination.

In particular, Charpy V-notch test is more related to the purpose of this article which is defining the strength of aluminum alloy wheels at different service conditions. To provide different service conditions, samples are climated at several temperatures. Shivkumar et al. worked on the Charpy impact energy of A356 alloy have been measured at different conditions and results show that there is not important change for impact energy, but these specimens were produced in sand moulds and water-cooled copper moulds [5].

1.1 Aim of the Thesis

In this study, the Charpy impact test of the rim used in car tires produced with AlSi7Mg0.3, which is an alloy of aluminium, at critical temperatures of -75° , 175° and between, and their examination are discussed. The purpose of this thesis is to estimate the strength of A356 alloy tire rims produced by the low-pressure casting method at these critical temperatures. We obtained this estimation by conditioning the samples we obtained in accordance with the ISO148-3 stands we made on the wheels we cast, at temperatures of -75° , 175° and between and subjecting them to a Charpy impact test.

1.2 Literature Survey

It is necessary to understand the methods used in rim production, the different effects of these methods, the mechanical and metallurgical properties of AlSi7Mg0.3, which is an aluminum alloy, and all the factors that affect these properties.

1.2.1 Classification of Cast Aluminium Alloy

The classification of purchases is made by the internationally recognized US Aluminum Association (EAA). EAA has established this notation system by compiling International Aluminum Identification and chemical component limit registers for cast aluminum alloys [17].

In the wrought alloy designation, the first number denotes the first alloying element. The second number is used to describe the change in the original alloy. This number is 0 for the original alloy. The last two numbers define the purity of aluminum in 1XXX series alloys. In all other series, it defines alloys with various properties [18]. (Table 1.1)

There is also a classification of aluminum casting alloys. For example, for the 1xx.x class, the second and third digits express the purity ratio of the alloy. If the last digit is 0,

it means casting and 1 means it is ingot. For example, 150.0 is a 99.5% pure cast alloy. (Table 1.1)

Table 1.1. Aluminum alloy designation system – Aluminum Association [19]

Castin alloys		Wrought alloys	
Alloy series	Principal alloying element	Alloy series	Principal alloying element
1xx.x		1xxxx	>99.00% aluminium
2xx.x	Aluminium-copper	2xxxx	Aluminium-copper
3xx.x	Aluminium-silicon plus copper and/or magnesium	3xxxx	Aluminium-manganese
4xx.x	Aluminium-silicon	4xxxx	Aluminium-silicon
5xx.x	Aluminium-magnesium	5xxxx	Aluminium-magnesium
6xx.x	Unused series	6xxxx	Aluminiummagnesium and silicon
7xx.x	Aluminium-zinc	7xxxx	Aluminium-zinc
8xx.x	Aluminium-tin	8xxxx	Other elements
9xx.x	Other elements	9xxxx	Unused series

The improvement of mechanical properties in alloys is possible with cold or hot applications. The strengthening degree is indicated by the temper designation T and H depending on whether the alloy can be heat-treated or hardenable. Other definitions indicate whether the alloy is annealed (O), dissolved (W) or used as produced (F). Numbers following T and H indicate the hardening amount, the actual type of heat treatment or other special manufacturing process status of the alloy [20].

Table 1.2. Temper Serial Numbers Definitions for Aluminium Alloys

Temper No	Definition
F	As Manufactured
O	Annealed
H	Cold-Shaped
W	Heat-Treated Solution
T	Aged

1.2.1.1 Properties of Aluminium Casting Alloys and Al-Si Eutectic Systems Used in Wheel Production

Aluminium casting alloys are known for its low density. Immaterial solubility for all gases outside of hydrogen, low melting temperature and good surface when the endpoint is reached are some of the aluminium alloy's advantages. A large amount of shrinkage as it solidifies is the biggest problem of aluminium alloys. Much attention should be paid to this in mold design to obtain a more uniform and dimensionally accurate product in casting and finishing or minimizing hot tearing.

Most metals can alloy with aluminium. However, very few of these have enough solid solubility to be major alloy additions. The most used elements have high solubility. These are: zinc, magnesium (both >10at. %), copper and silicone [21].

Table 1.3. Solid Solubility of Elements in Aluminium [21]

Element	Temperature(°C)	Maximum Solid Solubility	
		(wt.%)	(at.%)
Cadmium	649	0.4	0.09
Cobalt	657	<0.02	<0.01
Copper	548	5.65	2.40
Chromium	661	0.77	0.40
Germanium	424	7.2	2.7
Iron	655	0.05	0.025
Lithium	600	4.2	16.3
Magnesium	450	17.4	18.5
Manganese	658	1.82	0.90
Nickel	640	0.04	0.02
Silicon	577	1.65	1.59
Silver	566	55.6	23.8
Tin	228	0.06	0.01
Titanium	665	1.3	0.74
Vanadium	661	0.4	0.21
Zinc	443	82.8	66.4
Zirconium	660.5	0.28	0.08

The Al-Si binary system is composed of a eutectic reaction, which takes place at approximately 12.3 wt.% Si at a temperature of 577 °C. All the Al-Si compositions with less than 12.3 wt.% Si are known as hypoeutectic, with more than 12.3 wt.% Si, hypereutectic, and 12.3 wt.% Si, eutectic [19] (Figure 1.1).

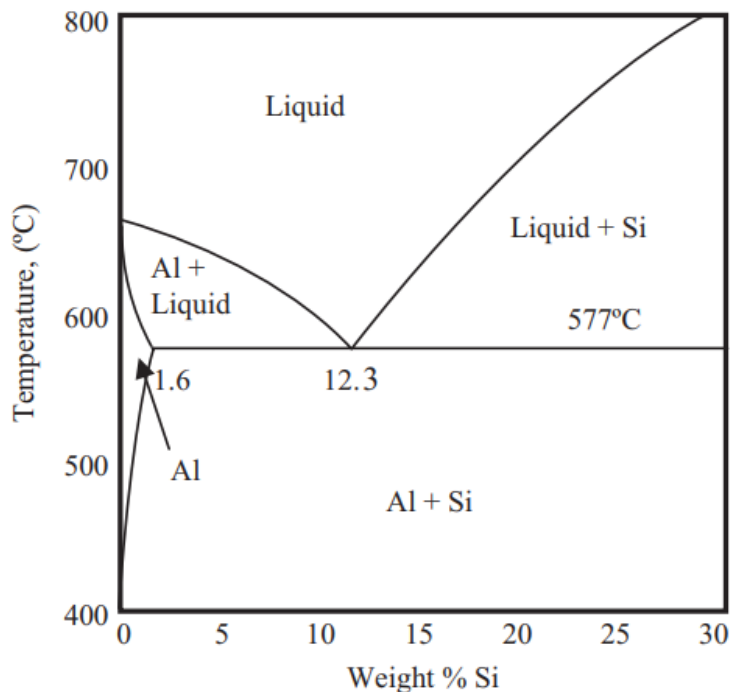


Figure 1. 1. Section of the binary Al-Si phase diagram that covers the most common Al-Si compositions for the 3xx.x series of alloys.

Alloys containing silicon as the main alloy addition are the most important of aluminium casting alloys, mainly due to the high fluidity provided by the comparatively large volumes of Al - Si eutectic. Fluidity is also supported because of the high heat of the fusion of silicon. Which is also increases "fluid life", particularly in hypereutectic compositions.

Well weldability, high corrosion resistance and the fact that the silicon phase decreases contraction during solidification and also decreases the coefficient of thermal expansion of the cast products are other advantages of AL-Si system-based casting. The eutectic is created between almost pure silicon and an aluminium solid solution including just over 1% silicon [21].

Eutectic consists of individual cells in which the silicon parts appear to be attached to each other. Alloys with eutectic exhibit low ductility due to the brittle nature of large silicon wafers. Rapid cooling greatly improves the microstructure. For this reason, the silicone phase takes a fibrous form. As a result, both tensile strength and ductility are greatly improved [21].

1.2.1.2 Al-Si Casting Alloys Used in Wheel Production

With a high degree of fluidity and low shrinkage, while solidifying, eutectic combinations have a special practice for thin-walled castings, e.g., Fig. 1.2. These alloys can be used

for castings where strength is not a priority. For example, some of these are cookware and certain car casting [21].

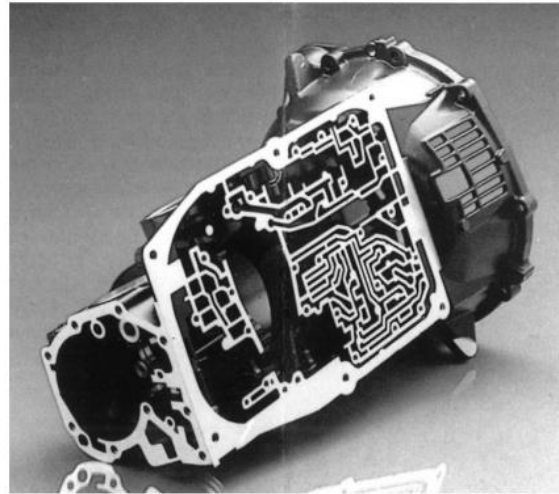


Figure 1.2. Al-Si cast alloy, Thin-walled transmission casing [21]

When alloys containing sufficient amounts of silicon are exposed to high temperatures, they begin to grow due to the precipitation of silicon from solid solution. Its dimensions can be stabilized by heating it for a few hours in a temperature range of 200-500 before use [21].

Al–Si–Mg Alloys

Sand and permanent mold castings are made from Al - Si - Mg alloys 356 (Al-7Si-0.3Mg) and 357 (Al-7Si-0.5Mg). Small magnesium additions cause the phases formed in this system to collapse, causing age hardening.

The solution process has a beneficial effect on silicon degradation and spheroidizing in modified alloys. On the other hand, it has little effect on unmodified particles. Alloy 357 which has higher magnesium content, results in higher tensile properties and rises the reaction to age hardening. But there is the drawback in that exceptionally huge particle of an intermetallic compound π ($\text{Al}_5\text{Si}_6\text{Mg}_8\text{Fe}_2$) may additionally shape. (Figure 1.3).

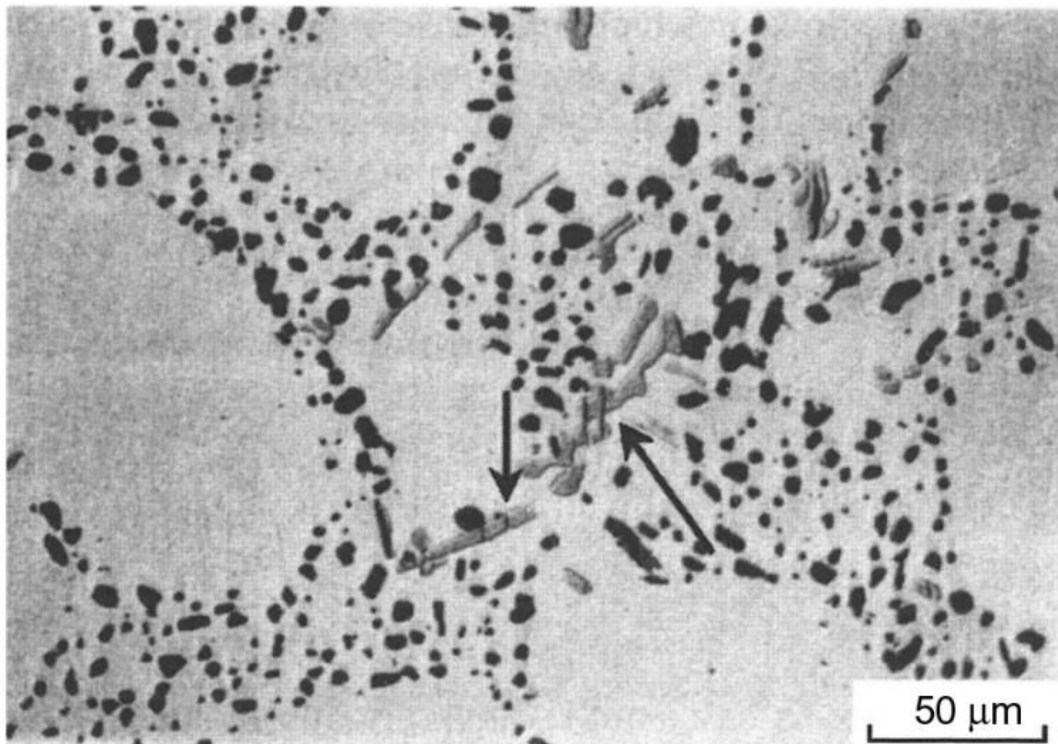


Figure 1.3 Microstructure of Alloy 357 with π phase [21]

In this figure, π phase particles can be seen together with small eutectic silicon particles. Arrows indicate π phase particles cracked when the alloy is deformed [21].

These particles tend to crack when the alloy is stretched. This makes the 357 less ductile compared to the 356, which contains less magnesium. Since the π phase reduces magnesium, its yield strength is less than it should be [21].

Al–Si–Cu Alloys

Adding copper to Al - Si alloy increases the strength of the alloy. Also supports age hardening and develops machinability. However, castability and ductility are decreased. Alloys generally contain between 3 and 10.5 percent silicon and 1.5 to 4.5 percent copper. Alloys with higher silicon content (e.g., Al–10Si–2Cu) are used in pressure die casting. Alloys with higher copper content (e.g., Al–3Si–4Cu) are used in permanent mold castings and sand castings [21]. The strength of these castings is advanced by unnatural aging.

Composition 390 (Al – 17Si – 4Cu – 0.55Mg) is a hypereutectic composition. This composition is used for sand and permanent mold casting of car parts made of aluminium alloys. Alloy 390 is also used for parts in automatic transmissions of vehicles and for casting small engines [21].

1.2.1.3 Factors Affecting the Mechanical and Metallurgical Properties of Al-Si Casting Alloys

Mechanical and metallurgical properties of Al-Si alloys; It is related to the grain refining process, and heat treatment [22]

Grain Refining Process

It is directly related to the fracture and tensile strength of aluminum casting alloys, and the distribution of shrinkage and gas voids is an important process in terms of reducing the tendency to hot tear and improving feed during casting. It provides fewer structural casting defects in the part and thus better mechanical properties.

There are aluminum dendrites consisting of the same core in the structure of the alloy and called the grain (Figure 1.4). The length of these dendrites is determined primarily by the solidification rate, and the slower the solidification rate, the longer the dendrites. There is a modifiable eutectic silica phase between the mentioned dendrite arms [23].

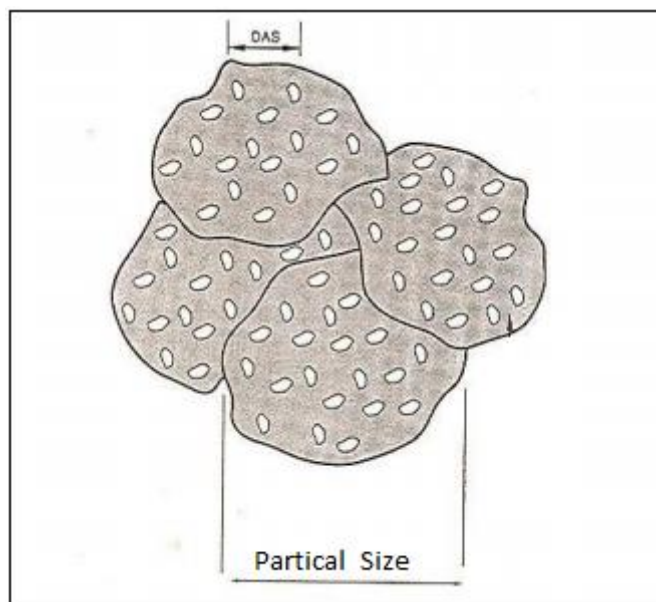


Figure 1.4 Main particles forming the Al-Si structure [23].

In general, grains in aluminum casting alloys are observed with a size of 1 - 10 mm, while DAS values are between 10 - 150 μm . The eutectic silica phase can be seen in these alloy systems as plates with a length of 2 mm or spheres with a diameter not exceeding 1 μm [23].

Heat Treatment

Commercial Al-Si-Mg alloys are generally T6 heat treated. For T6 heat treatment, the following steps are respectively processed (Figure 1.5).

- Solution taking process
- Quenching process
- Aging process

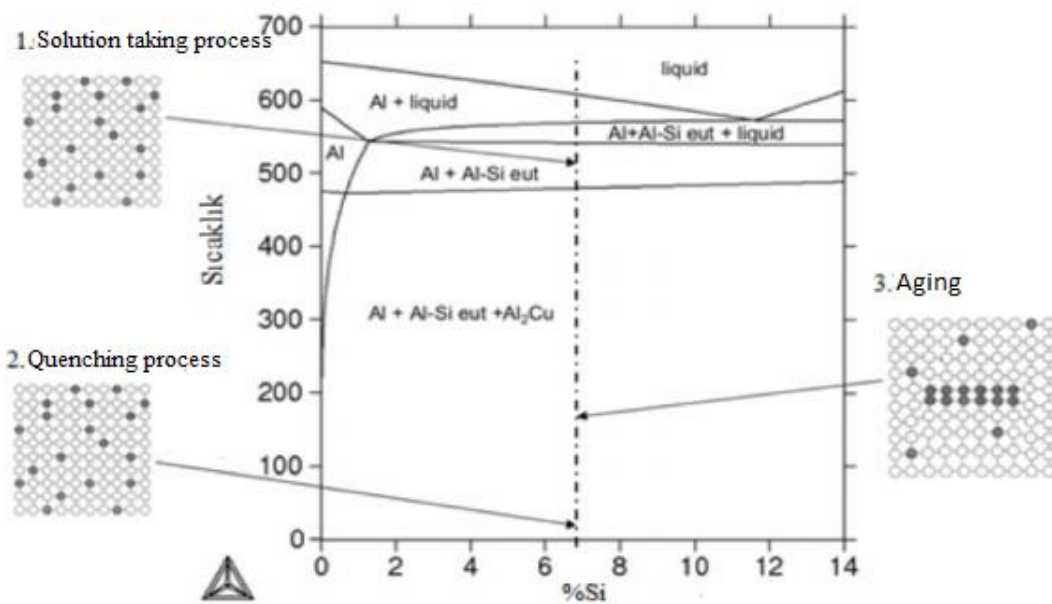


Figure 1.5 T6 heat treatment process [24]

The solution process is applied for homogenization of the cast structure, precipitation of intermetallic Mg₂Si phase and change of eutectic Si morphology. The time required for solutionization is related to the length of the dendritic structure and the solution temperature [25]. In order to increase the strength, Mg contained in Al-Si alloys has a high solubility in solidus temperature. It has been observed that as the solution temperature decreases, the solubility rate in the solid decreases. Since the melting temperature of aluminum is around 560 ° C, the processing temperature should be between 525 - 545 ° C [26].

If the solution process takes longer than necessary, it may cause high energy costs. Mg and Si alloying elements should precipitate homogeneously in order to increase the strength by settling during aging [26].

The purpose of the quenching process is to ensure that the components (Mg_2Si) that will precipitate in the aging phase and dissolved in the solution phase form a supersaturated solution at room temperature, to prevent this from occurring before room temperature [26].

The quenching rate is important between $450^{\circ}C$ and $200^{\circ}C$. In this range, precipitation occurs due to a high rate of oversaturation and high diffusion rate. Oversaturation decreases at higher temperatures. At low temperatures, the diffusion rate is not sufficient for precipitation to occur. The quenching rate should be below $4^{\circ}C/s$. The increase in yield stress at speeds above this value increases very slowly with increasing quenching rate. $4^{\circ}C/s$ is the optimum rate [26].

One of the most important steps in increasing the strength of aluminium alloys is the aging process. By controlling the aging time and temperature, many combinations of mechanical properties can be achieved. Aging can be performed at room temperature or at $90 - 260^{\circ}C$ by accelerating [26].

1.2.2 Automotive Wheel Production

Different shapes of rims can be produced to achieve different goals. These will be explained in this section.

1.2.2.1 Wheel Production by Forging Method

The forging method and rim production method are applied in cases where very low weight and very high strength are expected in aluminum alloy rims. Although the production of rims by forging method has similar processes to production with low pressure casting method, it is not so popular because it is much more costly for the manufacturer than low pressure casting method [27]

The rim is obtained from an aluminum billet. It takes the form of a block by being shaped under high temperature and pressure. Then the part is deburred, and the rim is put into the forming press. Heat treatment is applied to increase the mechanical properties of the rim. Finally, it goes through the CNC machining, drilling and painting processes and takes its final form. (Figure 1.6)

One of the most important features of forged rims is that defect types such as prosthesis and casting gap do not occur under any circumstances. And this means more reliable rims. Rims produced by the forging method can have a wider product range in terms of appearance as they are much more durable and lighter than those produced by the casting method [28].

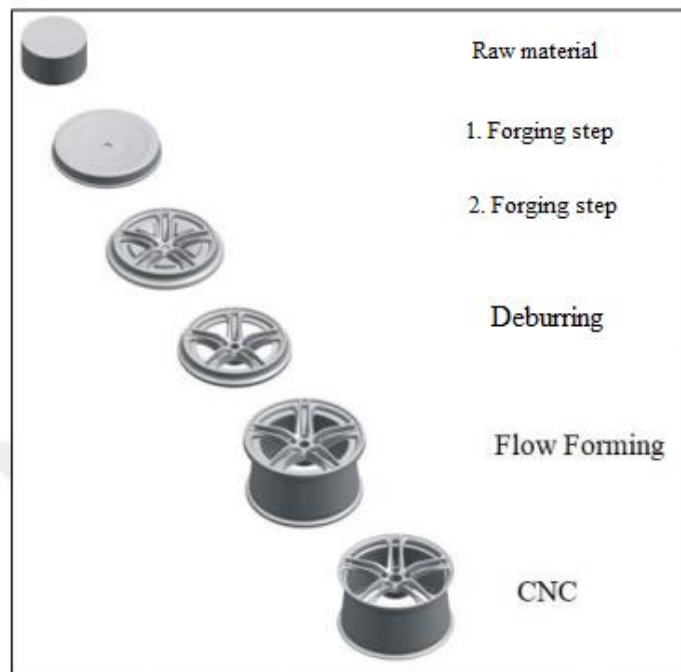


Figure 1.6 Wheel Production by Forging Method [27]

1.2.2.2 Wheel Production by Cold Forming Method

Rims can be produced from light metal alloy materials as well as from different materials. The cold forming method is used in steel wheel production. Generally, steel rims are used in trucks, forklifts, construction machines and commercial vehicles.

Rim production with cold forming technique consists of four main parts. The first two of these sections consist of the manufacture of pulleys and disc parts. In the third stage following these two stages, the pulleys and discs are assembled to each other. Finally, the rim is painted to give the desired color to the rim and to increase corrosion resistance [29].

This method offers various advantages to the manufacturers such as obtaining the produced part or product symmetrically at the end of the applied processes, low forming

cost and obtaining a very good surface quality and due to the changes in the internal structure of the metal after plastering, the shaped part can have much better mechanical properties [30].

The rim and hub, which are the two most important parts in segmented wheels, are manufactured separately and then assembled and made into a rim ready for final operations such as drilling and enlarging by welding.

The steel sheet raw material is firstly cut and curled on the guillotine machine in certain dimensions according to the size of the rim. Then the piece is inserted into the butt-welding operation.

Flash butt welding is very important in the cold shaping method. The most important reason for this is that the pulley carrying the tire is joined by the butt-welding method. If there is any problem with the source quality; a tire air leakage problem may occur as a result of rim cracking, puncture or tearing. After the butt-welding operation, the pulley production from the sheet plate is started.

During this process, the material, which has been curled and made round, is heated by the high current passing through the ends and the ends are centered by hitting each other. Excess metal scrapes caused by the high current are removed by deburring operation. The part, which goes through end cutting and grinding operations in order to correct its edges, is calibrated on a calibrated bench afterward. The calibrated pulley is put on the plastering bench to shape it by the plastering method. Here, with the help of plastering balls, shaping is completed in two stages.

1.2.2.3 Wheel Production by Low Pressure Die Casting Method

Casting is the process of melting metal or alloys and filling them into the desired mold. The casting of a part takes place by pouring the molten metal into a mold of the desired geometry and solidifying there. Thanks to this production method, it is possible to produce even the most complex parts. With this method, which is suitable for mass production, many parts are produced in a short time. The parts produced can be simple or complex in shape or can range from a few millimeters to several meters. Due to such advantages, casting has an important place among production methods [31, 32].

In low pressure castings, it uses metal molds to cast, but the molten metal is pressurized to allow the mold to fill faster and be better controlled. In the process, it uses up to 7 MPa pressure for special products, but generally, the pressure used is below 0.5 MPa [32].

It is the most widely used method in the automotive industry. It is used in the production of rims.

In the low-pressure casting method, after the mold is locked, the liquid metal is poured into a pump chamber heated to metal temperature or cold. The pump quickly passes the liquid metal through the feed section, during which time the air in the mold is ejected

through the escape gaps. After the mold cavity is completely filled, pressure is applied until the casting cools. The mold is then opened, and the casting material is then taken out. While the mold is open, it is closed after cleaning and oiling, and the previous process is applied again and again [33].

1.2.3 Wheel Test Methods

1.3 Charpy Impact Testing

In the Charpy impact test, the energy required to break the specimen containing notches under the impact effect is calculated. This value is called impact strength (Figure 1.7).



Figure 1.7 Charpy impact testing machine

The pendulum with mass G is at height h_1 , and its potential energy is

$$\text{Initial Potential energy} = G * h_1 \quad (1.1)$$

After the pendulum is released from this height, it breaks the sample and on the other hand, rises to the height h_2 . Thus, the potential energy in the final state of the pendulum

$$\text{Potential Energy in Second State} = G * h_2 \quad (1.2)$$

When frictional losses are neglected, the total energy of the Pendulum in the initial state is equal to the total energy in the final state and the energy lost due to the impact. The fracture energy of the sample:

$$G * h_1 = G * h_2 + \text{fracture energy} \quad (1.3)$$

$$\text{fracture energy} = G * (h_1 - h_2) \quad (1.4)$$

The samples used in impact tests are usually notched. When a notched sample is strained, a stress perpendicular to the bottom of the notch occurs. Fracture starts with the effect of this stress. In order for the sample to break, this vertical tension must be greater than the force holding the crystals together. If the sample breaks before the plastic deform, it is called a brittle fracture. The fractured surface is a smooth parting surface. Fracture surface: It is shimmery and granular.

1.4 Instrumented Charpy Impact Testing

Adding instrumentation to an impact system allows the engineer to “see” all kinds of previously unknown information, including beginner damage points and ductile brittle transition zones. With instrumentation, the load on the sample is continuously recorded depending on the time and/or deviation of the sample before it is broken. This gives a more complete representation of an effect than a single calculated value. Because failures are caused by the weakest point and spread from there, samples do not need to be broken down to be considered failures. Depending on the requirements, the fault can be identified by deformation, crack initiation, or complete fracture.

The CVN test can be applied using one of the following: an instrumented drop-weight system tup or a pendulum assembly, an Instrumented tup, but does not require identification energy expended. An instrumented setup provides more information about the processes that consume force as a function of load point displacement, the measured results required using a pendulum, contributing to the energy required for the sample to fail. Because the behaviour in an impact test can be complex, data interpretation and evaluation of the best practical implications for a well-Instrumented machine [34].

2. MATERIAL AND METHOD

2.1 Sample Production

The Charpy specimens were machined from cast aluminum alloy automotive wheels. Wheels are produced by a low-pressure die casting, and the material of these wheels is A356 aluminum alloy, hypoeutectic aluminum-silicon alloy, ingots form. The chemical composition of A356 alloy studied in this work is shown by Table 2.1.

Table 2.1.Chemical composition of A356 alloy

A356	Wt.%		Wt.%
AL	92.1661	Na	0.00035
Si	7.286	Ca	0.0014
Mg	0.277	Zr	0.0026
Ti	0.1213	V	0.0103
Fe	0.1116	Co	0.0006
Sr	0.0153	Sb	0.00001
Mn	0.021	P	0.00041
Cu	0.0012	B	0.0006
Zn	0.0041	Others	0.0044
Cr	0.0012		
Ni	0.0048		
Sn	0.0014		

5 wheels chosen for preparing specimens for V-Notched Charpy impact test, and they have 5 spokes with appropriate dimensions for taking specimens, conform with TS_EN_ISO_148_3.

These 5 wheels were produced from the same charge because of minimizing the error caused by melt alloy. An electric-induction furnace has used for melting material at 750 ± 5 °C. The wheels have 18-in diameter and 12.450 kg weight. Then they went to the heat treatment stage, which has 545 ± 2 °C taking into the solution for 3.5 hours, quenched in water the bath at 72 ± 2 °C, and then artificial aging applying with 165 ± 2 °C temperature for 2 hours. Additionally, wheels take the process in paint shop which is 200 °C temperature for 45-minute pre-treatment, 240 °C temperature for 45-minute powder coating, 220 °C temperature for 40-minute wet paint processes. After all, that wheels are ready to process for preparing V-notched specimens.

2.1 Sample Preparation

Charpy V-notched specimens drawn from same A356 wheels, as mentioned earlier they have cast same charge. These wheels have 5 spokes, and spokes are our target place, shown in Figure 2.1, for taking specimens. Attention was paid to designing specimens'

location that point of contact in 13° impact test should coincide at the point of contact with specimen and anvil in Charpy test.

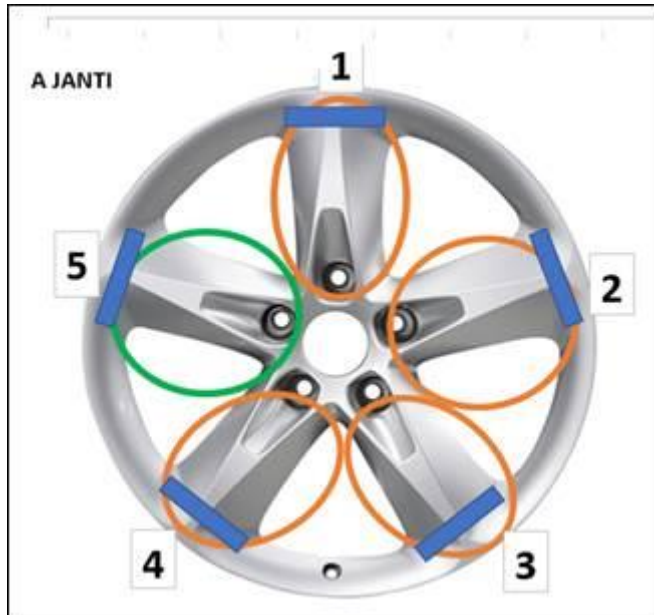


Figure 2.1 Display of samples taken from the wheel

The standard for Charpy V-notched tests is TS_EN_ISO_148_3, and to this standard, our specimens must have 5mmx10mmx55mm dimensions. To start the preparation sample process, each wheel was cut from the spokes ends with a band saw. Then these pieces were machined with highly precise CNC machines. The most crucial part of this machining is creating V-notched size. This V-notched size must have 2mm depth with $0.25\text{mm} \pm 0.025\text{mm}$ radius of root and $45^\circ \pm 1^\circ$ angle of the notch.

2.2 Sample conditioning

American Society for Testing and Materials Method E 23 includes very precise requirements concerning the determination and control of specimen test temperature. It specifies minimum soaking times dependent on the use of liquids or gases as the medium for thermally conditioning the specimen. The method also requires that the impact of the specimen occur within 5 s of removal from the conditioning medium. It does not, however, provide guidance regarding the choice of conditioning media. This investigation was mainly conducted to investigate the changes in specimen temperature which occur when water is used for thermal conditioning. A standard CVN impact specimen of alloy aluminum was instrumented with surface-mounted and embedded thermocouples [35]. To test the samples at a various temperatures between -75° and $+175^\circ$, acetone and dry ice mix used to cool the sample, and boiling water solution and electric-induction furnace was used to heating the samples.

3. TESTING AND DATA INTERPRETATION

3.1 Instrumented Charpy Impact Testing

The Instron CEAST 9050 impact pendulum machine is used for this work. Owing to this instrumented machine, we obtained the time-varying force and energy data for 6000 points, which we cannot obtain in a standard Charpy machine. In order to obtain data at 6000 points, the frequency was set to 2000 kHz and the working range was set to 100%. The data obtained were transformed into graphics using the software within the machine. OriginPro was used to produce more visually meaningful graphics.

3.2 Tests at Different Temperatures

To estimate the resistance of A356 aluminium wheels produced by the LPDC method at different operating temperatures, the samples were impact tested at temperatures of -75 °C, -40 °C, 0 °C, +20 °C, +60 °C, +95 °C and +175°C. Total impact energy, crack initiation energy and crack propagation energy data will be obtained from Charpy impact tests performed at these temperatures. With these data obtained, it was aimed to examine the strength of the sample at different temperatures.

Dry ice, acetone, boiling water and vacuum oven were used to reach the desired temperatures of the samples. Temperature monitoring was done with NÜVE EV 018 model digital thermometer throughout the process. A system made of foam, glass and polyurethane was used to prevent heat transfer.

3.2.1 Tests at 175 °C

NÜVE EV 018 model vacuum oven was used for the heating process (Figure 3.1). First, the oven was set at 175 ± 5 °C. After the temperature of the oven was stabilized, the temperature of the environment was controlled with a digital thermometer. 3 samples were placed in the oven and kept in the oven for 30 minutes. Later, the samples were taken from the furnace with the help of scissors within 5 seconds and broken in the impact machine.



Figure 3.1. NÜVE EV 018 model vacuum oven

After breaking each sample, time-dependent force and energy data of fracture were obtained from the software of the Instron CEAST 9050 impact pendulum machine.

The obtained Force-Time and Energy-Time data are visually arranged with OriginPro8.5 and shown in figure 3.2.

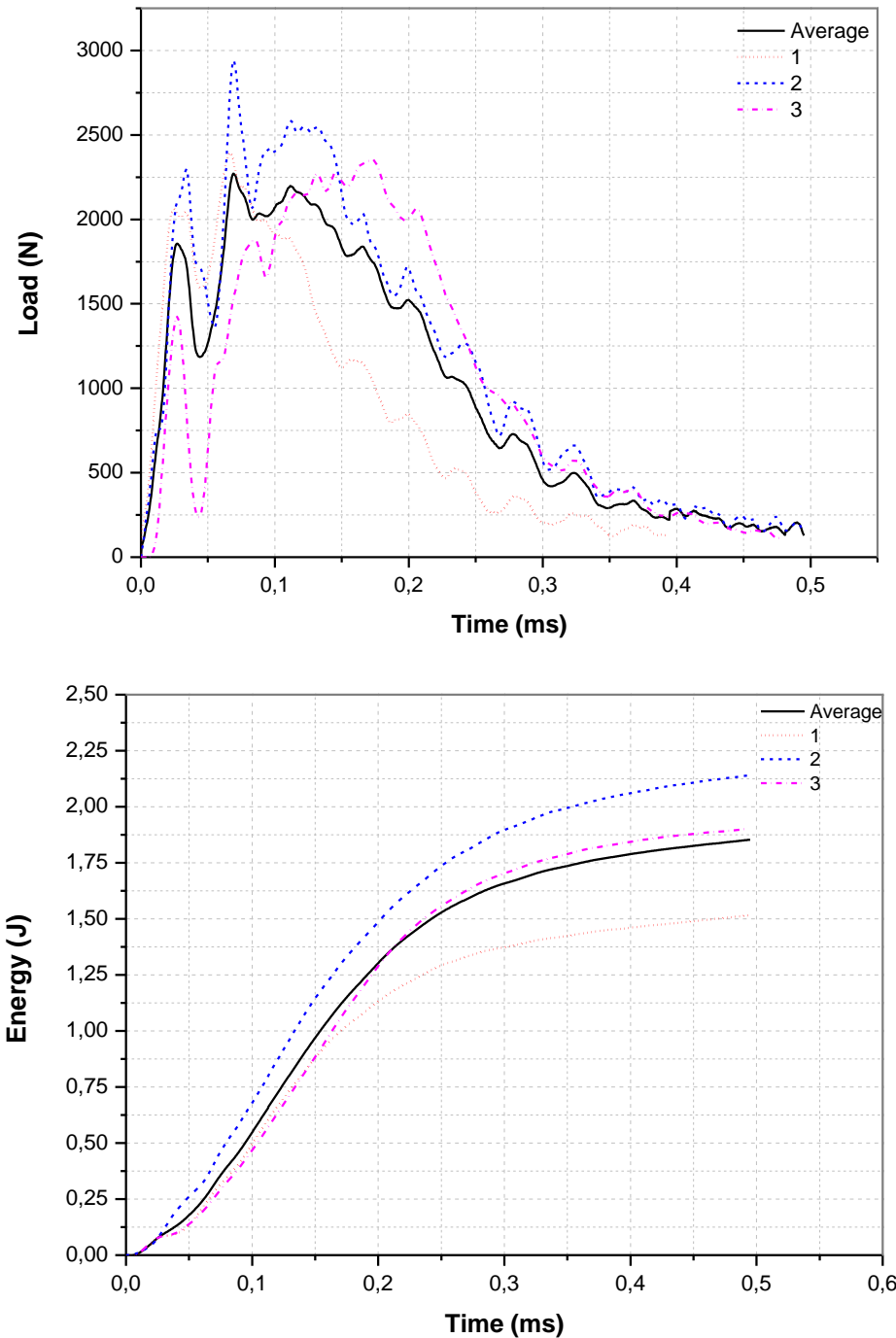


Figure 3.2. Load-time and Energy-Time graphs of 3 specimens at 175 °C temperature.

The results of the experiments performed at 175 °C degrees are given in Table 3.1. The average maximum load value of the samples was 2.56 kN, the average initiation impact energy value was 1.57 J/cm², the average total energy was 4.59 J/cm² and the average propagation energy was 3.02 J/cm². These impact energies were obtained by dividing the joule values taken from The Instron CEAST 9050 impact pendulum machine by the cross-sectional area of the sample (0.8cm²*5cm²).

Table 3.1. Charpy test results of samples at 175° C

	Sample1	Sample2	Sample3	Average Maximum Load (kN)
Temperature (°C)	Maximum Load (kN)			
175	2.40	2.94	2.36	2.57
	Initiation Impact Energy J			Average Wi J
	1.26	1.01	2.46	1.58
	Total energy J			Average Wt
	3.69	5.36	4.72	4.59
	Propagation Impact Energy J			Average Wp
	2.44	4.34	2.26	3.01

3.2.2 Tests at 95 °C

For the heating process, a mechanism was prepared in which the water was constantly boiling. First, it was determined that the temperature of the water in the apparatus was 95 ± 5 °C with a digital thermometer. The samples were placed in the setup and kept for 20 minutes. Later, the samples were taken from the assembly with the help of scissors within 5 seconds and broken in the impact machine.

After breaking each sample, time-dependent force and energy data of fracture were obtained from the software of the Instron CEAST 9050 impact pendulum machine. The obtained Force-Time and Energy-Time data are visually arranged with OriginPro8.5 and shown in figure 3.3.

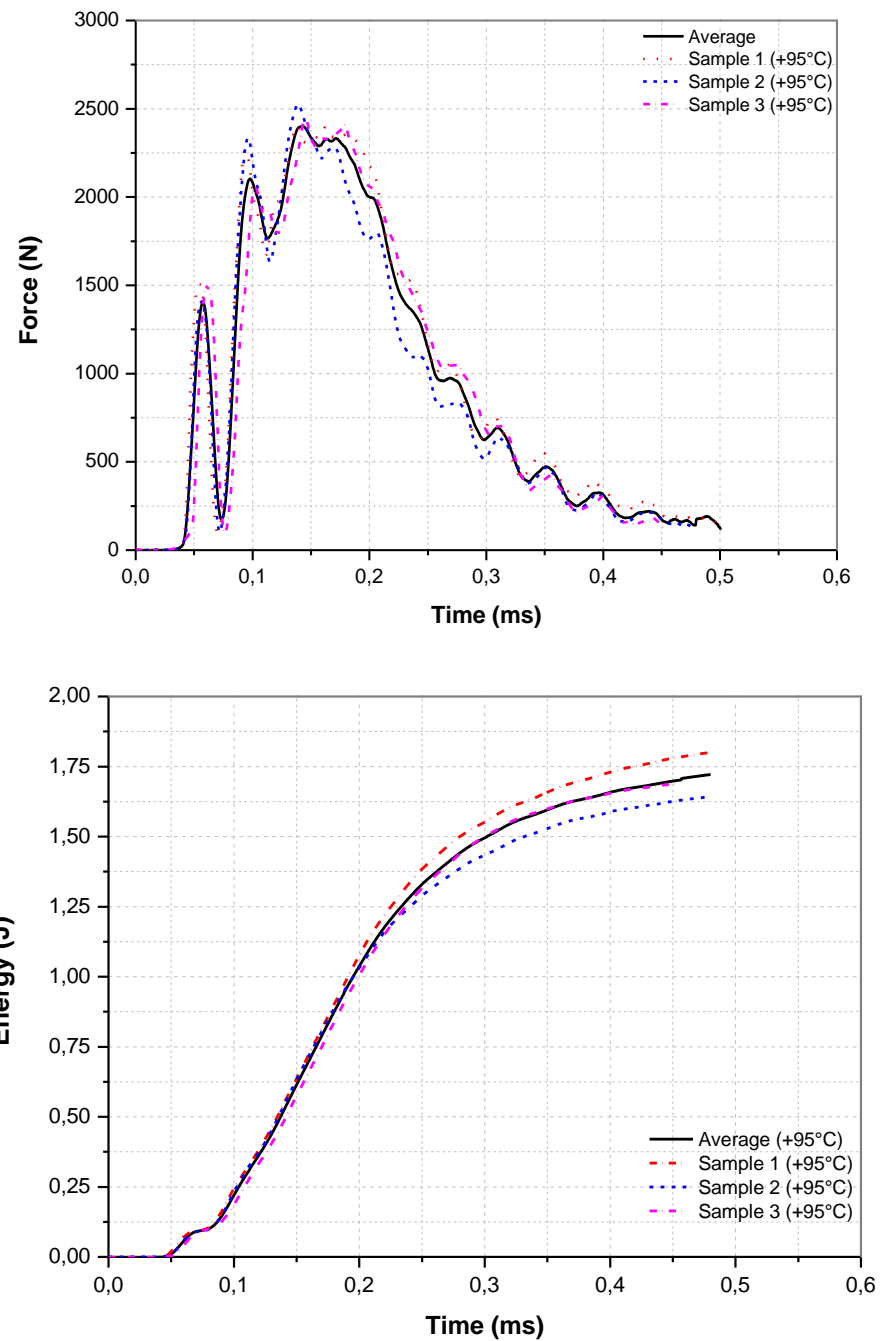


Figure 3.3. Load-time and Energy-Time graphs of 3 specimens at 95 °C temperature.

The results of the experiments performed at 95 °C degrees are given in Table 3.2. The average maximum load value of the samples was 2.46 kN, the average initiation impact energy value was 1.33 J/cm², the average total energy was 4.29 J/cm²and the average propagation energy was 2.96 J/cm². These impact energies were obtained by dividing the joule values taken from The Instron CEAST 9050 impact pendulum machine by the cross-sectional area of the sample (0.8cm²*5cm²).

Table 3.2. Charpy test results of samples at 95° C

Temperature (°C)	Sample1	Sample2	Sample3	Average Maximum Load (kN)
	Maximum Load (kN)			
95	2.41	2.53	2.45	2.46
	Initiation Impact Energy J			Average Wi J
	1.31	1.36	1.31	1.33
	Total energy J			Average Wt
	4.54	4.11	4.23	4.29
	Propagation Impact Energy J			Average Wp
	3.22	2.74	2.92	3.36

3.2.3 Tests at 60 °C

The apparatus for the heating operation was set at a temperature of 60 ± 5 ° C. Samples are placed. Hot water was added to the system at regular intervals to keep the temperature constant. Ambient temperature was monitored with a digital thermometer for 20 minutes. Later, the samples were taken from the assembly with the help of scissors within 5 seconds and broken in the impact machine.



Figure 3.4. Setting the samples to 60°C

After breaking each sample, time-dependent force and energy data of fracture were obtained from the software of the Instron CEAST 9050 impact pendulum machine. The obtained Force-Time and Energy-Time data are visually arranged with OriginPro8.5 and shown in figure 3.5.

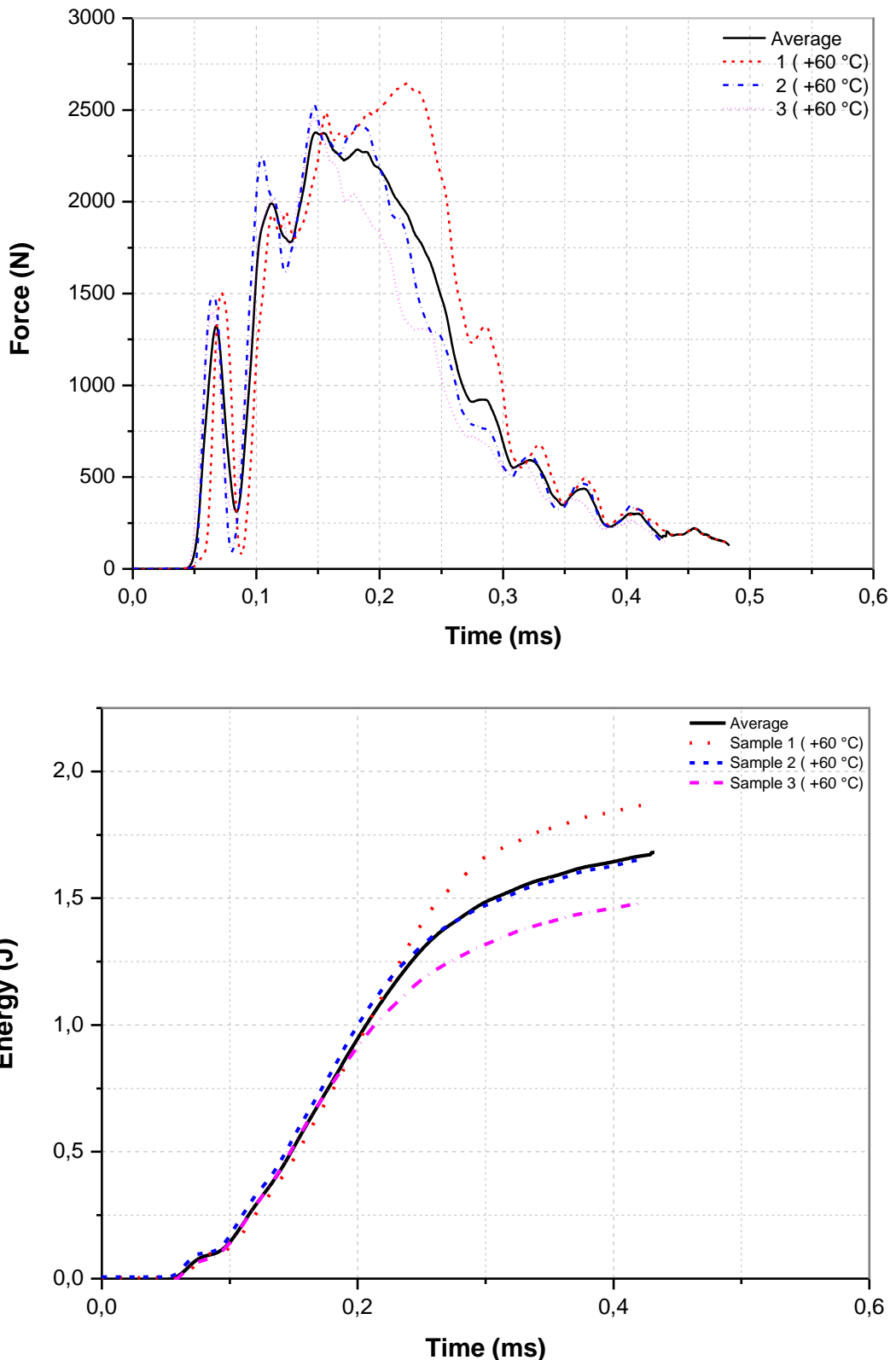


Figure 3.5 Force-time and Energy-Time graphs of 3 specimens at 60 °C temperature.

The results of the experiments performed at 60 °C degrees are given in Table 3.3. The average maximum load value of the samples was 2.55 kN, the average initiation impact energy value was 1.79 J/cm², the average total energy was 4.21 J/cm² and the average propagation energy was 2.42 J/cm². These impact energies were obtained by dividing the joule values taken from The Instron CEAST 9050 impact pendulum machine by the cross-sectional area of the sample (0.8cm²*5cm²).

Table 3.3. Charpy test results of samples at 60° C

	Sample1	Sample2	Sample3	Average Maximum Load (kN)
Temperature (°C)	Maximum Load (kN)			
60	2.65	2.53	2.46	2.55
	Initiation Impact Energy J		Average Wi J	
	2.84	1.32	1.23	1.80
	Total energy J		Average Wt	
	4.78	4.14	3.72	4.21
	Propagation Impact Energy J		Average Wp	
	1.94	2.82	2.49	2.42

3.2.4 Tests at 20 °C

The temperature of the experimental environment was measured with a digital thermometer as 20 ± 3 °C. The samples were kept in a room environment for one day. Later, the samples were taken from the assembly with the help of scissors within 5 seconds and broken in the impact machine.

After breaking each sample, time-dependent force and energy data of fracture were obtained from the software of the Instron CEAST 9050 impact pendulum machine. The obtained Force-Time and Energy-Time data are visually arranged with OriginPro8.5 and shown in figure 3.6.

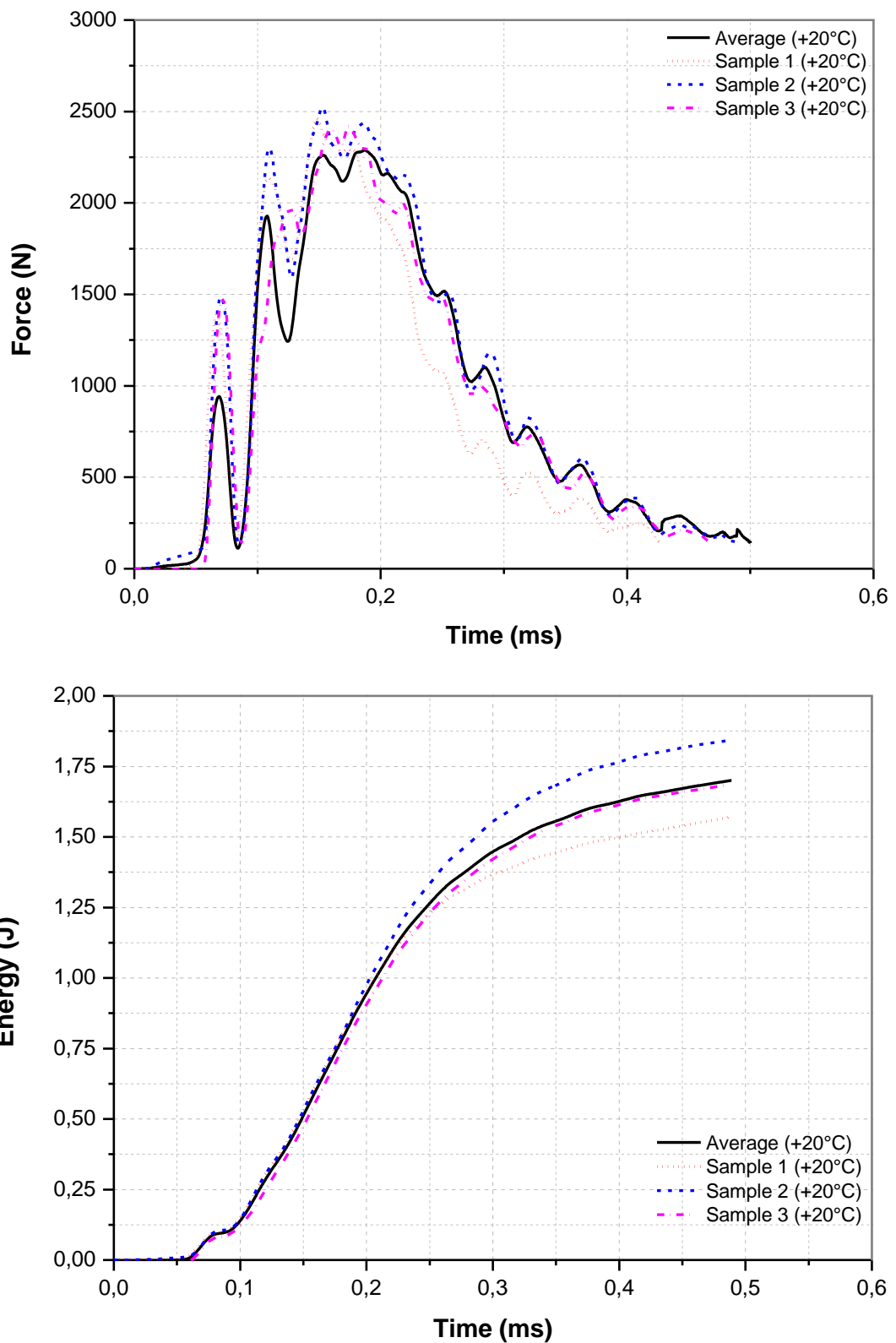


Figure 3.6. Force-time and Energy-Time graphs of 3 specimens at 20 °C temperature.

The results of the experiments performed at 20 °C degrees are given in Table 3.4. The average maximum load value of the samples was 2.47 kN, the average initiation impact energy value was 1.45 J/cm², the average total energy was 4.20 J/cm² and the average propagation energy was 2.75 J/cm². These impact energies were obtained by dividing the joule values taken from The Instron CEAST 9050 impact pendulum machine by the cross-sectional area of the sample (0.8cm²*5cm²).

Table 3.4. Charpy test results of samples at 20° C

	Sample1	Sample2	Sample3	Average Maximum Load (kN)
Temperature (°C)	Maximum Load (kN)			
20	2.46	2.53	2.42	2.47
	Initiation Impact Energy J			Average Wi J
	1.30	1.39	1.65	1.45
	Total energy J			Average Wt
	3.80	4.61	4.17	4.20
	Propagation Impact Energy J			Average Wp
	2.51	3.21	2.52	2.75

3.2.5 Tests at 0 °C

A water-ice mixture was added to the apparatus for cooling. With the help of a digital thermometer, it was observed that the temperature was 0 °C. Samples were added to the assembly and kept at 0 °C with a digital thermometer for 20 minutes. Later, the samples were taken from the assembly with the help of scissors within 5 seconds and broken in the impact machine.



Figure 3.7. Setting the samples to 0°C

After breaking each sample, time-dependent force and energy data of fracture were obtained from the software of the Instron CEAST 9050 impact pendulum machine. The obtained Force-Time and Energy-Time data are visually arranged with OriginPro8.5 and shown in figure 3.8.

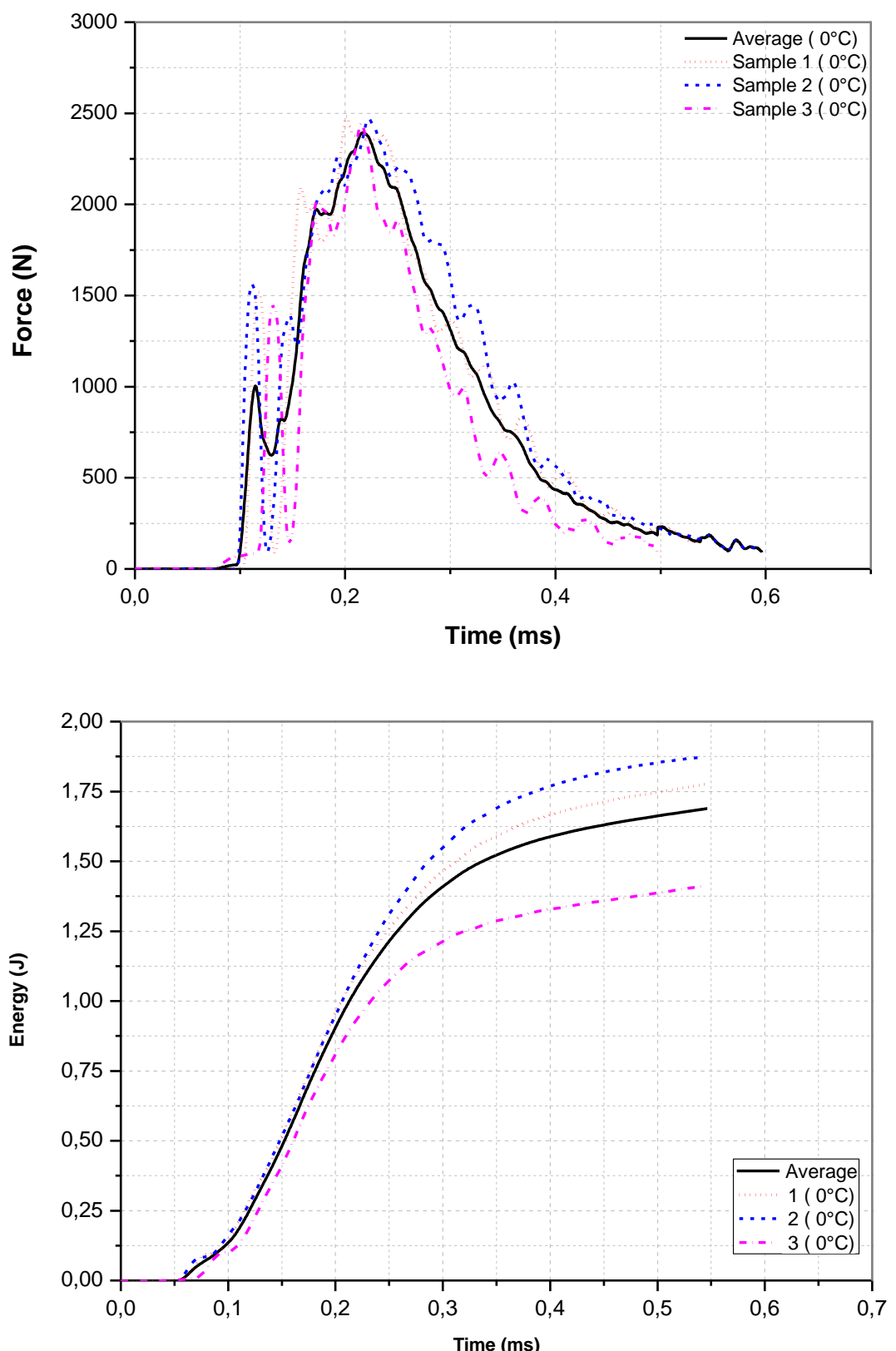


Figure 3.8. Force-time and Energy-Time graphs of 3 specimens at 0 °C temperature.

The results of the experiments performed at 0 °C degrees are given in Table 3.5. The average maximum load value of the samples was 2.47 kN, the average initiation impact energy value was 1.47 J/cm², the average total energy was 4.14 J/cm² and the average propagation energy was 2.67 J/cm². These impact energies were obtained by dividing the joule values taken from The Instron CEAST 9050 impact pendulum machine by the cross-sectional area of the sample (0.8cm²*5cm²).

Table 3.5. Charpy test results of samples at 0° C

	Sample1	Sample2	Sample3	Average Maximum Load (kN)
Temperature (°C)	Maximum Load (kN)			
0	2.48	2.47	2.45	2.47
	Initiation Impact Energy J			Average Wi J
	1.31	1.76	1.36	1.48
	Total energy J			Average Wt
	4.35	4.69	3.39	4.14
	Propagation Impact Energy J			Average Wp
	3.04	2.92	2.03	2.67

3.2.6 Tests at -40 °C

A mixture of acetone and dry ice was added to the bowl for cooling. Samples were added when the temperature of the assembly reached -40 ± 5 ° C. Dry ice was added to the apparatus at regular intervals for 20 minutes to maintain the temperature. The setup was followed by a digital thermometer throughout the process. Later, the samples were taken from the assembly with the help of scissors within 5 seconds and broken in the impact machine.



Figure 3.9. Setting the samples to -40°C

After breaking each sample, time-dependent force and energy data of fracture were obtained from the software of the Instron CEAST 9050 impact pendulum machine. The obtained Force-Time and Energy-Time data are visually arranged with OriginPro8.5 and shown in figure 3.10.

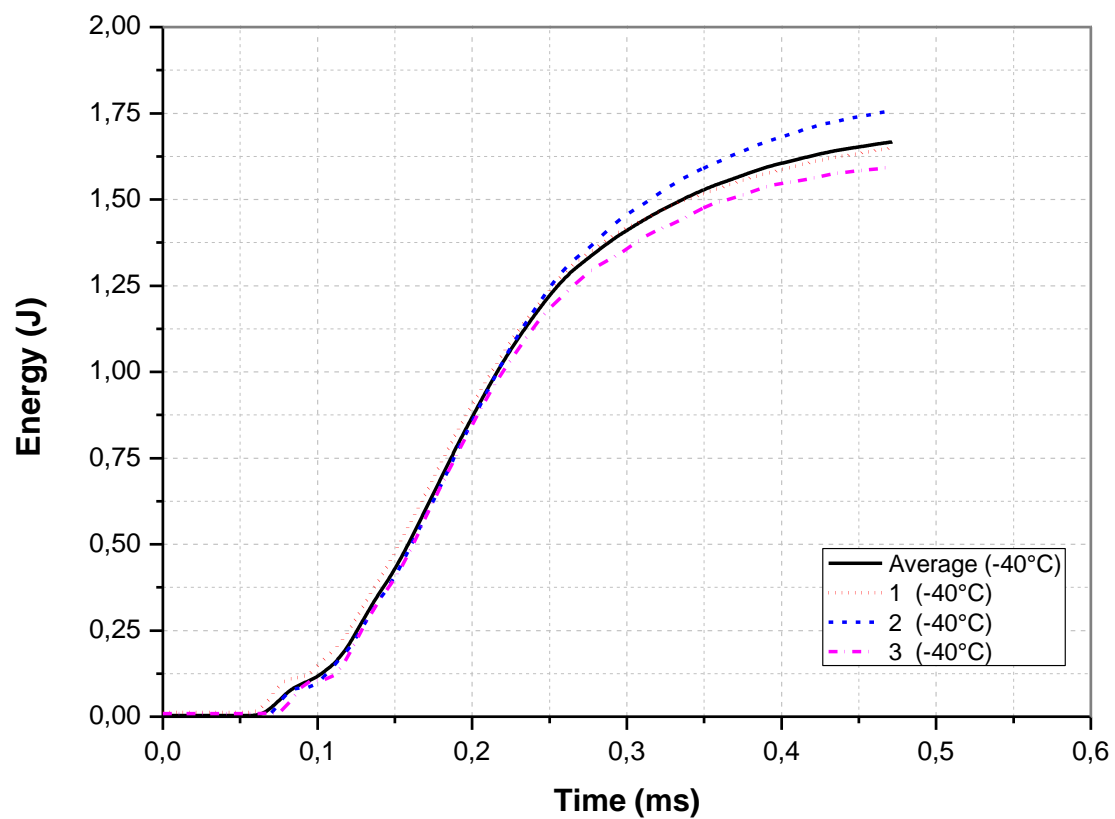
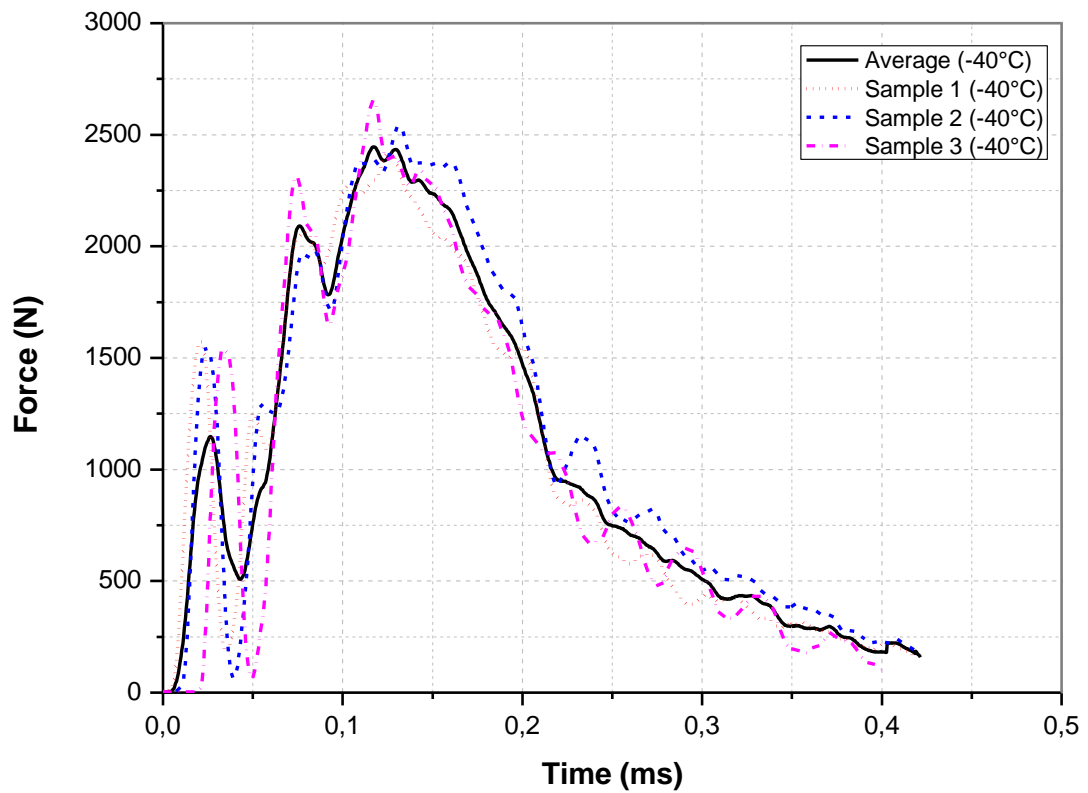


Figure 3.10. Force-time and Energy-Time graphs of 3 specimens at -40 °C temperature.

The results of the experiments performed at -40 °C degrees are given in Table 3.6. The average maximum load value of the samples was 2.54 kN, the average initiation impact energy value was 1.61 J/cm², the average total energy was 4.16 J/cm² and the average propagation energy was 2.55 J/cm². These impact energies were obtained by dividing the joule values taken from The Instron CEAST 9050 impact pendulum machine by the cross-sectional area of the sample (0.8cm²*5cm²).

Table 3.6. Charpy test results of samples at -40° C

	Sample1	Sample2	Sample3	Average Maximum Load (kN)
Temperature (°C)	Maximum Load (kN)			
-40	2.42	2.54	2.65	2.54
	Initiation Impact Energy J		Average Wi J	
	1.74	1.72	1.37	1.61
	Total energy J			Average Wt
	4.13	4.39	3.96	4.16
	Propagation Impact Energy J		Average Wp	
	2.38	2.67	2.59	2.55

3.2.7 Tests at -75 °C

Dry ice was added to the apparatus for cooling. The temperature of the dry ice was measured as -75 ± 5 °C. The samples were put into the setup and kept for 20 minutes. The process was followed by a digital thermometer. Later, the samples were taken from the assembly with the help of scissors within 5 seconds and broken in the impact machine.

After breaking each sample, time-dependent force and energy data of fracture were obtained from the software of the Instron CEAST 9050 impact pendulum machine. The obtained Force-Time and Energy-Time data are visually arranged with OriginPro8.5 and shown in figure 3.11.

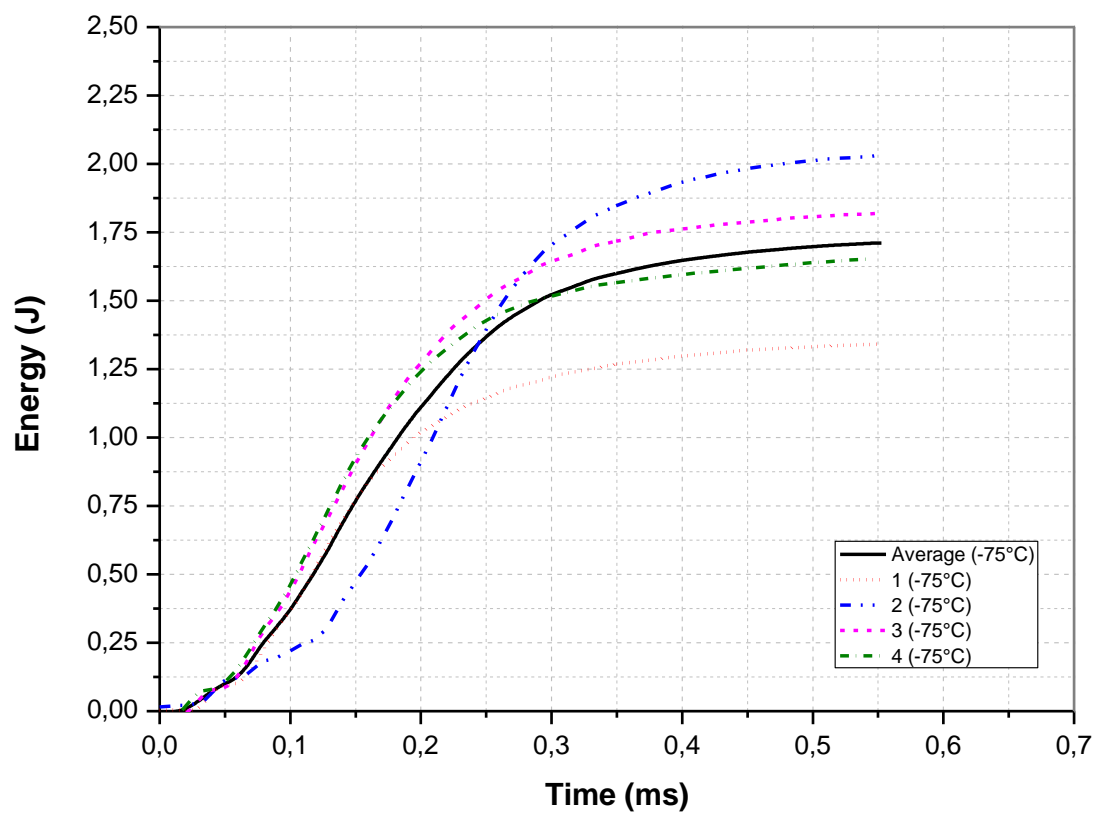
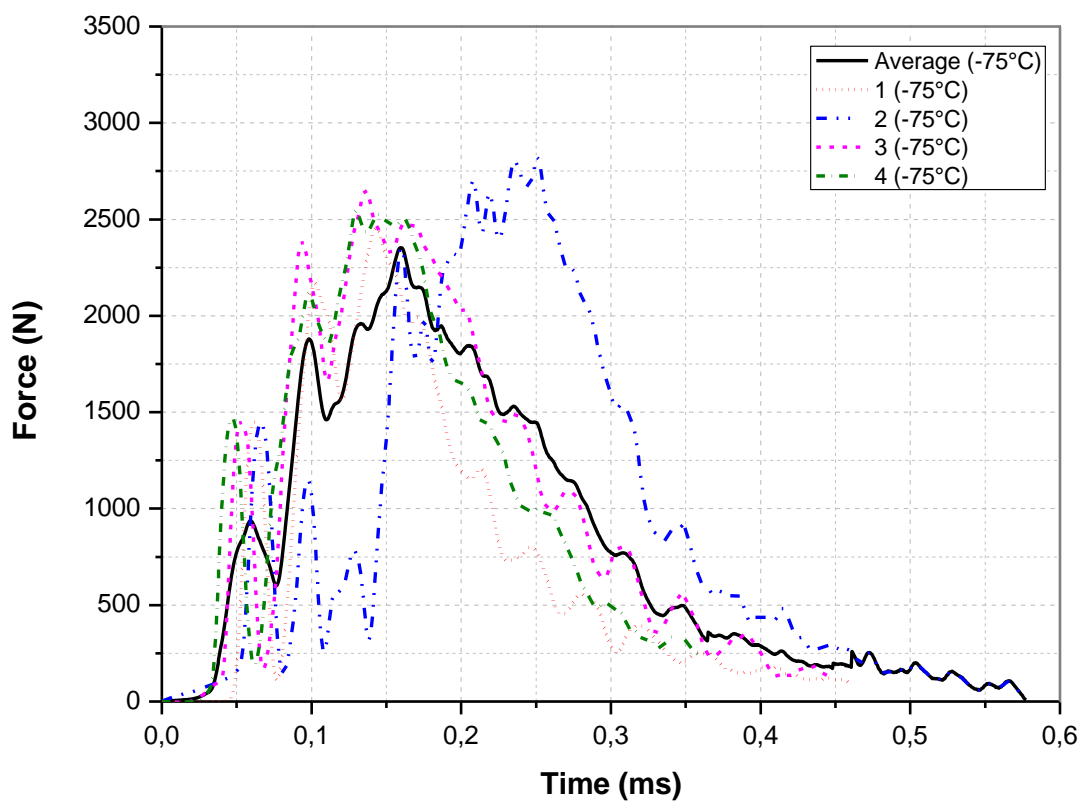


Figure 3.11. Force-time and Energy-Time graphs of 4 specimens at -75 °C temperature.

The results of the experiments performed at -75 °C degrees are given in Table 3.7. The average maximum load value of the samples was 2.56 kN, the average initiation impact energy value was 1.75 J/cm², the average total energy was 4.17 J/cm² and the average propagation energy was 2.42 J/cm². These impact energies were obtained by dividing the joule values taken from The Instron CEAST 9050 impact pendulum machine by the cross-sectional area of the sample (0.8cm²*5cm²).

Table 3.7. Charpy test results of samples at -75° C

	Sample 1	Sample 2	Sample 3	Sample 4	Average Maximum Load (kN)		
Temperature (°C)	Maximum Load (kN)						
-75	2.46		2.59		2.65		
					2.54		
	Initiation Impact Energy J				Average Wi J		
	1.29	3.06	1.37	1.28	1.75		
	Total energy J				Average Wt		
	3.28	5.07	4.44	3.90	4.17		
Propagation Impact Energy J				Average Wp			
				1.99	2.01		
				3.07	2.61		
				2.42			

3.3 Charpy Impact Resistance Variation with Temperature

The impact test is performed by calculating the amount of energy absorbed during fracture to determine the impact resistance and toughness of materials. Temperature can affect the toughness of a material. Impact tests were performed at different temperatures to reveal any influence on impact energy. Another reason for various temperatures is that to show the relationship of ductile to brittle transition in absorbed energy. Should be careful to select the service temperature. Only BCC structure materials experience ductile to brittle transition temperature. Increasing temperature allows more slip systems to operate more plastic deformation. FCC and HCP do not experience ductile to brittle transition; therefore, they give the same energy absorption at any temperature.

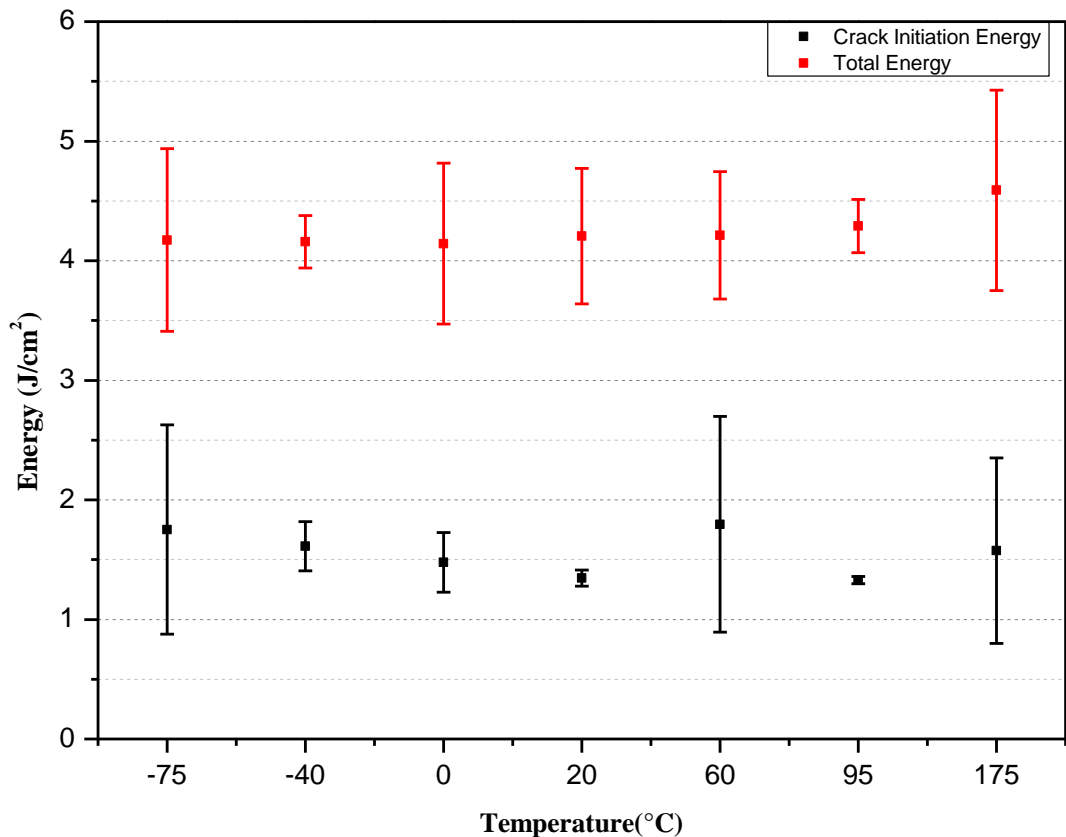


Figure 3.12. Crack Initiation and Total Energy to Temperature graph

4. MACROSCOPIC and MICROSCOPIC EXAMINATION

4.1 Microscopic Examination of Sample

The microstructure emerges because of examining the geometric structure of the sizes and distributions of the phases existing in metal composites, ceramics and alloys and how they are distributed in the volume under the microscope, and this morphological structure plays an important role in predicting the mechanical behavior of the metal or alloy. In general, the strength is closely related to the nature of the grains, and the distribution and grain size of the existing phases within the grains directly affects the mechanical behavior. The strength of small-grained micro-structured materials is superior to larger-grained micro-structured materials.

In two-phase alloys, one phase is generally harder and more brittle than the other. If this phase creates a continuous network within the structure, fractures or cracks will follow this line, so the material will become brittle. Reinforcement elements (such as particles and fibers) affect microstructure and strength. Therefore, preparation of samples for microscopy, examination of the prepared samples under the microscope, and interpretation of the photographs (micrographs) taken under the microscope are of vital importance to understand the source of material properties.

4.1.1 Sample Preparation

The sample examined should be representative of the part about which information is desired to be obtained. For example, If the damage investigation is to be carried out, samples are taken from the place where the damage occurred and the area that was not damaged and compared. In general-purpose examinations, it should be considered that the sample reflects all the properties of the part to be examined. Examination by taking many samples will increase the reliability while increasing the cost.

4.1.1.1 Sampling

While the samples are being cut from the main part, care should be taken not to overheat the sample and not to deform excessively. This may cause a change in the microstructure. According to the examination to be made, a transverse or longitudinal section should be taken. In this study, transverse and longitudinal sections were taken. To detect whether there is a deterioration in the isotropy of the microstructure. The most ideal cutting method is to use a water-cooled rotating disc (Fig. 4.1).



Figure 4.1. Abrasive Cutter.

These are called metallographic sectioning discs. There is a cutting disc suitable for every material. These discs contain abrasive materials such as SiC, Al₂O₃, diamond dust, and therefore these discs are called abrasive cutting discs. Coolant should be used to reduce heat build-ups during the cutting process. The coolant used can consist of oil and oil mixtures that do not corrode the sample. This liquid removes both excess heat and particles from the cutting area. STRUERS DISCOTOM-5 model machine was used in this study. Two samples were cut transversely and longitudinally from the samples created for the impact test.

4.1.1.2 Moulding

If the sample size to be examined is small or the sample is too complex to stand on a flat surface, it should be moulded or held with the help of a sample clamp. The moulding process can be done either hot or cold. Different types of resins are used in both methods. The sample to be moulded is sanded to 400 grits if possible and dried after cleaning the surface with alcohol. Hot moulding requires a moulding device, while cold moulding does not use any device. In this study, STRUERS ProntoPress-10 model hot moulding machine was used (Fig. 4.2).



Figure 4.2. Hot Moulding Machine.

In hot moulding, there is a chamber inside the device. We place the sample to be examined in the chamber of the Bakelite device with its surface facing down. Then we pour the hot Bakelite powder onto the sample. Considering that the sample powders will be compressed here, it should be noted that after the compaction takes place, the Bakelite powder must be poured in such a way that the length of the Bakelite exceeds the sample length, and the Bakelite must completely cover the back surface of the sample. The sample and Bakelite powder are kept for a certain period at a temperature not exceeding one-third of the melting temperature of the sample placed in the chamber. Since the sample used in this research is an aluminium alloy, it was processed at 180 °C for 12 minutes.



Figure 4.3. Specimen after moulding.

4.1.1.3 Grinding

The surface of a sample cut for microscopic examination is rough and scratched. An extremely smooth surface is needed to take images under the microscope. The deformed layer on the surface should be removed to see the internal structure to be examined. The sample must be grinded and polished to remove this deformed layer. Grinding and polishing operations are carried out in stages, and finer abrasives are used at each stage than the previous one. Thus, the scratches and deformations that occur in the sample at every stage are minimized. The sample is then polished to a mirror shine and brought to final gloss and smoothness before etching. Abrasives are produced by bonding hard and abrasive grains such as SiC, Al₂O₃ onto water-resistant paper or fabric. The number of sandpapers is related to the number of abrasive grains. The smaller the grain size, the greater the number of grains per 1 in². In other words, as the sanding number increases, the abrasive particle size decreases and the sandpaper becomes thinner. Grinding process is done from coarse to fine sandpaper with 180, 320, 600, 800, 1000, 1200, 2400 sandpaper. Water is used or sanding is done under running water to prevent the sample from heating up and to prevent the broken particles from scratching the sample surface and to remove them from this area. When switching to a fine abrasive, the specimen should be rotated 90° and the specimen moved from the outer surfaces of the disc towards the centre. If the sample is rotated 90°, it can be more easily understood that the traces of the previous sanding are removed. The sanding time is longer than the previous sanding time to remove scratches. While sanding, the surface should not be pressed too much. Otherwise, the scratches on the sample will increase and the sanding time will be longer. Struers Dap-7 grinding device was used.



Figure 4.4. Grinding and specimen after grinding.

4.1.1.4 Polishing

It can be done mechanically, automatically, electrolytically or chemically. Since only mechanical polishing will be done in this laboratory study, this method will be explained. For rough polishing, lint-free fabrics such as canvas are dressed on a rotating disc rotating at a speed of 150- 600 rpm for polishing. For fine polishing, hairy, broadcloth, velvet, etc. fabrics are dressed. Abrasives such as Al₂O₃, Cr₂O₃, MgO and diamond powder are poured on the cloth-covered discs and polishing is performed. The sample should be moved against the direction of rotation on the disc and rotated a quarter turn from time to time. To see whether the polishing is sufficient, it is examined visually and under an

optical microscope at 100X magnification. When viewed with the eye, it should have a mirror shine and no scratches should be seen when viewed with a microscope.

Struers LaboPol-21 polishing device was used for polishing as seen in figure 4.5. Polishing was done by abrading the surface of the sample with a cloth broadcloth and aluminium oxide (Al_2O_3).



Figure 4.5. Polishing device.

4.1.1.5 Etching

Etching is necessary for the phases and grain boundaries in the internal structure to be visible in the metal microscope. Etching can be chemical, electrolytic, or physical. Since chemical etching will be done in this laboratory study, chemical etching will be mentioned in the leaflet. In the chemical etching process, "etching reagent and etching reagent", which consists of a mixture of various chemical substances, and which are different for each material, are used.

For the etching process, 1 gram of Sodium Hydroxide and 100 grams of distilled water were put into the test cup. The sample was kept in solution for 8 seconds for etching.



Figure 4.6. After etching

4.1.2 Optical Microscope Results

Bakelite formed from the surfaces indicated was examined at different magnifications. NIKON EPIPHOT 300 microscope was used to examine the sample surfaces of the A356 aluminium alloy produced with LPDC. The regions where the samples to be examined under the microscope in bakelite were taken from the Charpy impact test sample are shown in Figure 7.

5x, 10x and 20x zoomed samples were taken with the aid of the microscope used. 5x, 10x and 20x zoomed versions of the transverse surface are shown in figure 4.8 5x, 10x and 20x zoomed versions of the longitudinal surface are shown in figure 4.9.

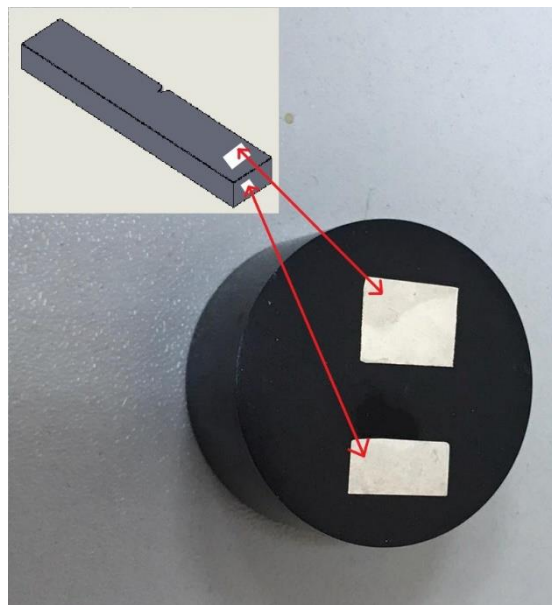


Figure 4.7. The regions of samples

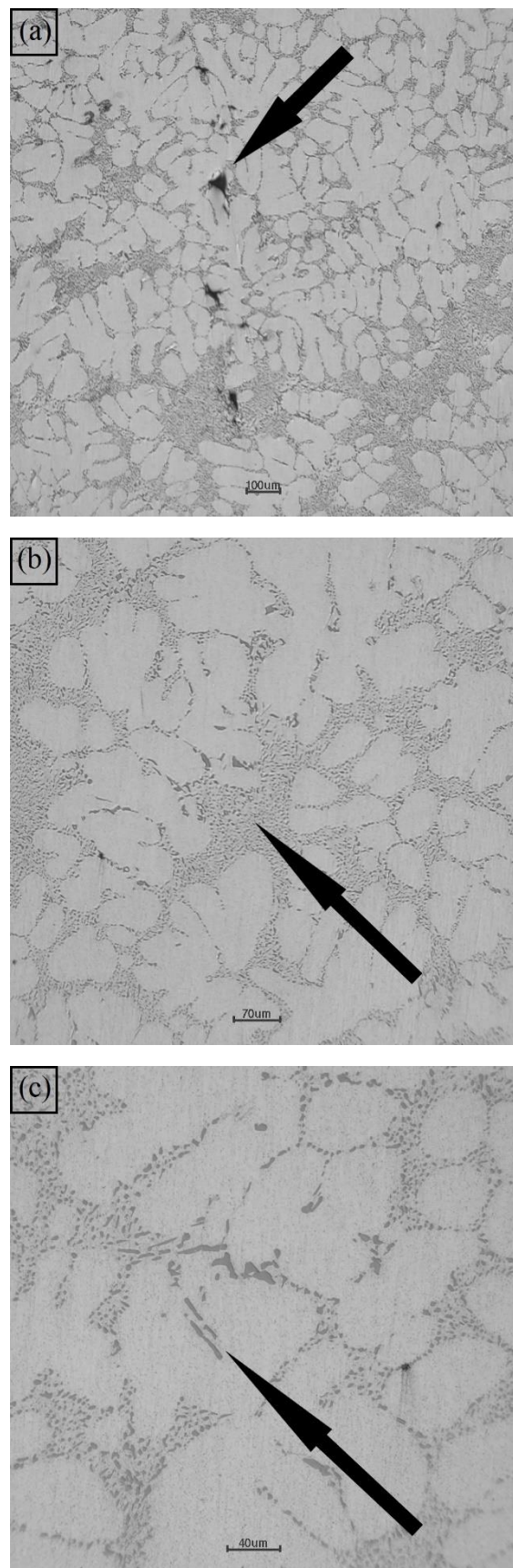


Figure 4.8. Optic results of the transverse surface by (a)5x (b)10x and (c)20x

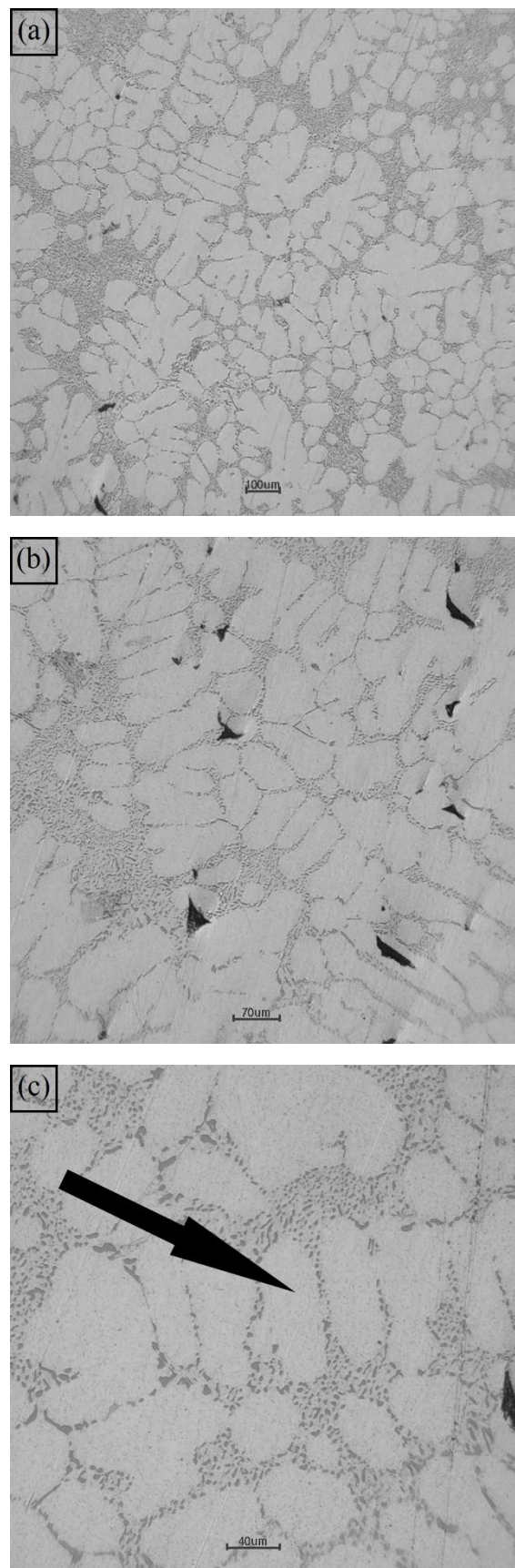


Figure 4.9. Optic results of longitudinal surface by(a)5x (b)10x and (c)20x

Structural defects were observed in figure 4.8 (a) and figure 4.9 (b). These defects may also be caused by the casting stage of the product, the cooling process, or the grinding process of the sample while preparing it for optical examination.

As shown in Figure 4.9 (c), α -Al is the most observed structure in the microstructure of the sample. Al-Si structure was observed in the sample as shown in figure 4.8 (b). It shows that the Si particles are uniformly distributed in the Al matrix. β -AlFeSi structure is observed in figure 4.8 (c).

4.2 Optical Examination of Fracture Surface

A fracture can generally be defined as the splitting of an object into two or more pieces under stress. Fracture is a result of plastic deformation. Two or more surfaces are formed because of the fracture. The stages of fracture are fracture formation and fracture propagation. There are five types of metal-based fracture in the natural process. They are ductile, brittle, adiabatic shear, creep, and fatigue shear. In this study, the variation of the fracture surface structure of the sample at different temperatures was investigated. Ductile and brittle properties were taken as the basis for the examination. The impact test sample will be prepared for the optical examination and the fracture surface will be examined.

4.2.1 Sampling

In order to examine the sample with an optical microscope, the size of the sample must be suitable between the microscope stage and the objective lens of the microscope. STRUERS DISCOTOM-5 model machine was used to cut the sample to make the sample size available. After this process, Struers Dap-7 model grinding device was used for grinding to keep the sample on the table properly and to be cleaned of burrs.

4.2.2 Optical Results

Fracture profiles have been analysed by optical microscopy in order to understand the behaviour of the sample at different temperatures. NIKON SMZ 1500 model optical microscope was used to examine the prepared sample. The fracture surfaces of the Charpy Impact test specimens, which were broken at +175, +20 and -75 degrees, were examined. 20x and 70x magnifications of the optical microscope were used.

Despite these observed differences, no transition from ductile to exactly brittle was observed for our material.

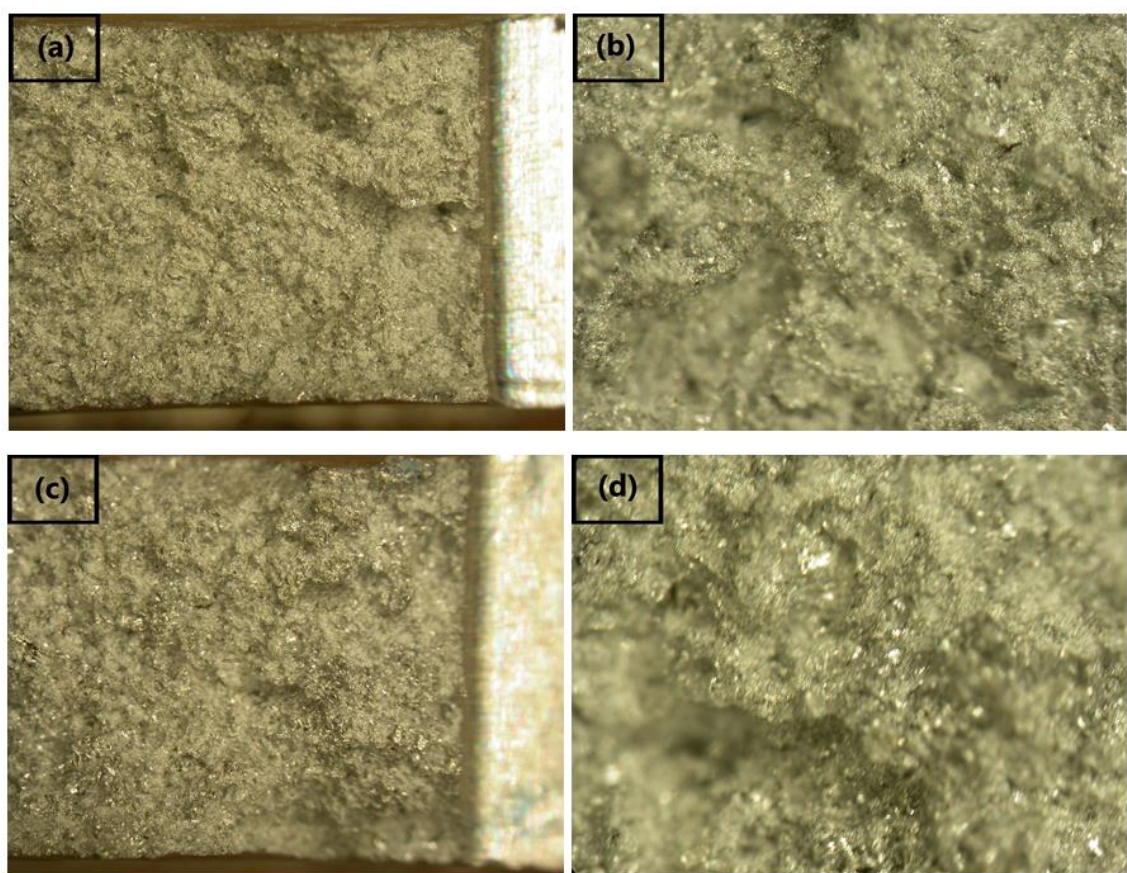


Figure 4.10. Fracture image of the sample at $+175\text{ }^{\circ}\text{C}$. (a) 20x and (b) 70x magnification images of the first sample. (c) 20x and (b) 70x magnification images of the second sample.

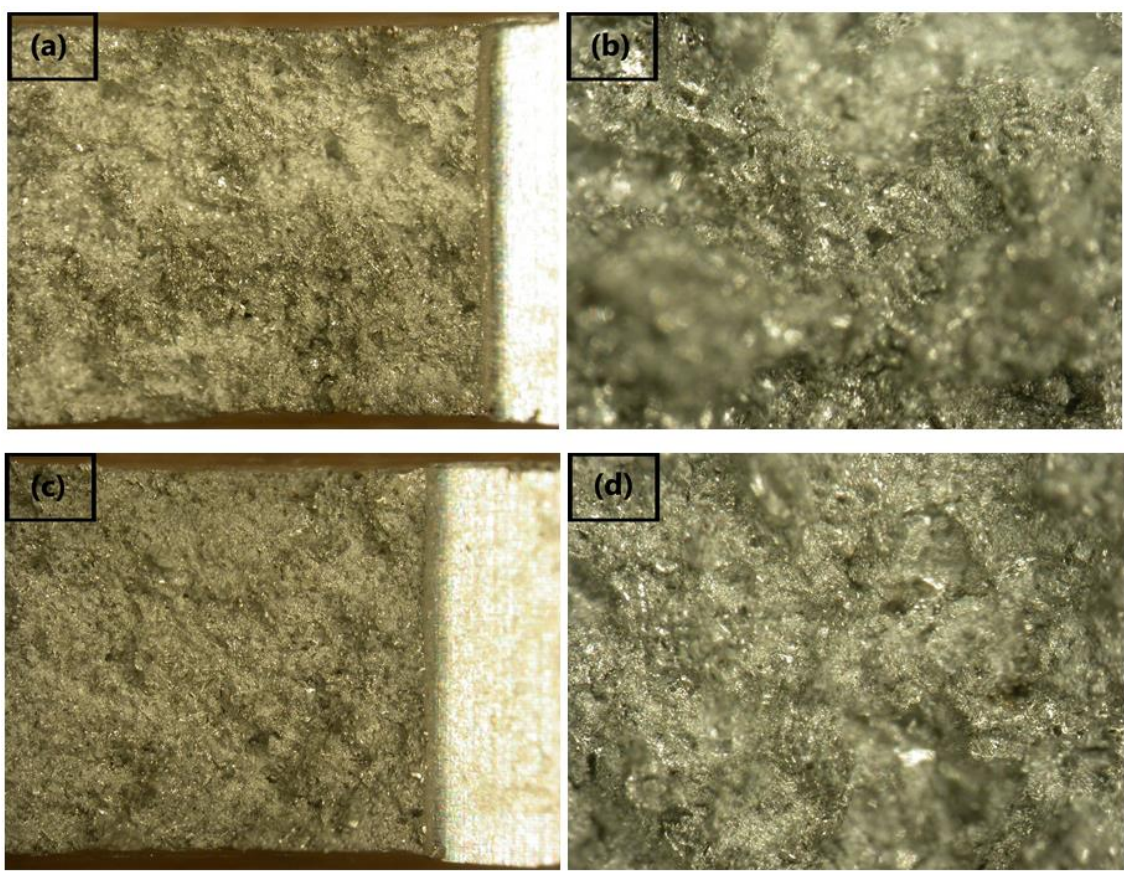


Figure 4.11. Fracture image of the sample at +20 °C.(a) 20x and (b) 70x magnification images of the first sample. (c) 20x and (b) 70x magnification images of the second sample.

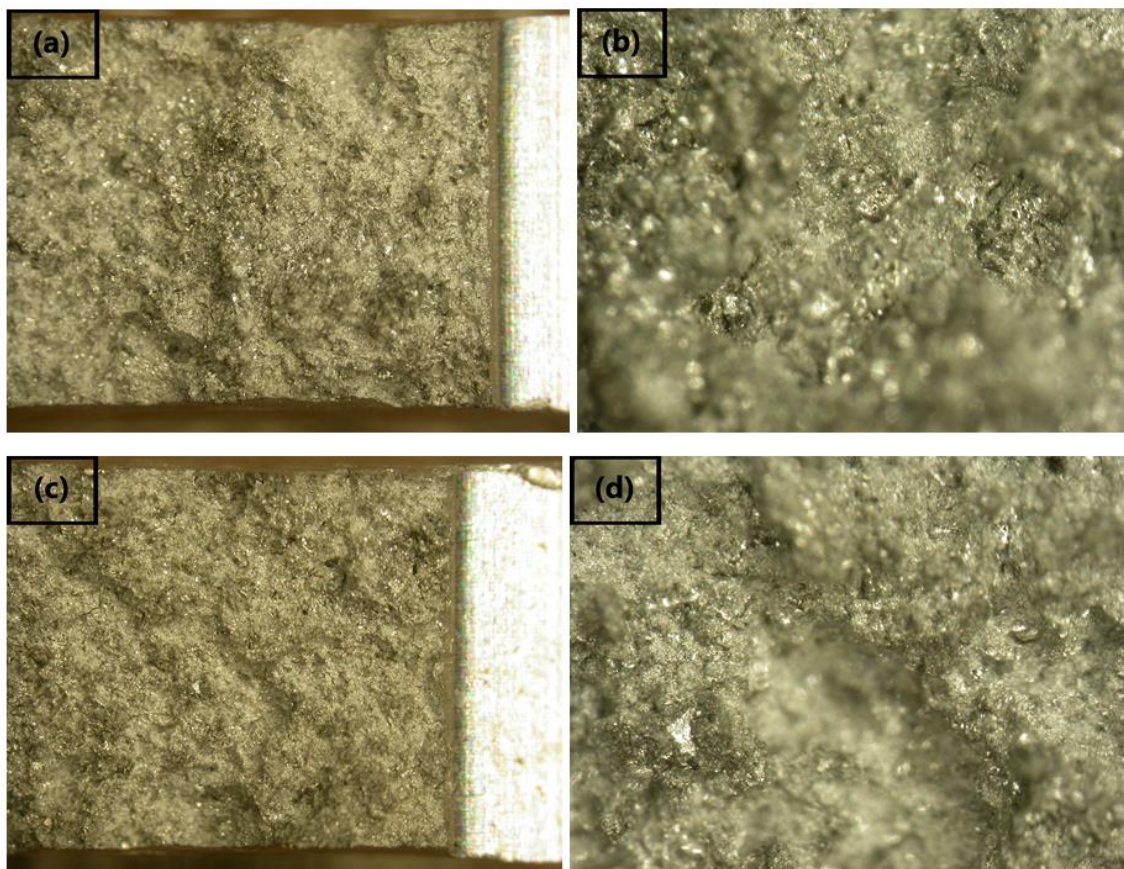


Figure 4.12. Fracture image of sample at -75 °C.(a) 20x and (b) 70x magnification images of the first sample. (c) 20x and (b) 70x magnification images of the second sample.

In the examined fractured surfaces, the highest dimple formation was observed in the samples that were fractured at +175 degrees (Figure 4.10). As the test temperature increased, it was determined that there was an increase in the recessed-protruding and fibrous structures on the fracture surfaces of the samples. (Figure 4.13 (c)). It was also observed that the plastic deformation on the fractured surfaces increased with temperature (Figure 4.13(a)).

Despite these observed differences, no transition from ductile to exactly brittle was observed for our material.

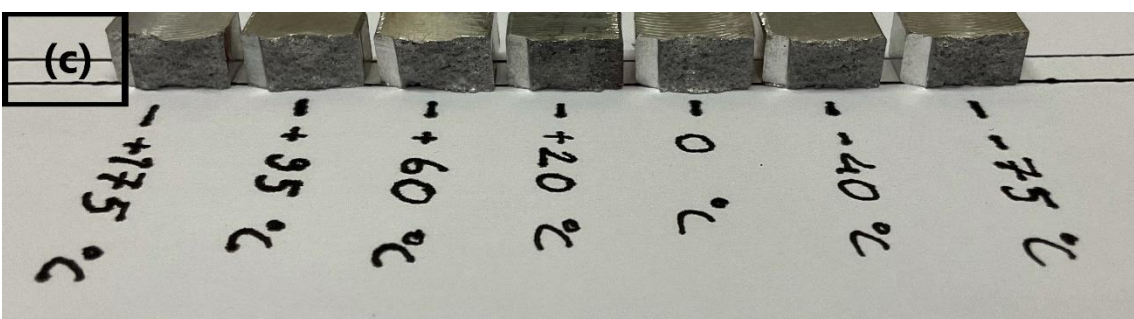
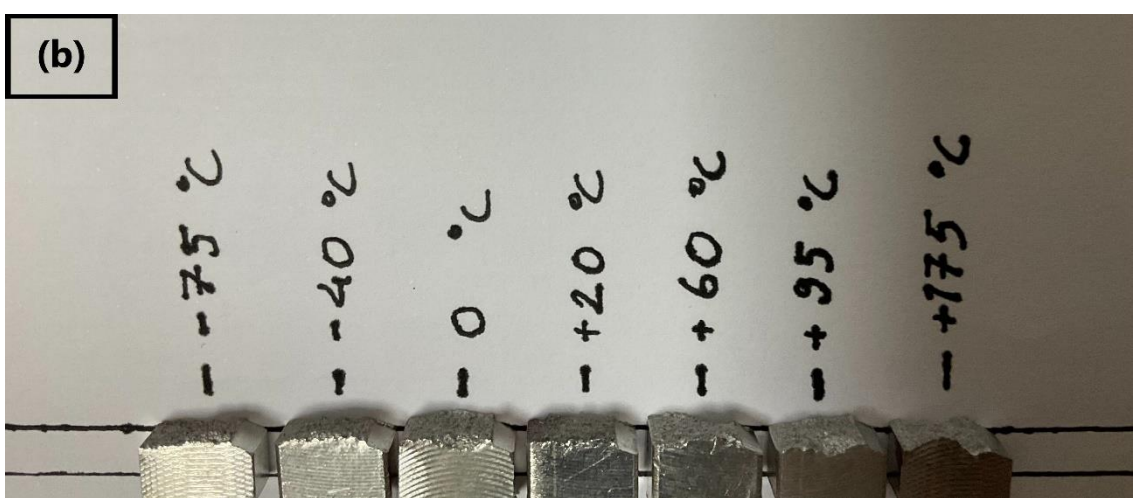
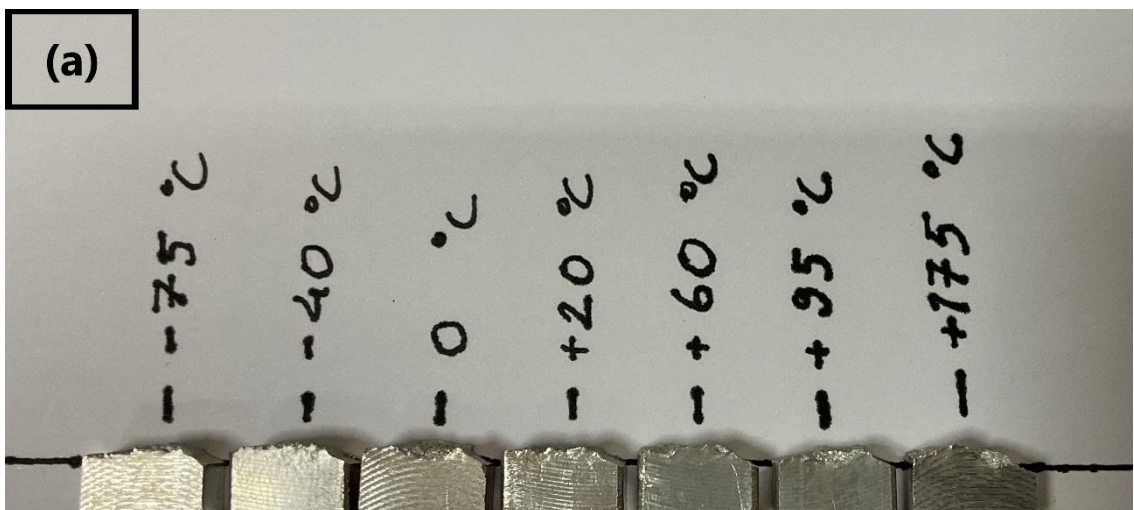


Figure 4.13. Fractured surface images of Charpy impact test specimen fractured at different temperatures.

4.3 SEM and EDS Examination of Fracture Surface

The main purpose of Scanning Electron Microscopy is to take surface images at high magnifications. However, various chemical analyses can also be performed.

Basically, the device consists of three parts (electron gun, magnetic lenses and detectors). Accelerated electrons from the electron gun are focused on the sample by means of magnetic lenses. Electrons scattered because of electron-sample interaction are analysed by various detectors.

By detecting these scattered electrons, imaging analysis of the structures in the material can be performed at the micro and nano level. In addition, qualitative and quantitative elemental analysis can be performed within the sample, and the distribution of elements can be monitored with the mapping technique.

Chemical analysis can be done with the EDS detector in the SEM device. Therefore, it can be learned quickly how many percent of which element is present in the material.

In this study, fracture surface samples used in the optical examination were used. Since the sample material is metallic, copper plating was used only to increase the surface contact in the samples (figure 4.14). Quorum SC7620 Sputter Coater model device was used for coating (Figure 4.15). ZEISS model device was used for SEM examination (Figure 4.16).

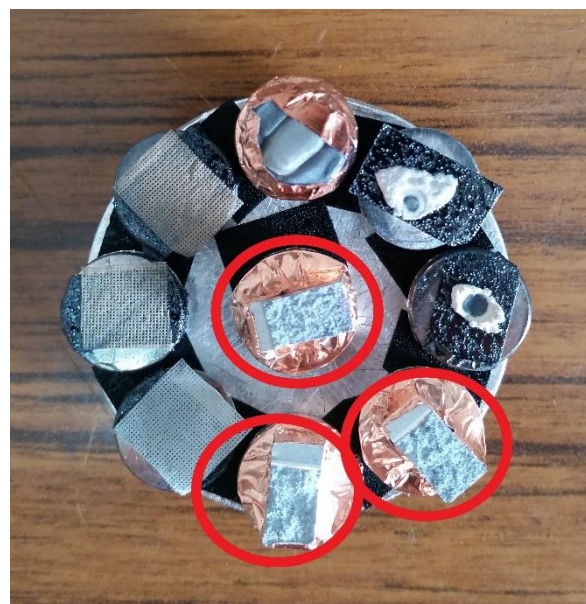


Figure 4.14. Samples inside the red circle for SEM+EDS



Figure 4.15. Sputter coater



Figure 4.16. ZEISS model SEM device

4.3.1 SEM and EDS Results

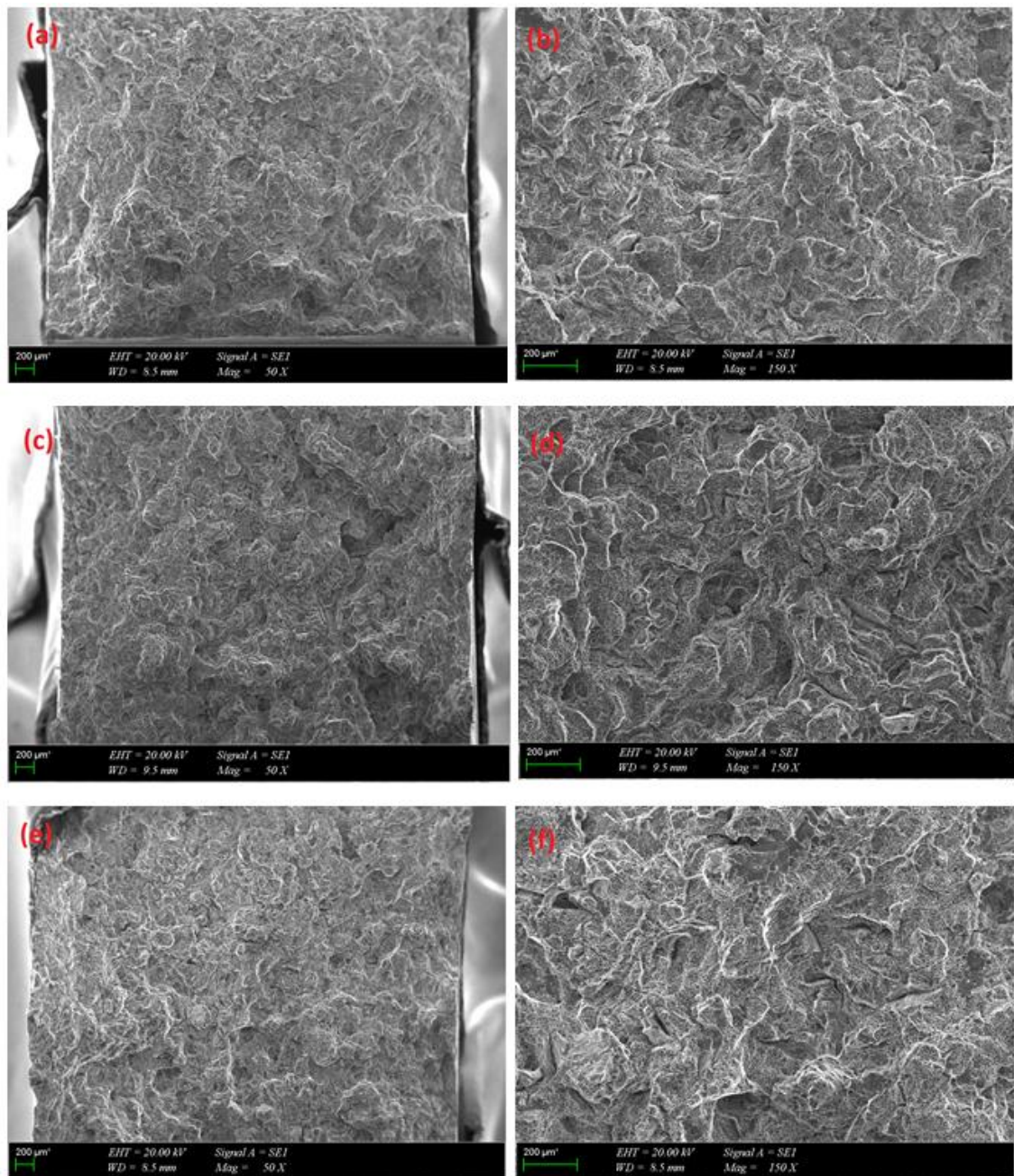


Figure 4.17. SEM micrographs of fracture surface after impact tests; (a) -75°C, 50X magnification, (b) -75°C, 150X magnification, (c) 20°C, 50X magnification, (d) 20°C, 150X magnification, (e) 175°C, 50X magnification, (f) 175°C, 150X magnification

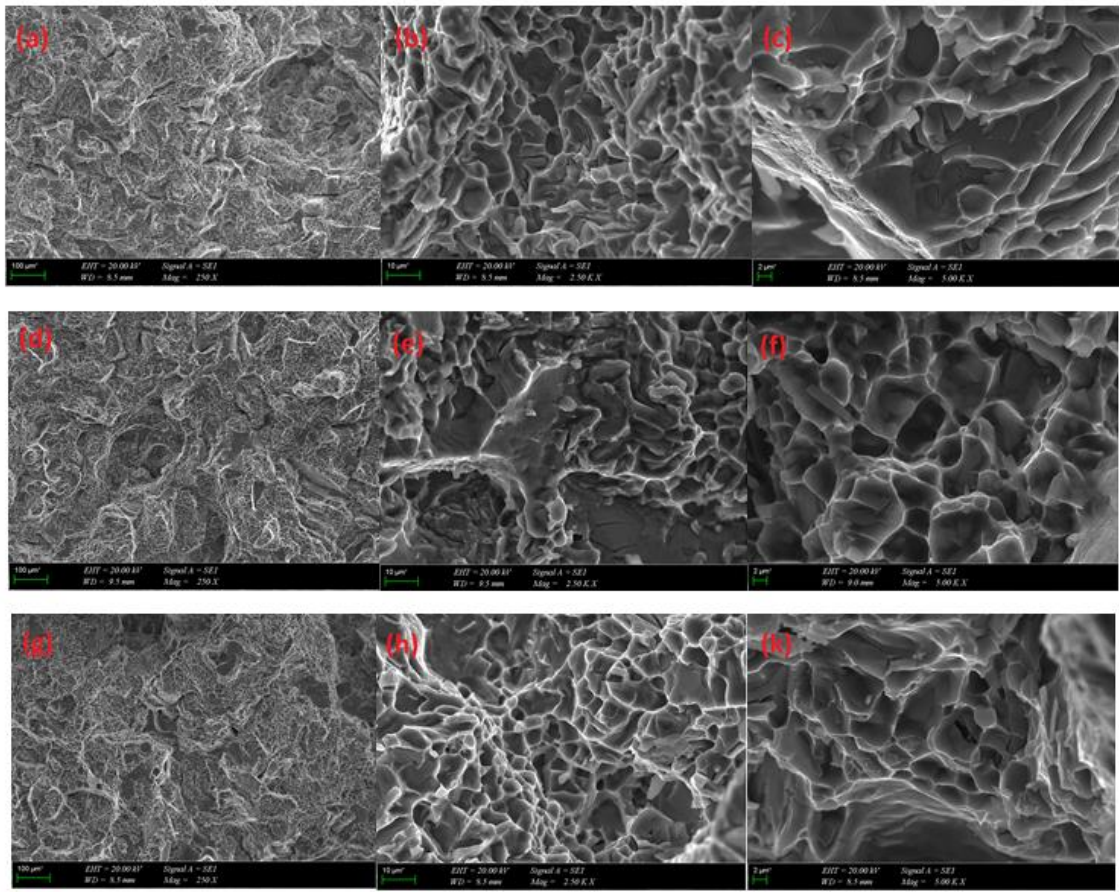


Figure 4.18. SEM micrographs of fracture surface after impact tests; (a) -75°C, 250X magnification, (b) -75°C, 2.5KX magnification, (c) -75°C, 5KX magnification, (d) 20°C, 250X magnification, (e) 20°C, 2.5KX magnification, (f) 20°C, 5KX magnification, (g) 175°C, 250X magnification, (h) 175°C, 2.5KX magnification, (k) 175°C, 5KX magnification

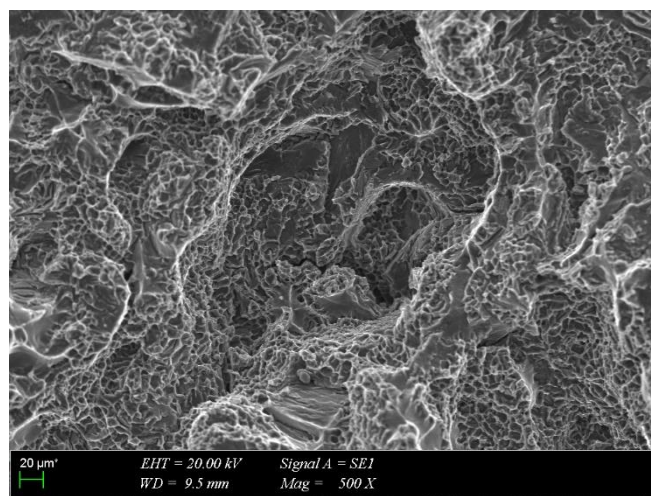


Figure 4.19. Detail of Fig.18. (d). (20°C). Morphology of the fracture surface around the deep secondary crack in the biphasic region. Well-protected conformation zones can be seen at the interfaces between α -aluminium and silicon.

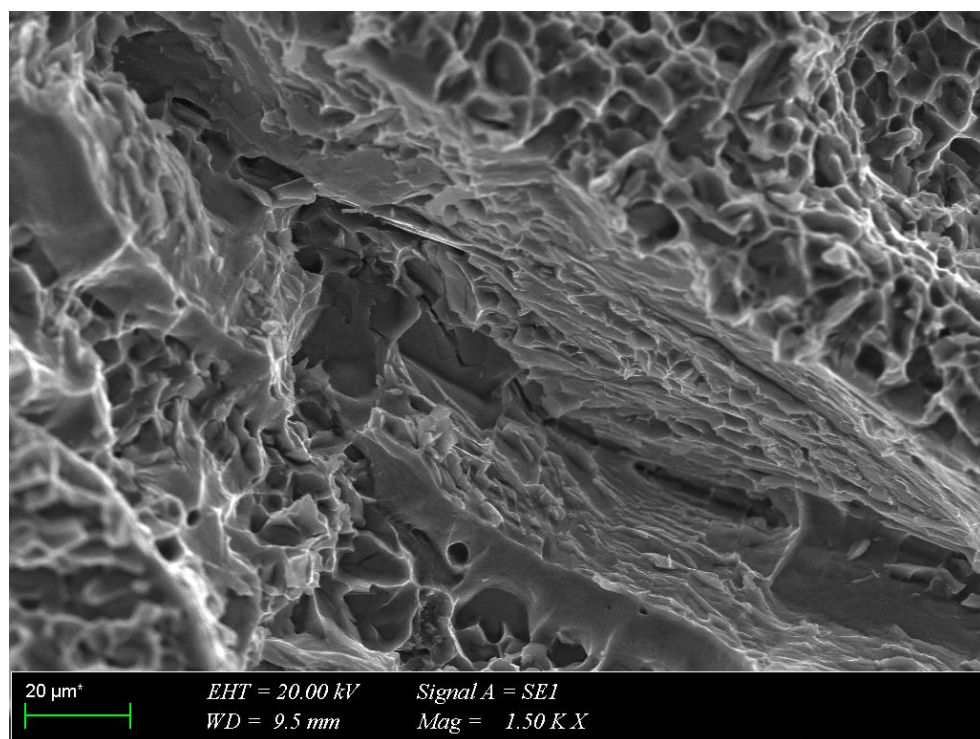


Figure 4.20. Detail of in Fig. 18(d). (20°C). Fracture of mixed morphology. Oval shear dimples are situated near the cleavage facet.

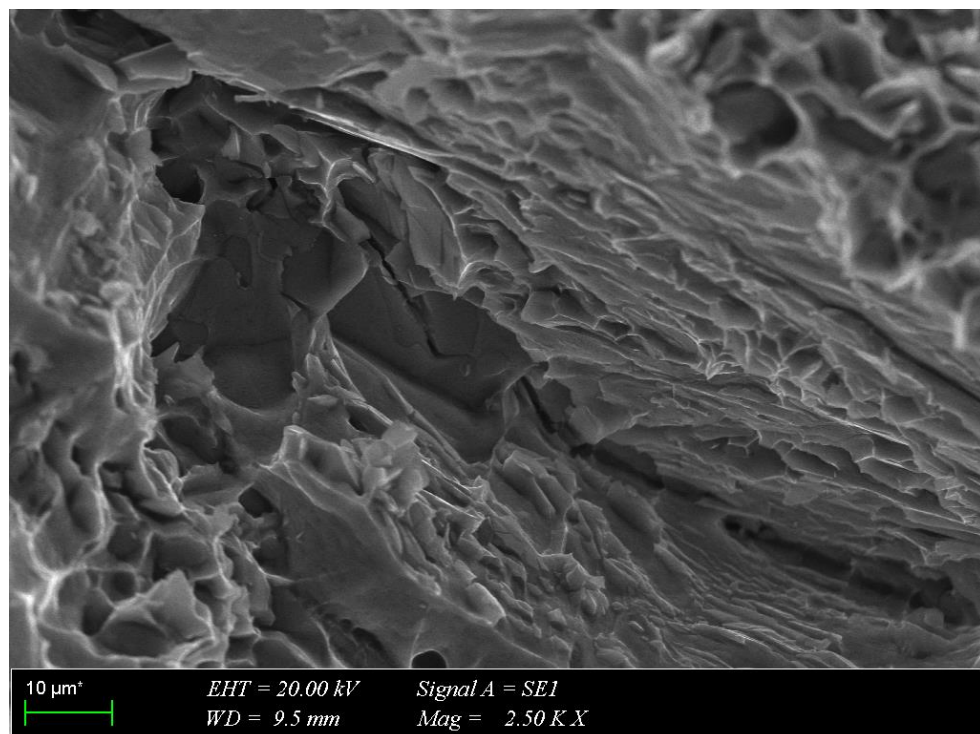


Figure 4.21. Detail of Fig. 20. (20°C). The secondary brittle crack took place on the interface between α -Aluminium and silicon.

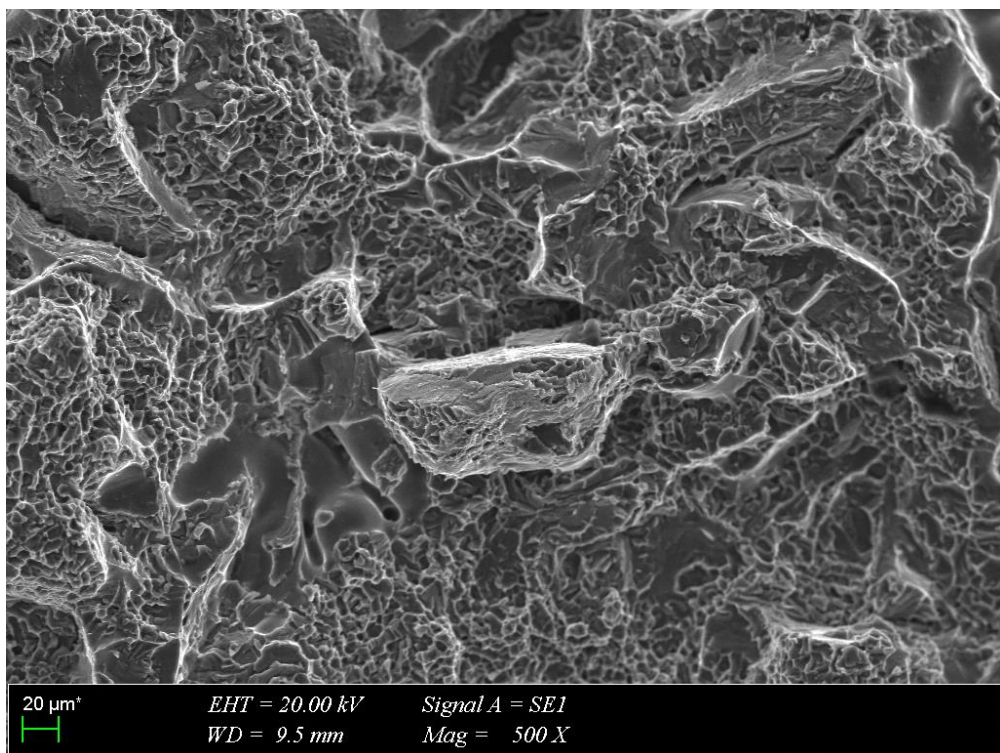


Figure 4.22. Detail of Fig. 17(d). (20°C). 500X

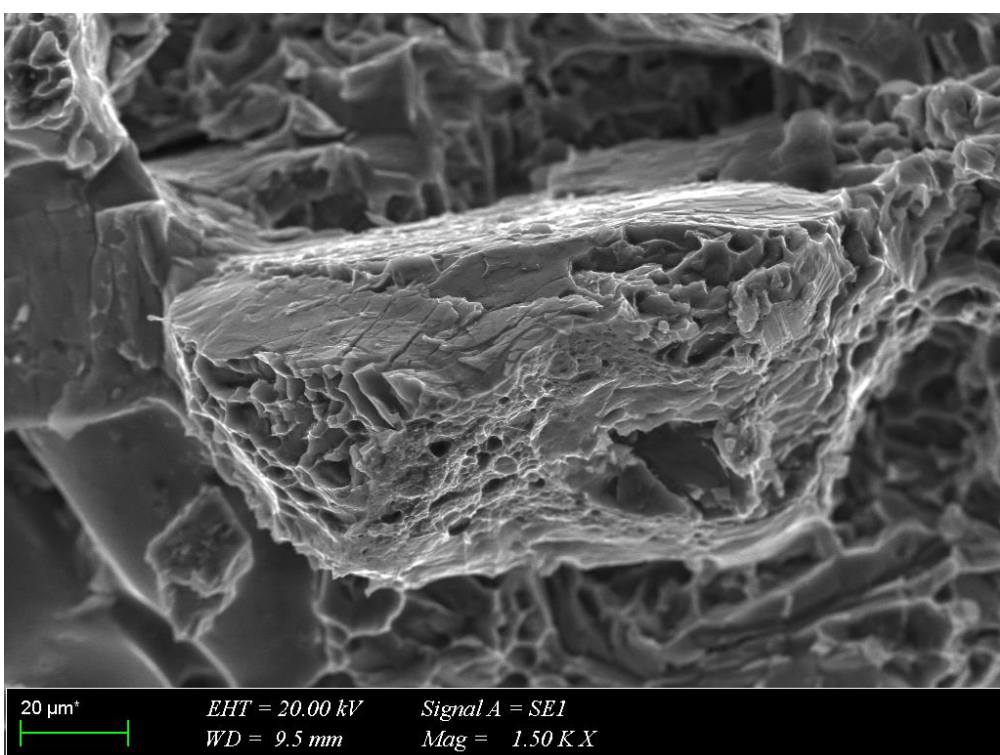


Figure 4.23. Detail of Fig. 22. (20°C). 1500X

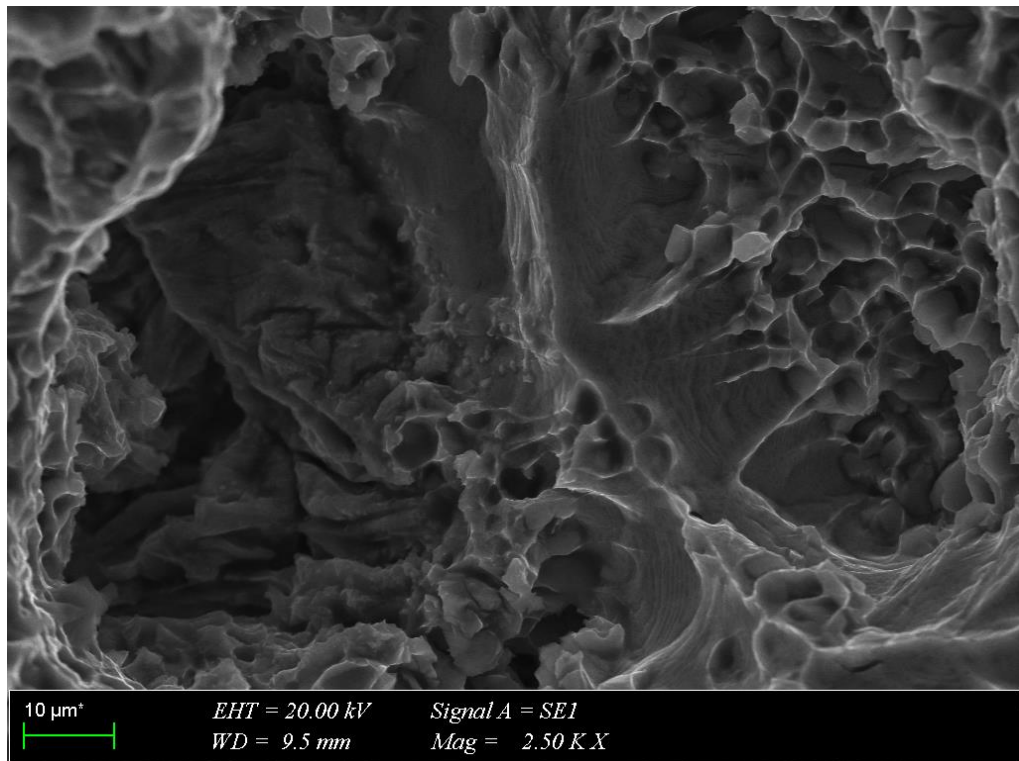


Figure 4.24. Morphology of the fracture surface in the deformed α -Aluminium solid solution. The shelves of the oval dimples are shown. (20°C). 2500X

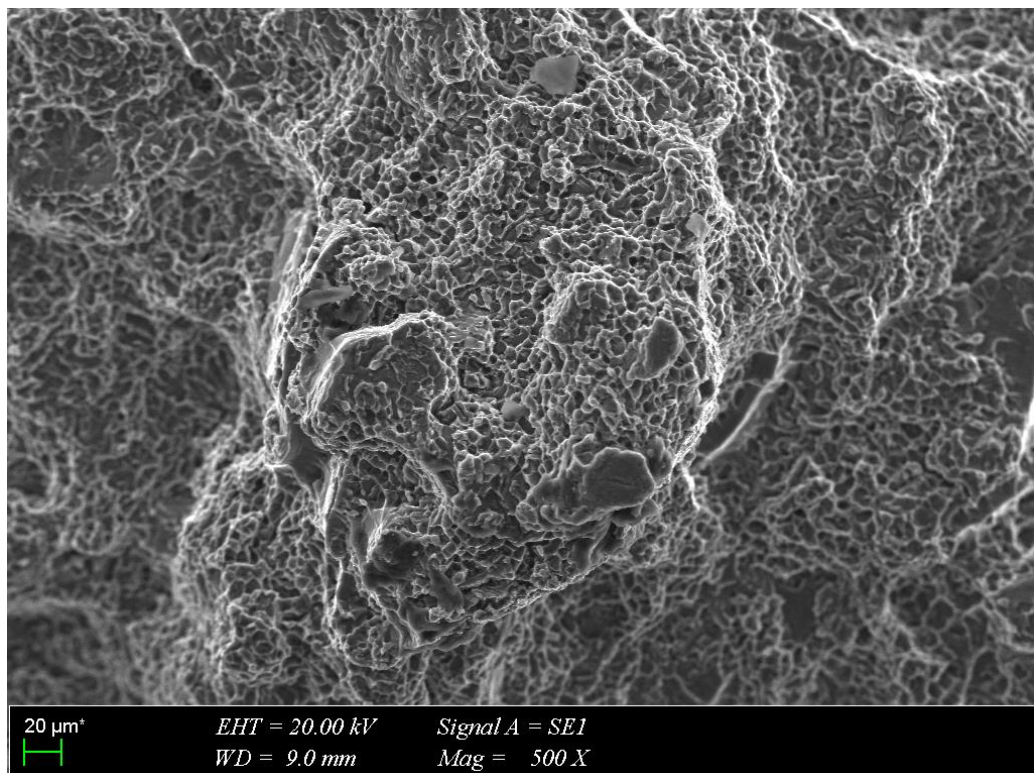


Figure 4.25. (20°C). 500X

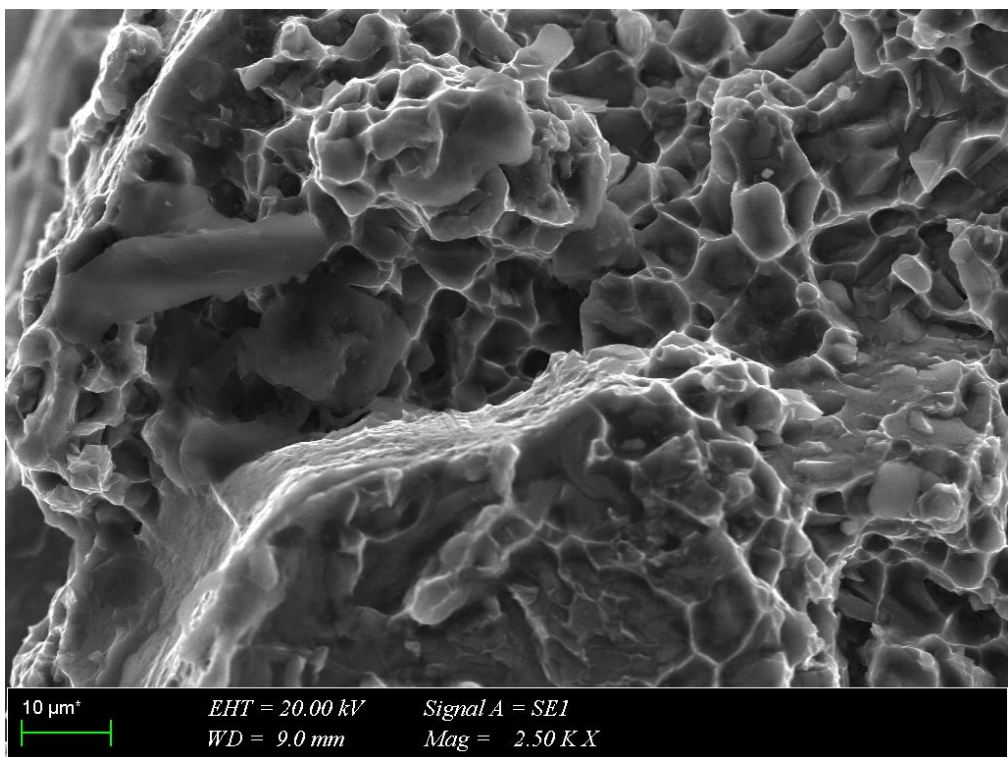


Figure 4.26. (20°C). 2500X

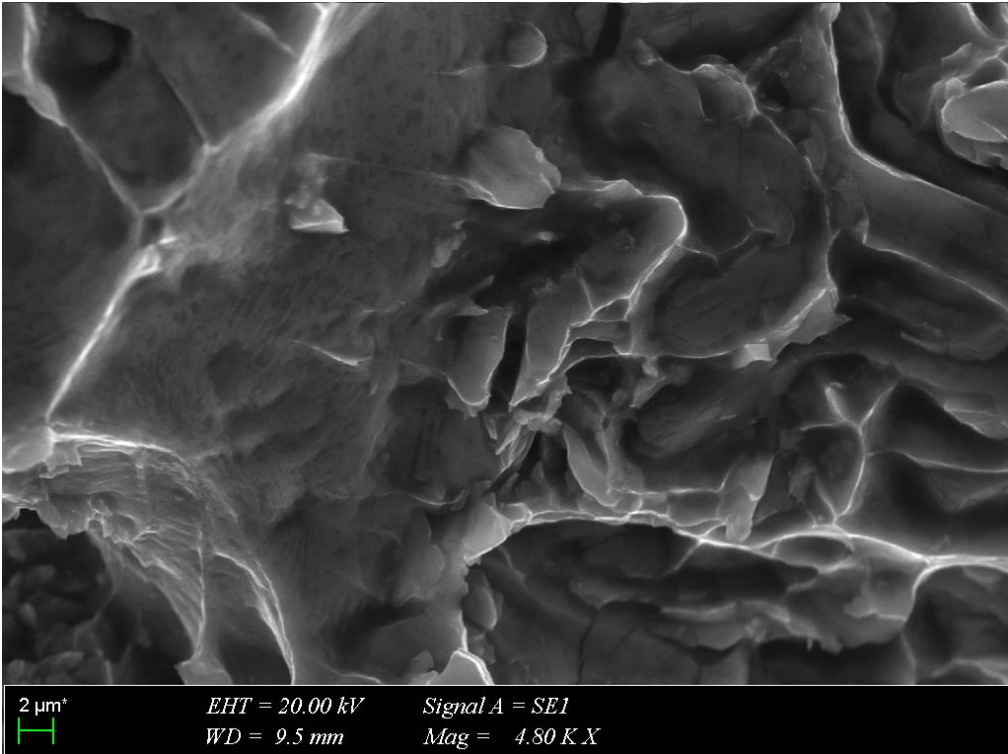


Figure 4.27. Detail in Fig. (20°C). 18(e)

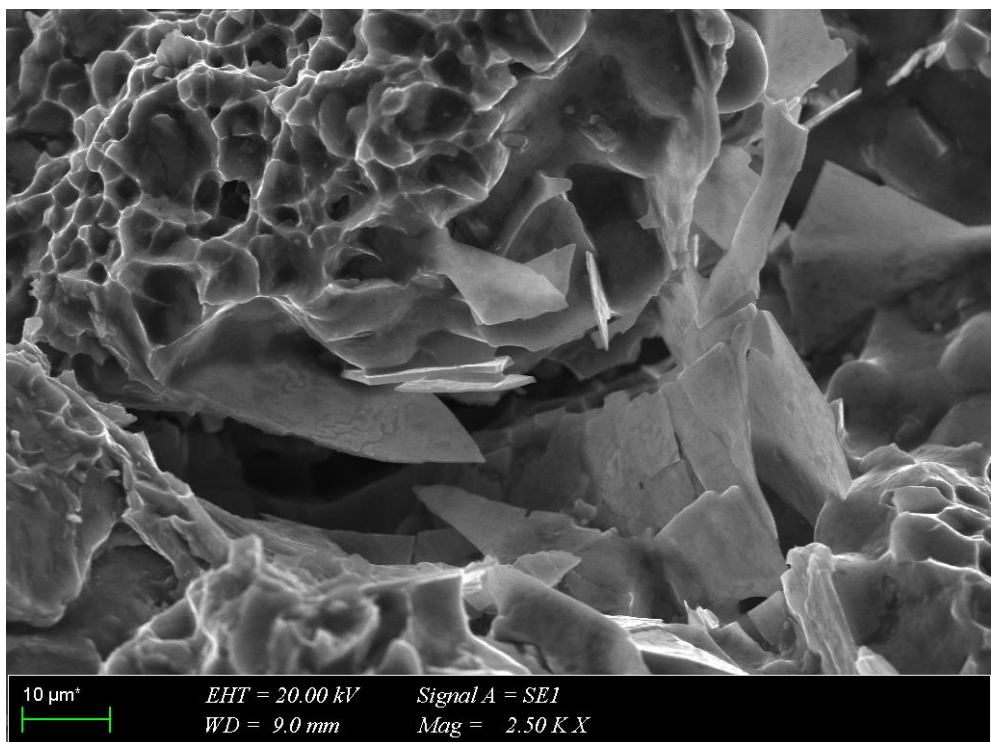


Figure 4.28. (20°C), 2500X

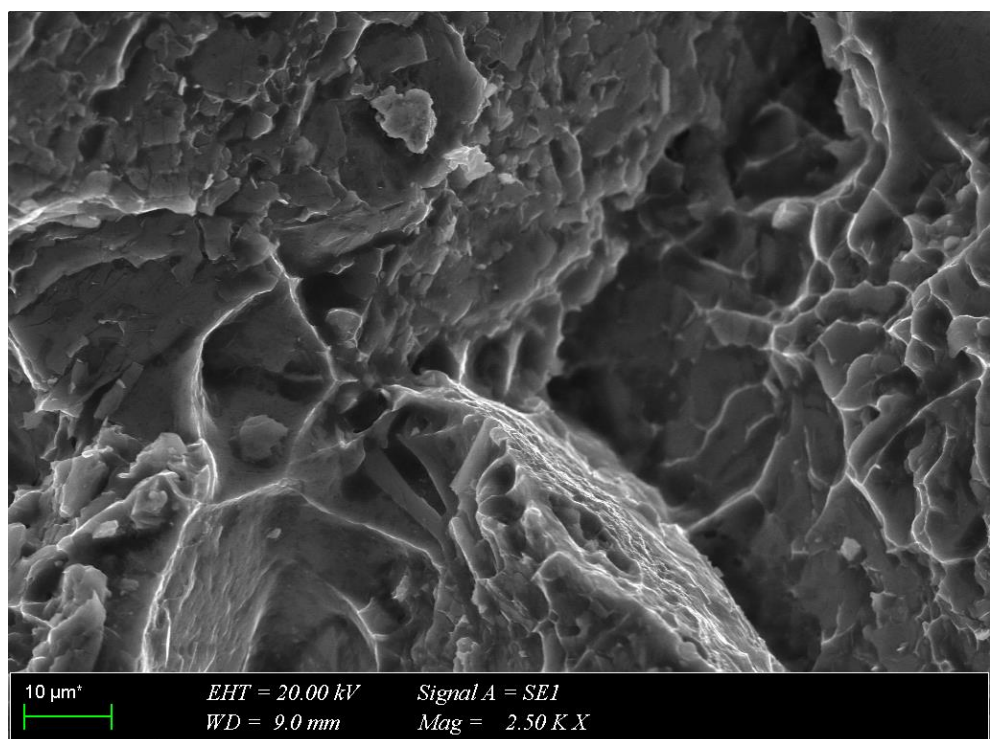


Figure 4.29. (20°C), 2500X

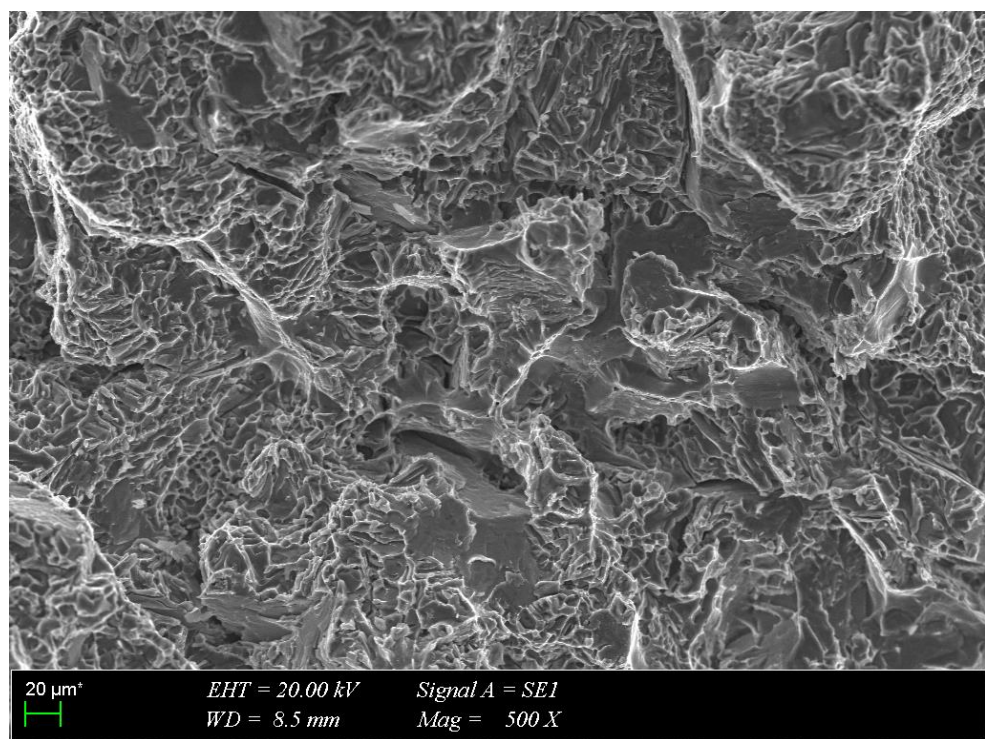


Figure 4.30. Transcrysalline fracture with the greatly developed surface. The main crack crossed the silicon precipitate in the cleavage planes of different orientations in relation to the average fracture plane. The rectilinear secondary cracks, the branched cleavage steps, and the tear ridges have formed in the α - Aluminium solid solution. (-75°C), 500X

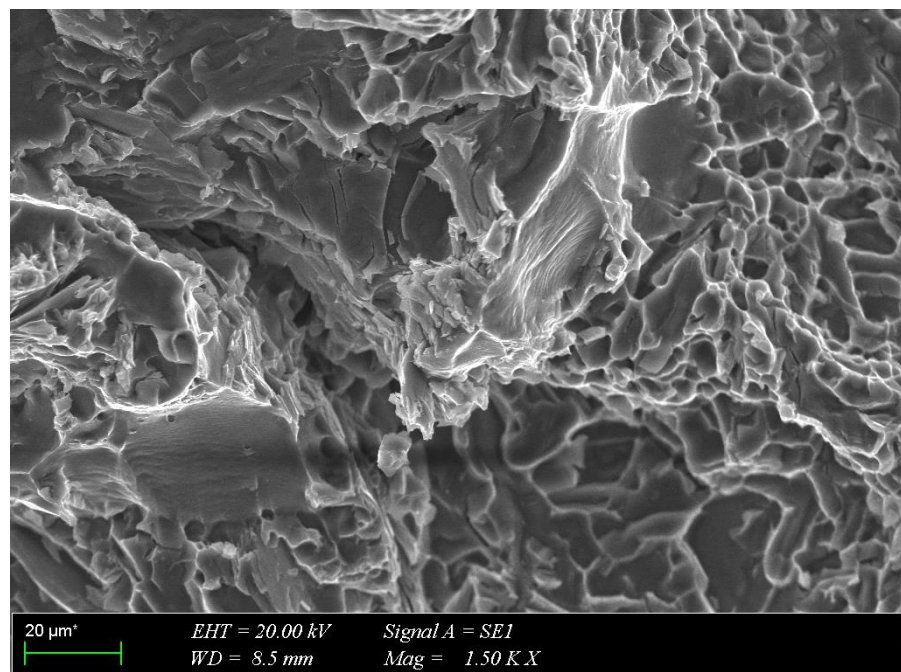


Figure 4.31. Surface of the silicon plate cracked several times. The crack front crossed the numerous cleavage planes of different orientations. (-75°C), 1500X.

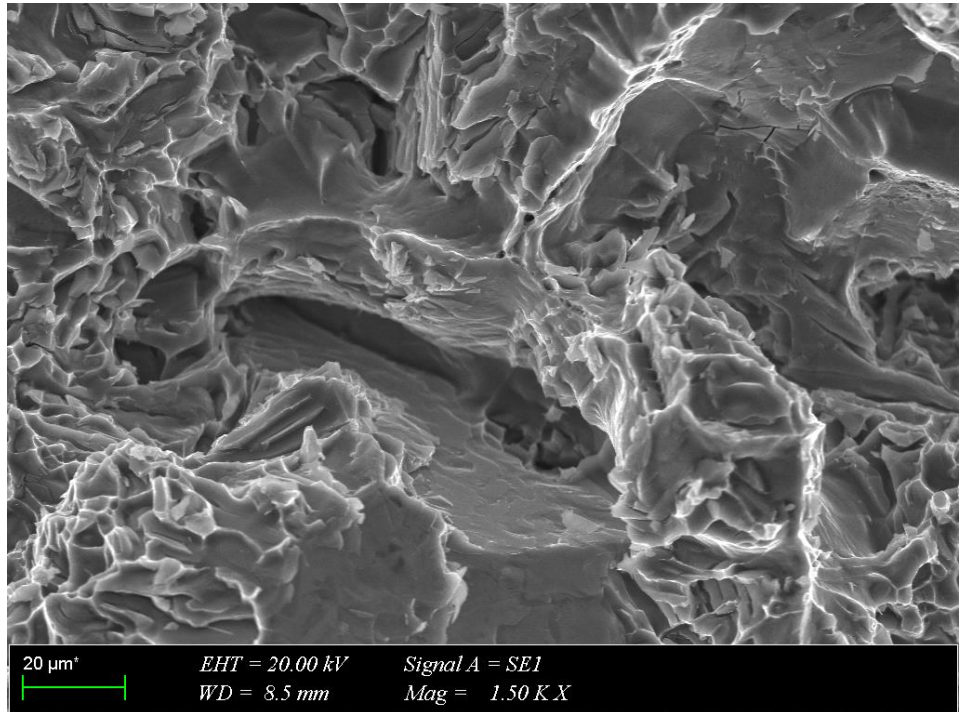


Figure 4.32. Detail of Fig.30, numerous secondary cracks are visible. (-75°C). 1500X

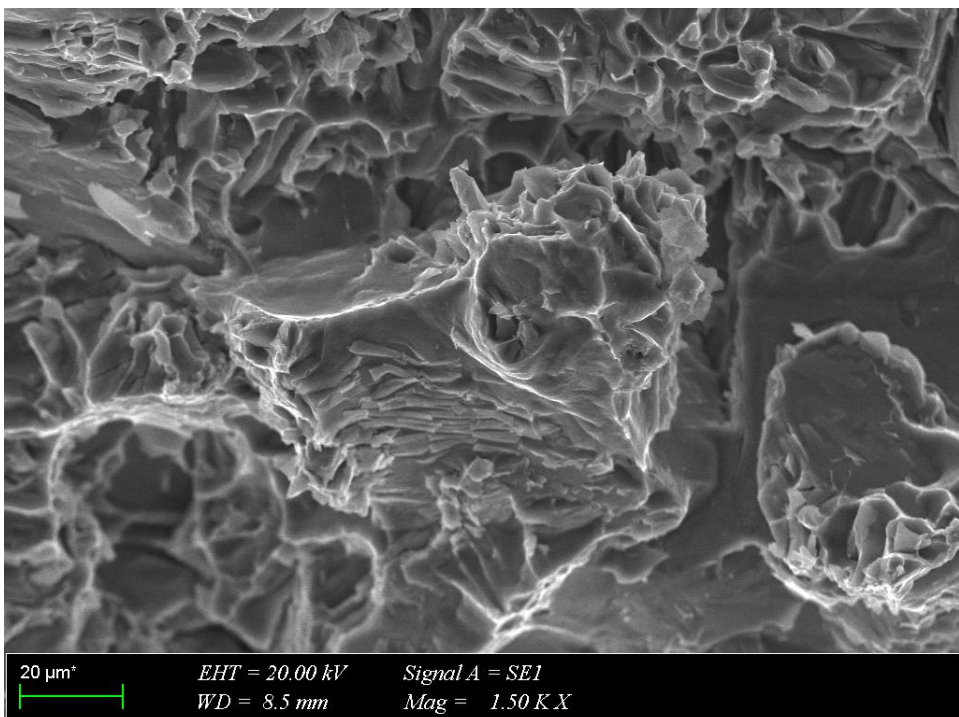


Figure 4.33. Cleavage steps formed in the branched particles. The cleavage step system is a result of the crack front propagation on the successive cleavage planes. (-75°C), 1500X

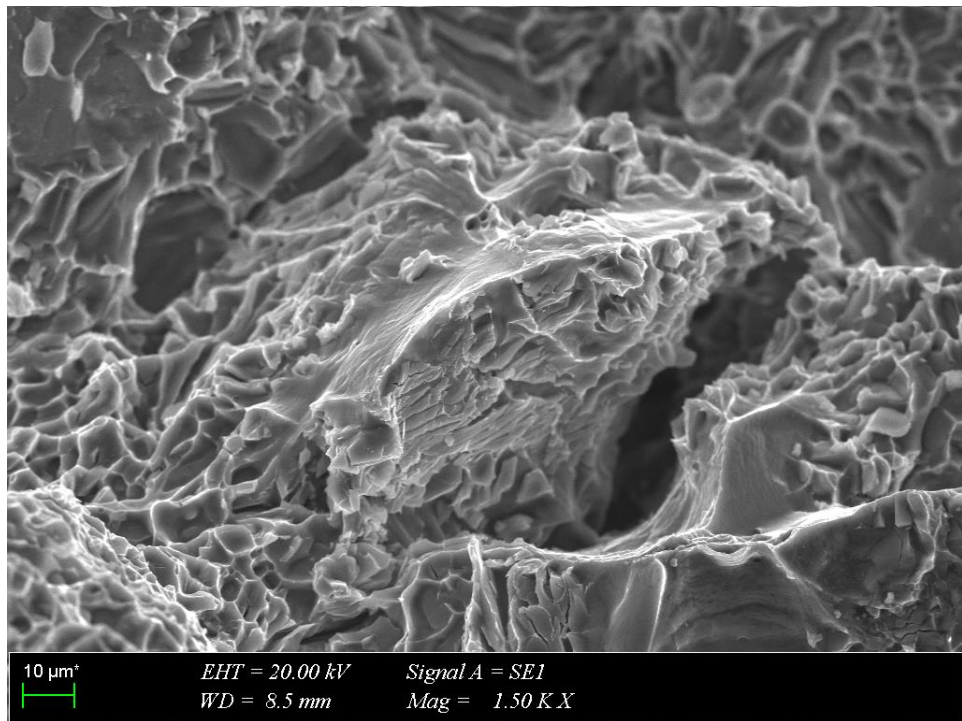


Figure 4.34. (-75°C), 1500X

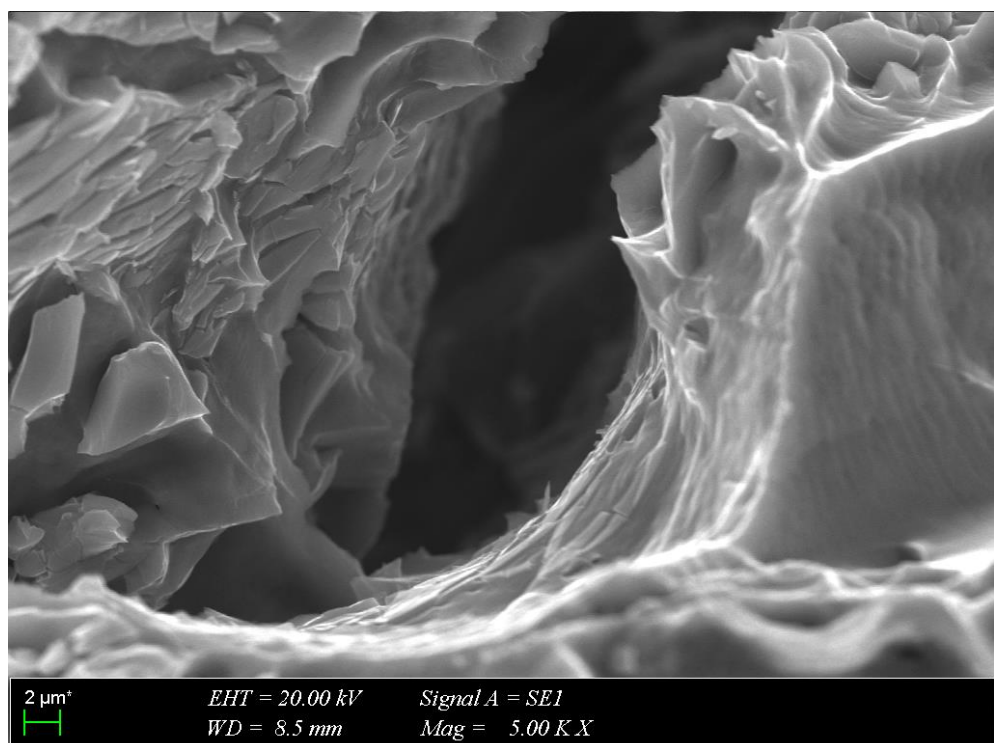


Figure 4.35. Detail of Fig.34 (-75°C), 5000X

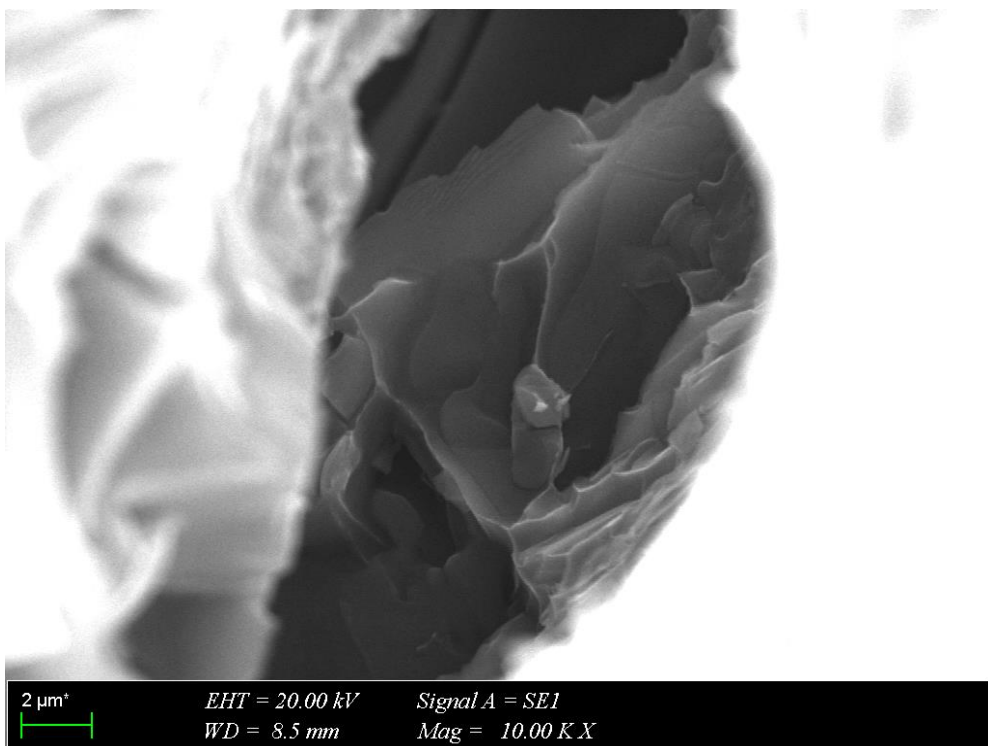


Figure 4.36. Detail of Fig.35 (-75°C), 10000X

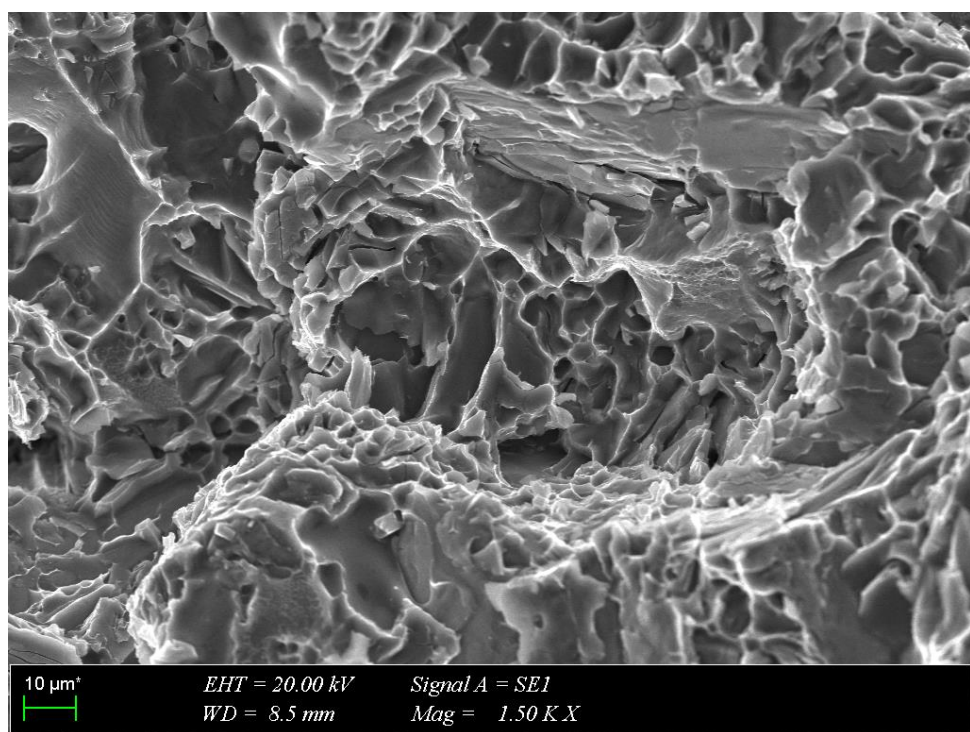


Figure 4.37. Transcrysanthine fracture of medium-developed surface. The areas of fracture of both cleavage and cellular features are visible (175°C), 1500X

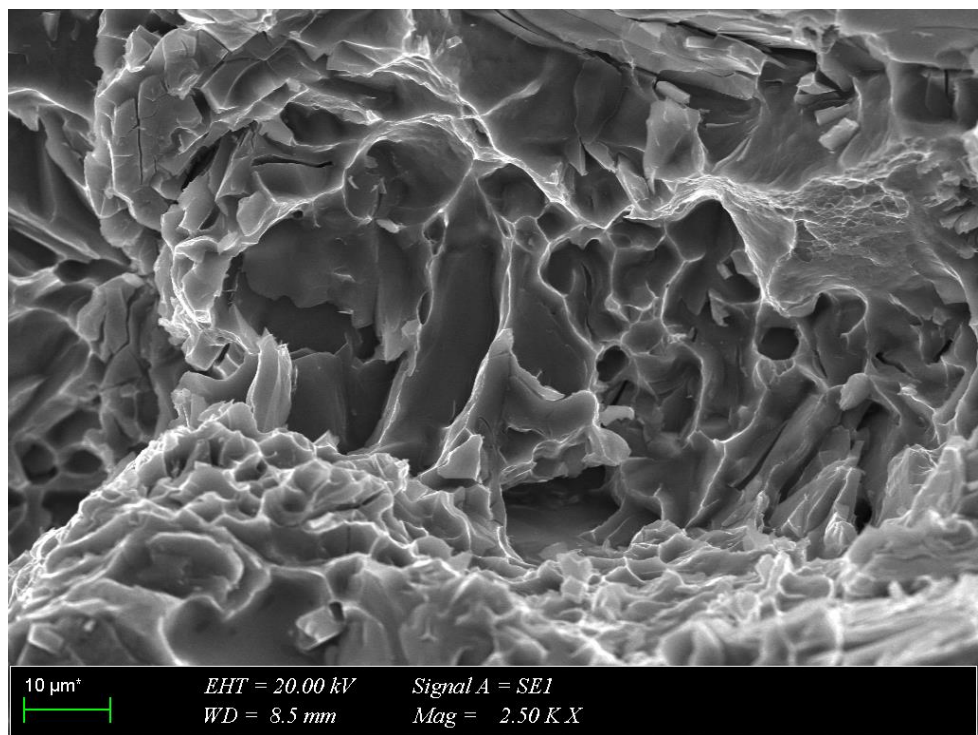


Figure 4.38. (175°C), 2500X

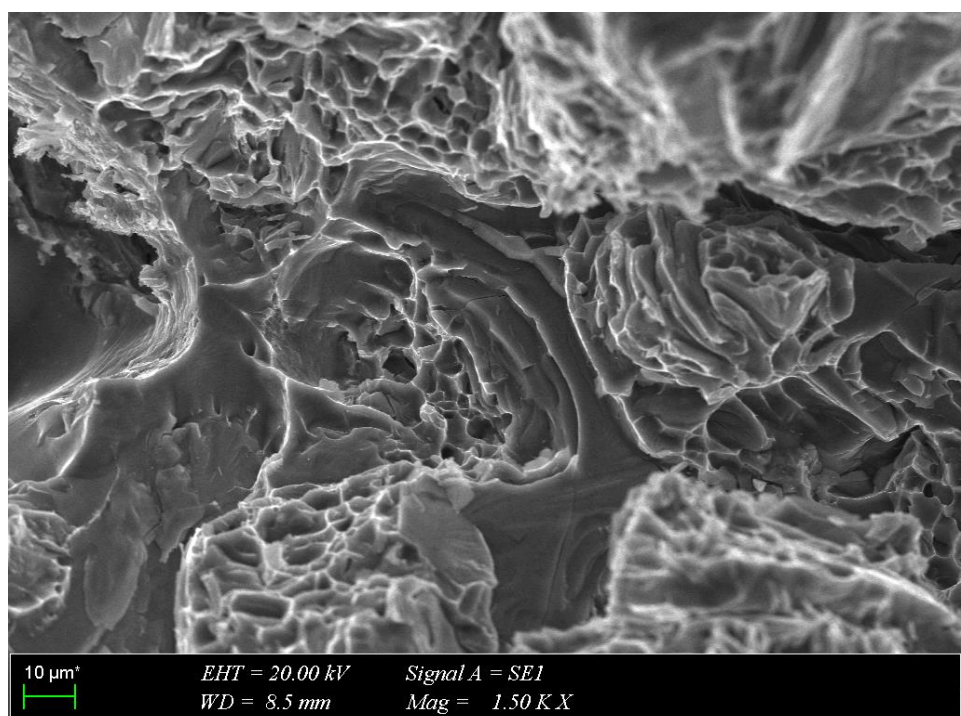


Figure 4.39. (175°C), 1500X

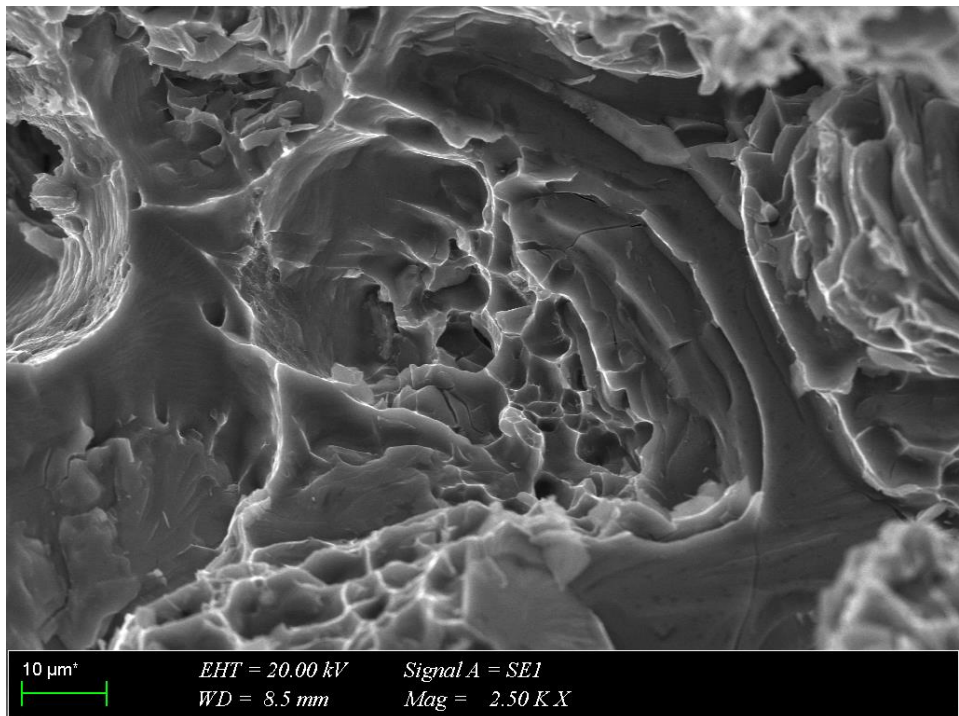


Figure 4.40. (175°C), 2500X

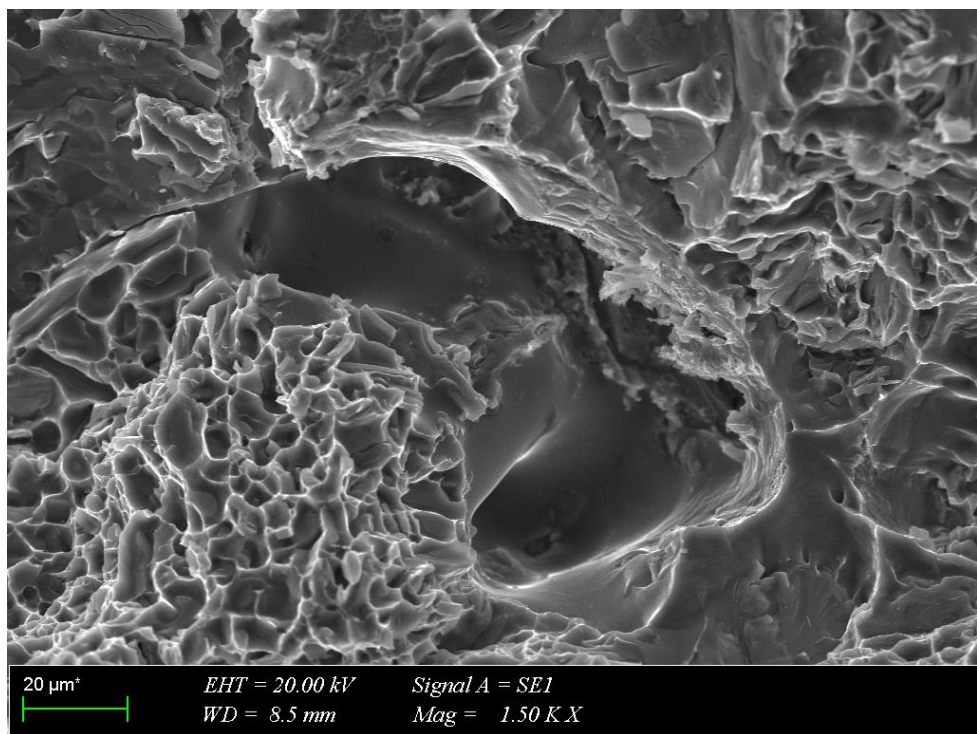


Figure 4.41. (175°C), 1500X

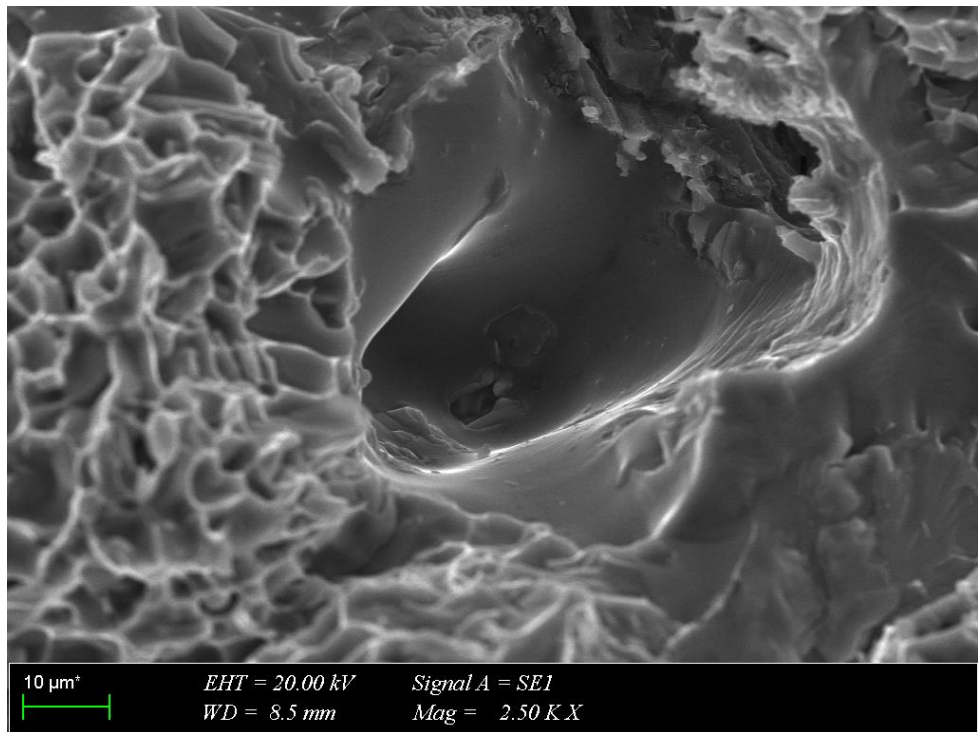


Figure 4.42. Fracture in two-phase region. The cell is formed from a deformed matrix band around the cracked silicon particles. The zone of the interface cohesion is present on the interface between α -Aluminium and silicon. In the silicon particle, numerous cleavage cracks are visible. In the microregion of the solid solution the oval and open shear dimples are revealed. Detail of Fig.41, (175°C), 2500X

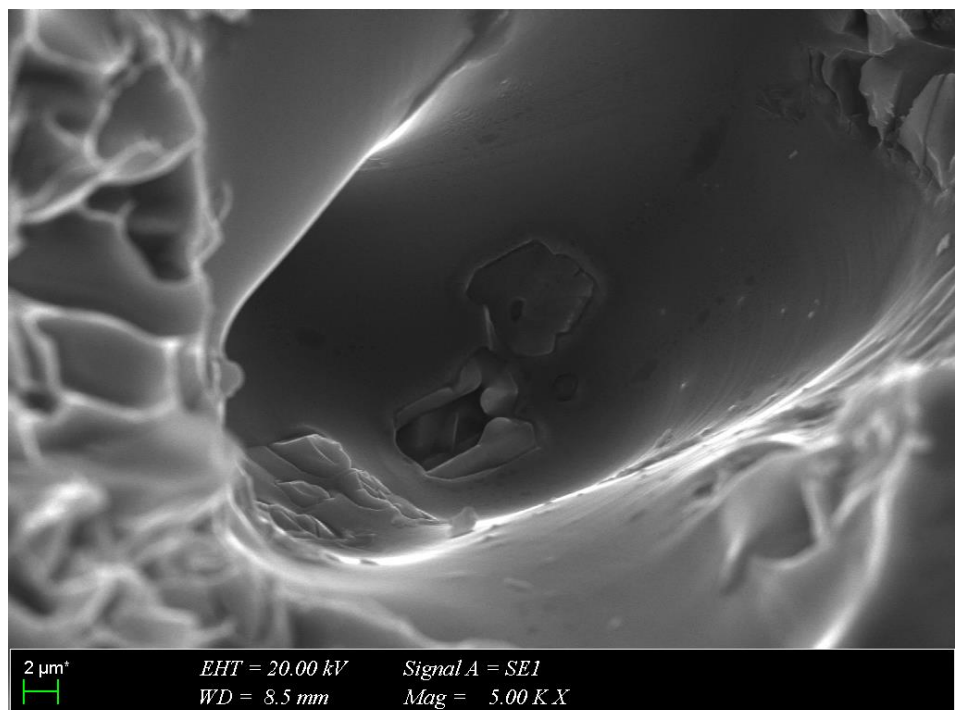
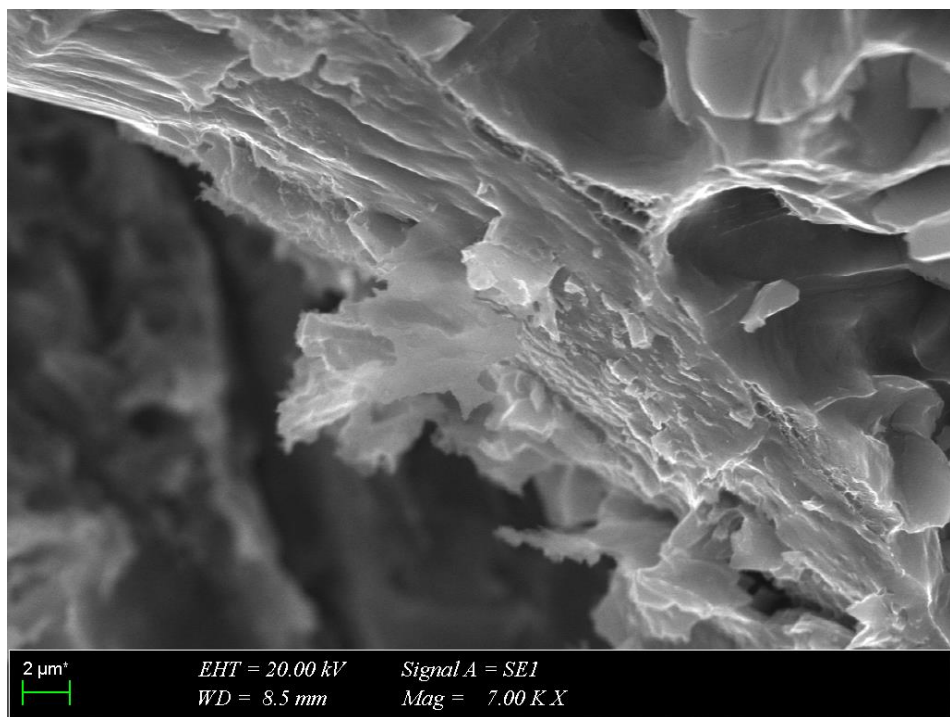


Figure 4.43. Detail of Fig.42, (175°C), 5000X

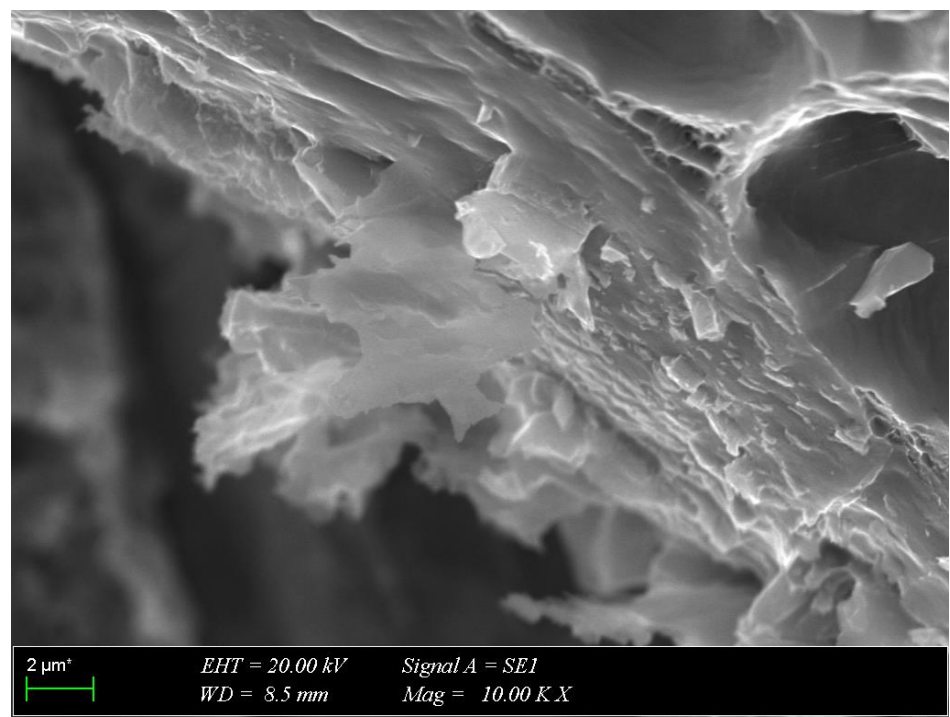


2 μm^*

EHT = 20.00 kV
WD = 8.5 mm

Signal A = SEI
Mag = 7.00 KX

Figure 4.44. (175°C), 7000X



2 μm^*

EHT = 20.00 kV
WD = 8.5 mm

Signal A = SEI
Mag = 10.00 KX

Figure 4.45. (175°C), 10000X

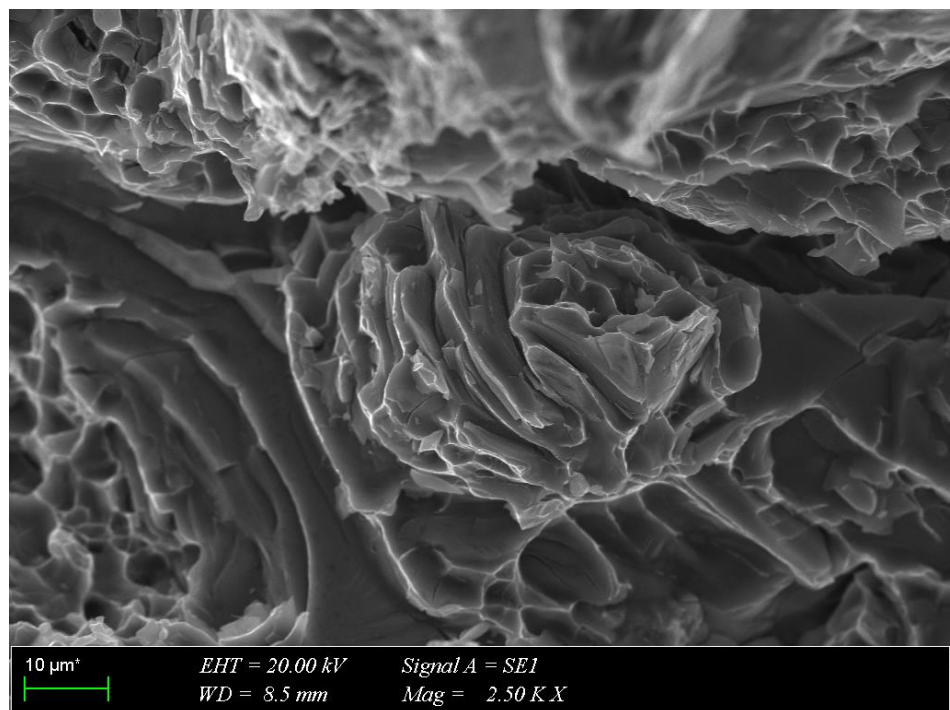


Figure 4.46. (175°C), 2500X

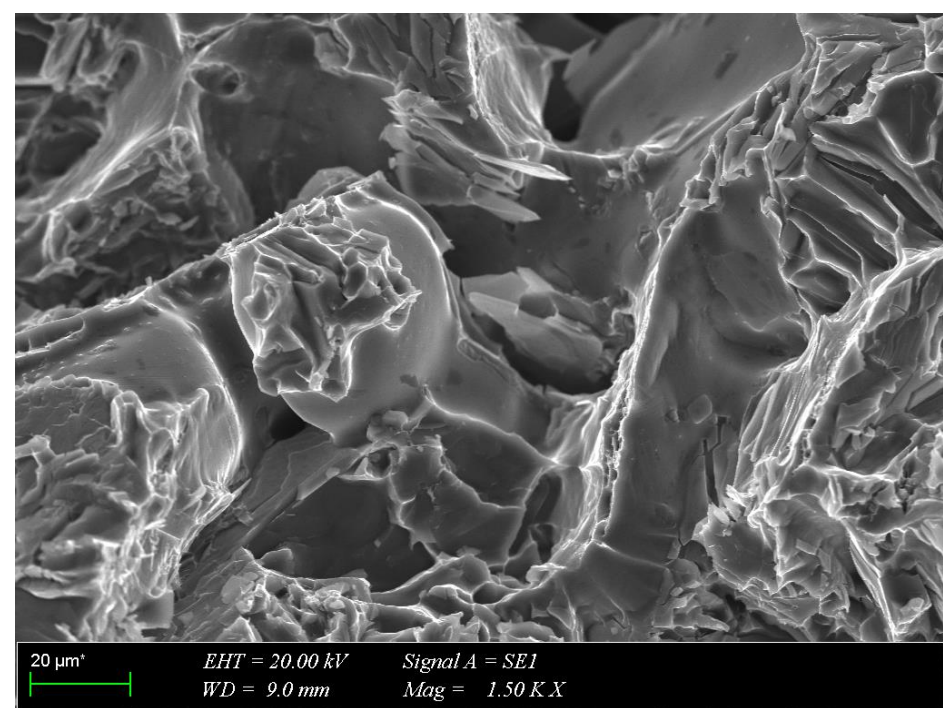


Figure 4.47. (175°C), 1500X

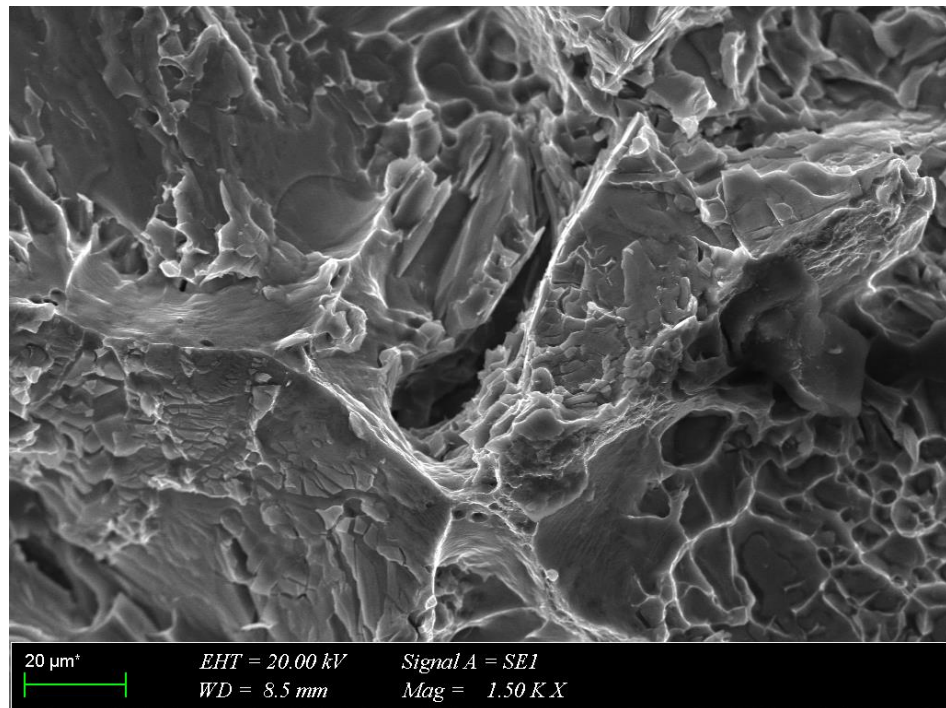


Figure 4.48. (175°C), 1500X

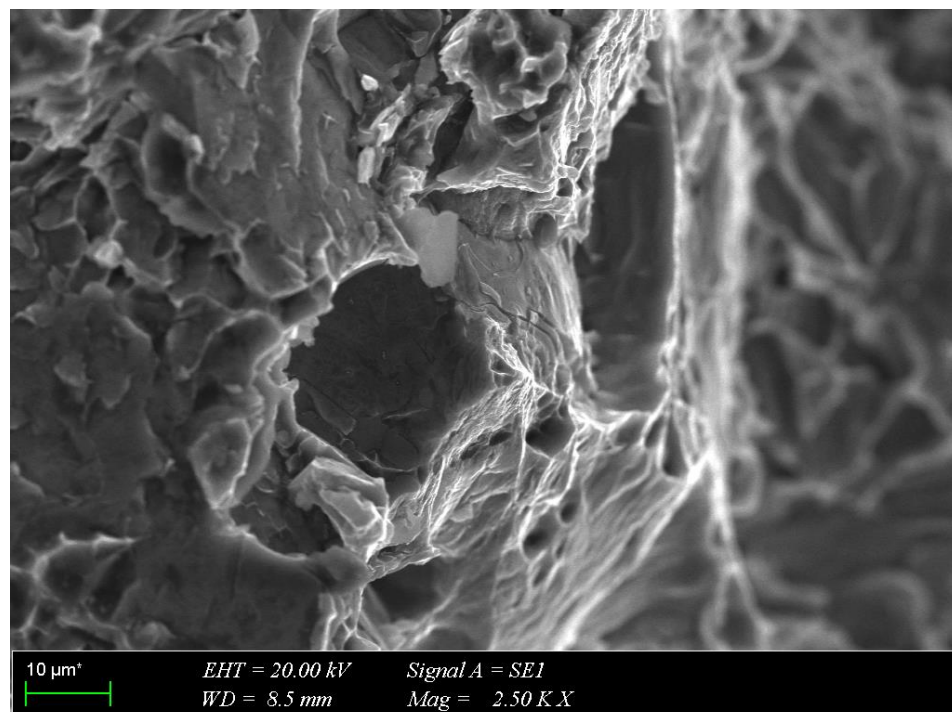


Figure 4.49. (175°C), 2500X

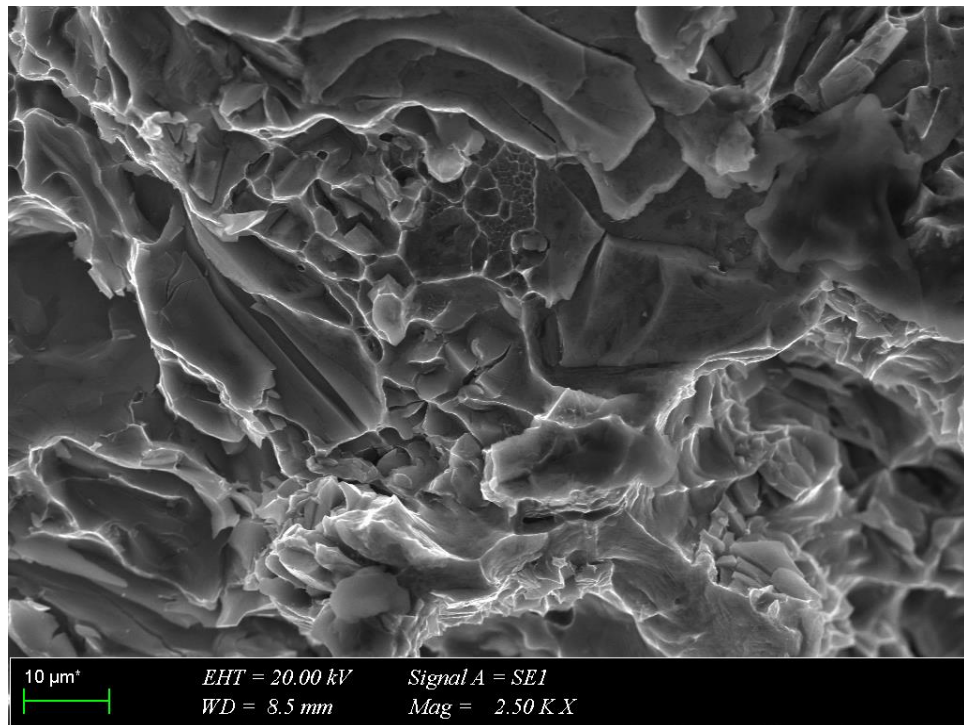


Figure 4.50. (175°C), 2500X

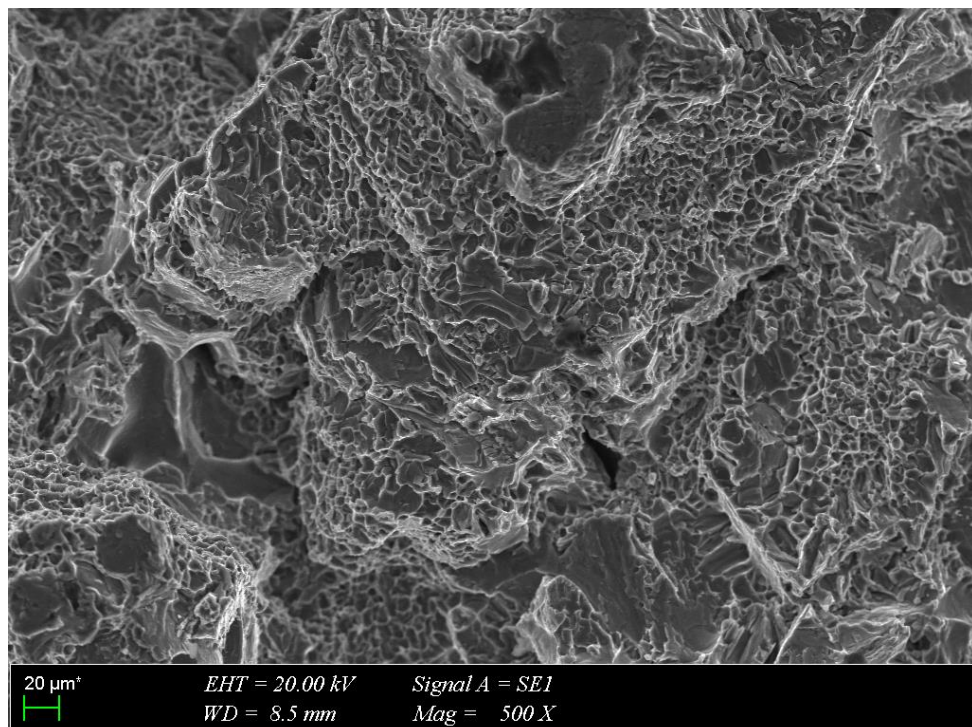


Figure 4.51. (175°C), 500X

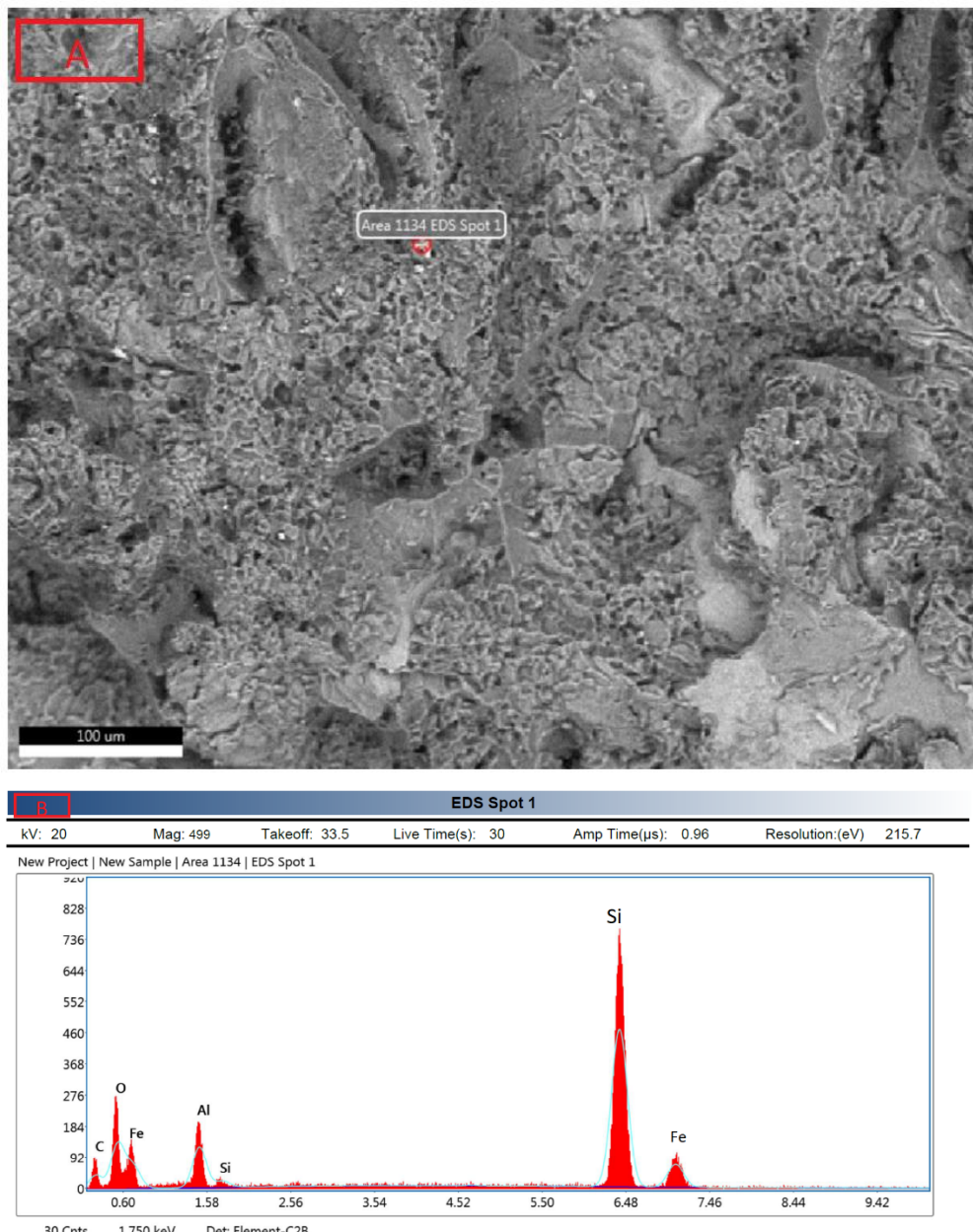


Figure 4.52. Area 1 of sample at 20°C, (a) SEM view of fracture surface, (b) EDS analyses

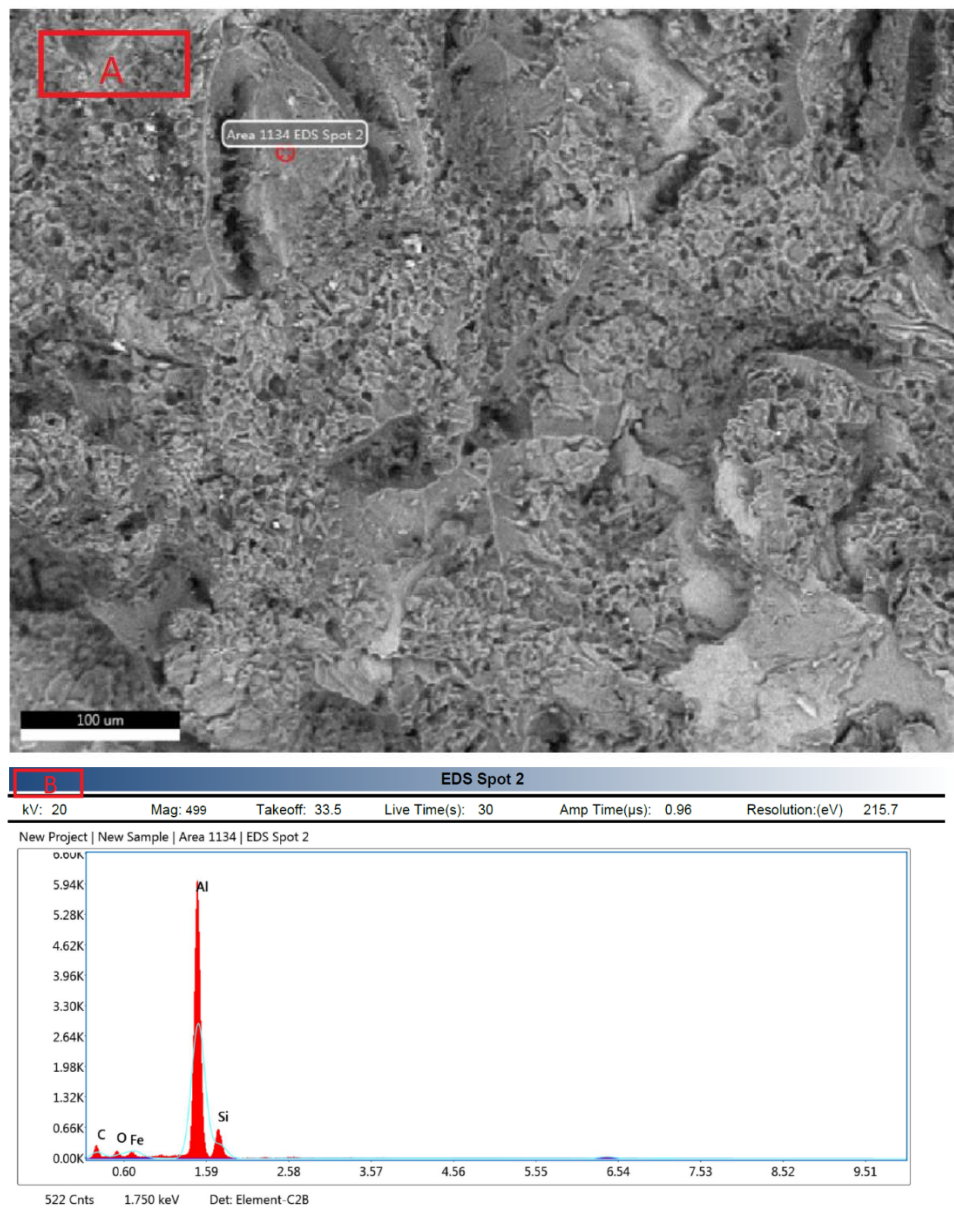


Figure 4.53. Area 2 of sample at 20°C, (a) SEM view of fracture surface, (b) EDS analyses

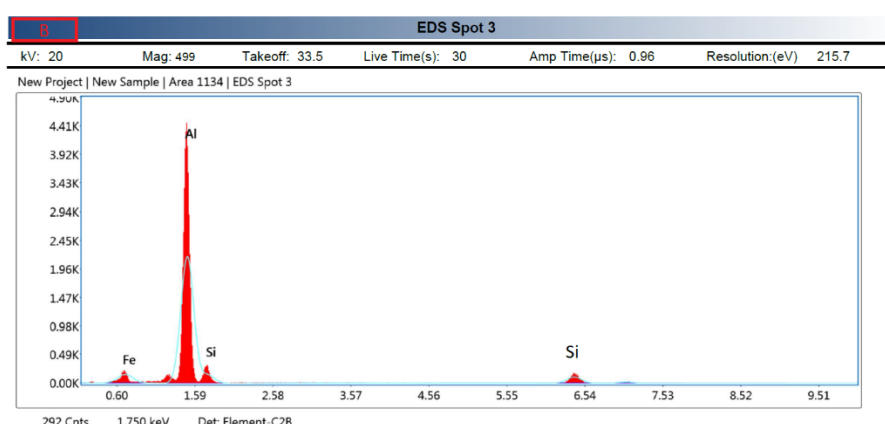
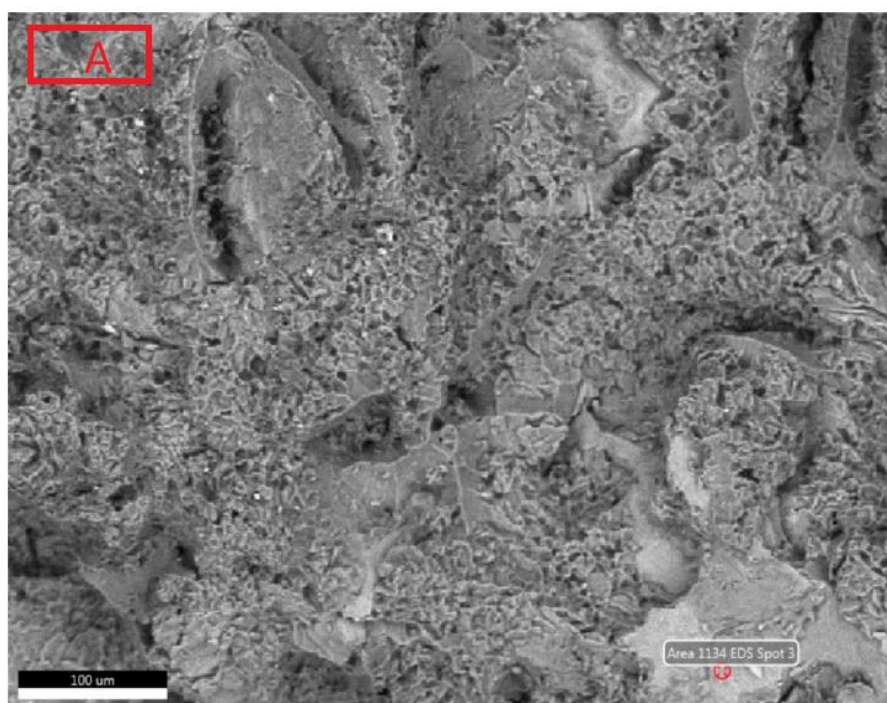


Figure 4.54. Area 3 of sample at 20°C, (a) SEM view of fracture surface, (b) EDS analyses

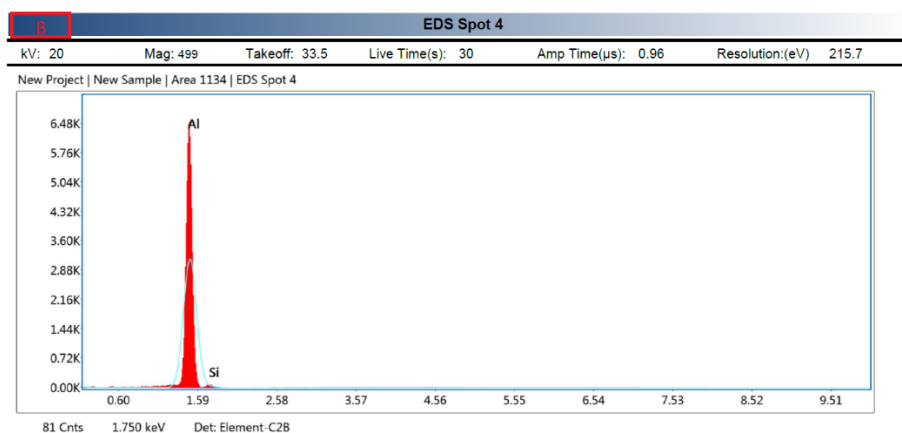
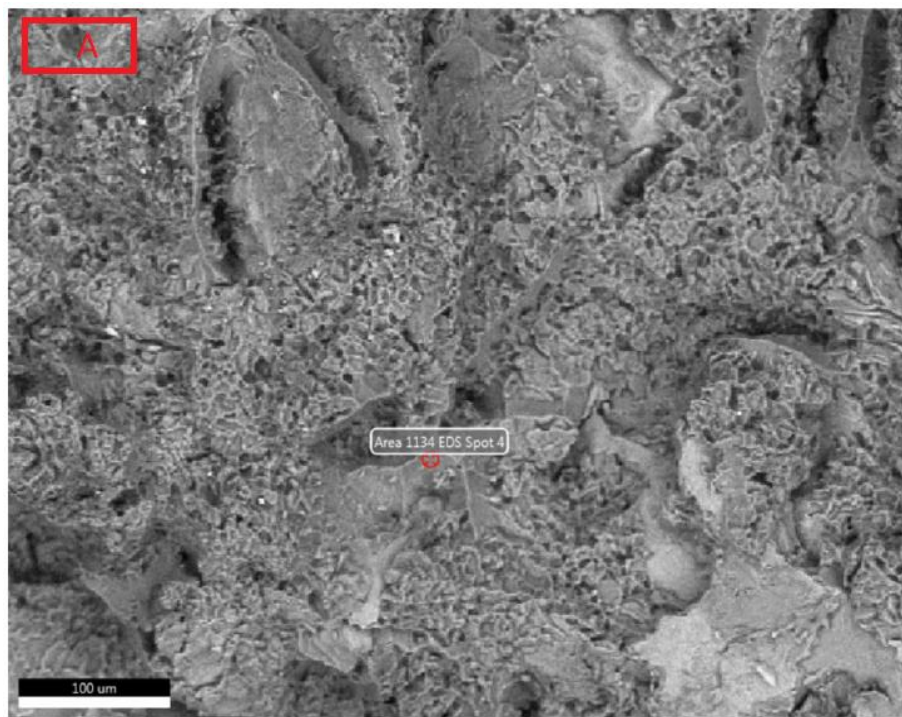


Figure 4.55. Area 4 of sample at 20°C, (a) SEM view of fracture surface, (b) EDS analyses

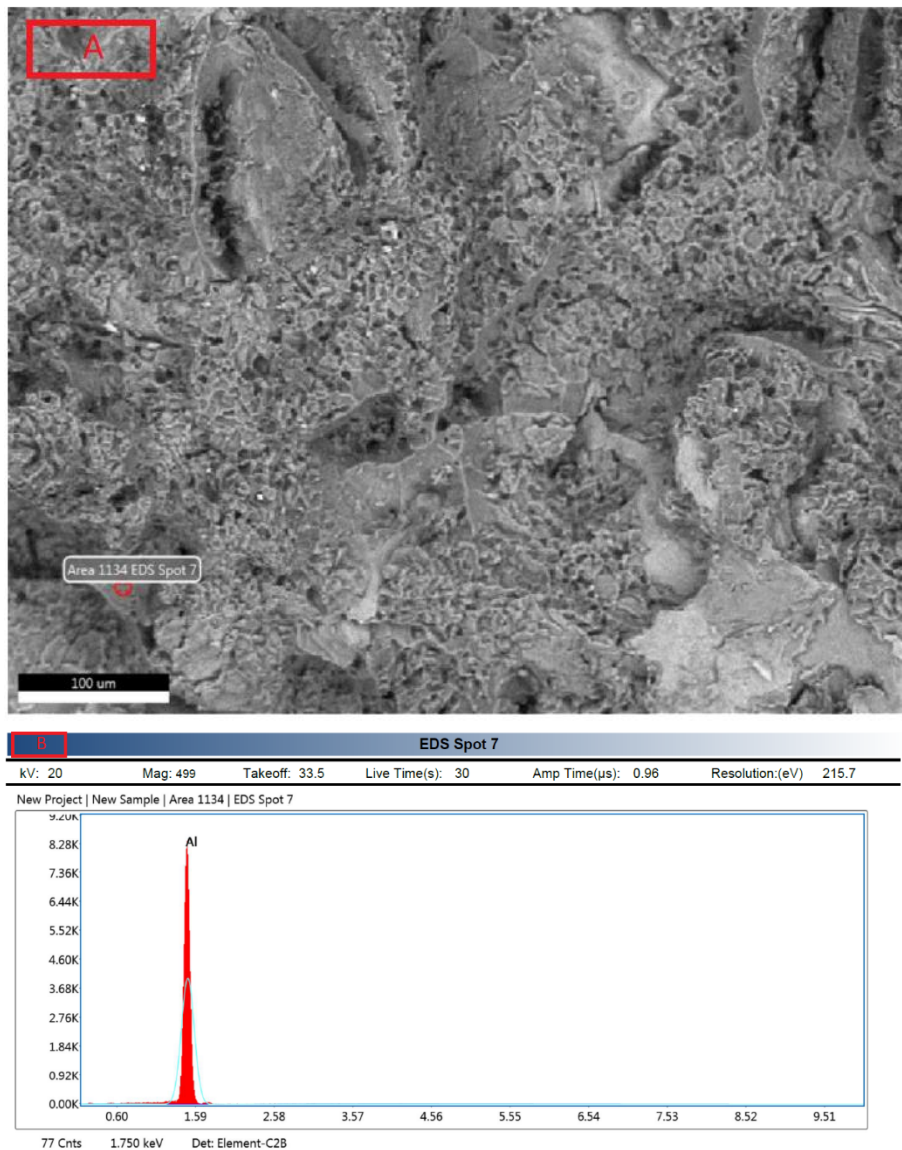


Figure 4.56. Area 5 of sample at 20°C, (a) SEM view of fracture surface, (b) EDS analyses

5. RESULTS and DISCUSSION

The findings of this study clearly show that as the temperature increased between -75 °C to 175°C, the impact energy showed a simple linear proportionality pattern. As with other metallic materials with face-centered cubic crystal (FCC) structure, ductile-brittle transition temperature (DBTT) was not observed within that temperature range. It was observed that the crack initiation energy decreased slightly with the increase in temperature. These findings show that the crack propagation energy increases with the increase in temperature.

Shivkumar et al. [5] tested V-Notched Charpy impact test samples produced from A356 aluminium alloy with different methods at different temperatures from 25 degrees to 200 degrees and they also did not observe a DBTT or big change in impact energies.

In order to investigate the ductile-brittle transition temperature, which cannot be observed in the impact energy-temperature graph, in more detail, the fracture surface of the broken samples in the impact test was examined under optical microscopy and scanning electron microscopy (SEM). In order to better understand the change in impact energies of the samples, the microstructure of a selected sample was examined. Structural defects were observed. These defects may also be caused by the casting stage of the product, the cooling process, or the grinding process of the sample while preparing it for optical examination. The Si particles are uniformly distributed in the Al matrix. It has been observed that the Si phase develops a fibrous form. Also, β -AlFeSi structure is observed.

The fracture surfaces of the samples broken at different temperatures were first examined comparatively by the naked eye. In this examination, it was clearly observed that as the test temperature increased, the plastic deformation on the fracture surface of the samples increased. Characteristic features of ductile fracture such as dull appearance and dimple formation were observed on the fractured faces of all samples.

The SEM analysis was performed to observe that the fracture properties of the samples tested at temperatures of -75°C, 20°C and 175°C degrees showed a ductile construction and a brittle construction. In this analysis, many fracture structures of brittle and ductile fracture characteristics were observed. In general, the formation of internal cracks and their accumulation in the dimple was observed at low temperatures. Therefore, it can be interpreted that the samples broken at this temperature show a relatively low impact energy absorption value. It was also found that the size of the dimples increased as the temperature increased. As a result of the SEM analysis, it was observed that the general fracture pattern of the A356 Charpy impact test specimens fractured at these temperatures was a ductile fracture.

The limiting factor of this research is that the digital thermometer cannot be placed inside the sample, but rather placed in the air-conditioned environment. For this reason, the temperature values we received during the test may vary by $\pm 3^\circ\text{C}$ degrees.

6. CONCLUSIONS

6.1 Main Conclusions

In this research study, it was tried to estimate the strength of the wheels produced from A356 aluminium alloy by LPDC method at different operating temperatures. V-notch Charpy impact tests were carried out to estimate strength under different operating conditions.

The samples were subjected to the impact test within 5 seconds after being conditioned at temperatures of -75°C, -40°C, 0°C, 20°C, 60°C, 95°C and 175°C degrees. The reason for applying these graded temperatures was to determine the DBTT point. In this way, the transition temperature of the samples from the ductile structure to the brittle structure would be determined and the safe operating temperature ranges of the products produced from these samples with the same method could be determined.

The V-Notch Charpy impact test results obtained show that the A356 alloy does not show a DBTT point. The fracture surfaces of the samples were subjected to microscopic and macroscopic analyses for possible ductility-brittleness structure transition.

The microstructure and fracture surface of two different surfaces of the sample were examined with an optical microscope. The production quality of the rim in the examined microstructure and its effect on the impact energy of the sample were investigated.

In the optical examination of the fractured surface, it was tried to determine whether the character of the fracture structure of the samples was ductile or brittle. In this examination, it was observed that as the test temperature increased, the plastic deformation of the fracture surface of the sample increased.

SEM analysis, which is a more detailed study, was applied for the detection of ductile-brittle transition. 3 samples were analysed at -75°C, 20°C and 175°C test temperatures. Although brittle structure samples were detected on the fracture surface of the sample fractured at -75°C temperature in the analysis, more ductile fracture structure samples were detected in all samples.

As a result, we have shown that there is no significant change in the impact energy of the wheels produced with the A356 alloy and the LPDC method at temperatures of -75°C and 175°C. Based on these findings, it can be interpreted that these temperatures tested will not cause a significant change in the fracture structure of the wheels produced by the method in this study.

6.2 Recommendations for Further Work

With the improvement of the world's transportation infrastructure day by day, it is now expanding in geographies where cars can be used. The expansion of the geography to be used may bring with it new extreme working conditions. As this work progresses, the test temperature range may be extended further in the future. In addition, thermometers used for temperature measurements can be placed inside the sample. In this way, we can

measure not only the outdoor temperature of the sample but also the actual internal temperature.

6.3 Evaluation of the Work from MUDEK Perspective

6.3.1 Economic Analysis

One of the main purposes of engineering studies is to provide economic benefit. One of the aims of this study is to prevent major economic losses that may occur. An example is the sinking of the titanic ship. At low operating temperature, the ship's material changed from ductile to brittle, its strength decreased, and fractures occurred, and the ship sank. Similarly, tests as in this study have an important place to prevent similar incidents in cars to be used at extreme temperatures.

6.3.2 Real Life Conditions

The samples used in this study were taken from certain wheels produced for automobiles. The tests were carried out according to international standards. Everything in the study was carried out according to real life conditions.

6.3.3 Producibility

Manufacturability is critical to the research and development, design and analysis of a product. Products produced by taking into account manufacturability can be put into use if they pass quality tests. In this study, it can be counted at the stage of quality tests and is of vital importance to produce a product that can withstand working conditions.

6.3.4 Constraints

In this study, heat transfer and limited extreme temperature values can be given as examples of limiting factors. In addition, the fact that the digital thermometer measures the temperature of the environment outside the sample limits us to learn the actual temperature value of the sample.

REFERENCES

- [1] Essienubong, I. A., Ikechukwu, O., & Ebunilo, P. O. (2016). Comparison of Aluminium Wheel to Steel Wheel in Relation to Weight and Fuel Consumption (Energy) in Automobiles, *Industrial and Systems Engineering, Engineering*, Vol. 1, No. 1, pp. 1-9
- [2] Elahi, M. A., & Shabestari, S. G. (2016). Effect of various melt and heat treatment conditions on impact toughness of A356 aluminum alloy. *Transactions of Nonferrous Metals Society of China*, 26(4), 956-965.
- [3] Do Lee, C. (2013). Variability in the impact properties of A356 aluminum alloy on microporosity variation. *Materials Science and Engineering: A*, 565, 187-195.
- [4] Alexopoulos, N. D., & Stylianos, A. (2011). Impact mechanical behaviour of Al–7Si–Mg (A357) cast aluminum alloy. The effect of artificial aging. *Materials Science and Engineering: A*, 528(19-20), 6303-6312.
- [5] Shivkumar, S., Wang, L., & Keller, C. (1994). Impact properties of A356-T6 alloys. *Journal of Materials engineering and performance*, 3(1), 83-90.
- [6] Ma, Z., Samuel, A. M., Doty, H. W., Valtierra, S., & Samuel, F. H. (2014). Effect of Fe content on the fracture behaviour of Al–Si–Cu cast alloys. *Materials & Design*, 57, 366-373.
- [7] Murali, S., Raman, K. S., & Murthy, K. S. S. (1992). Effect of magnesium, iron (impurity) and solidification rates on the fracture toughness of Al 7Si 0.3 Mg casting alloy. *Materials Science and Engineering: A*, 151(1), 1-10.
- [8] Caceres, C. H., Davidson, C. J., Griffiths, J. R., & Wang, Q. G. (1999). The effect of Mg on the microstructure and mechanical behavior of Al-Si-Mg casting alloys. *Metallurgical and materials transactions A*, 30(10), 2611-2618.
- [9] Y. G. Kim, H. Fujii, T. Tsumura, T. Komazaki, and K. Nakata, “Fracture behaviour of grain refined A356 cast aluminium alloy: tensile and Charpy impact specimens,” *Mater. Sci. Eng. A*, vol. 415, no. 1, pp. 250–254, 2006.
- [10] Wang, Q. G., & Cáceres, C. H. (1998). The fracture mode in Al–Si–Mg casting alloys. *Materials Science and Engineering: A*, 241(1-2), 72-82.
- [11] Samuel, A. M., Doty, H. W., Valtierra, S., & Samuel, F. H. (2014). Effect of grain refining and Sr-modification interactions on the impact toughness of Al–Si–Mg cast alloys. *Materials & Design* (1980-2015), 56, 264-273.
- [12] Tillová, E., Chalupová, M., Borko, K., & Kucharíková, L. (2016). Changes of fracture surface in recycled A356 cast alloy. *Materials Today: Proceedings*, 3(4), 1183-1188.
- [13] Merlin, M., Timelli, G., Bonollo, F., & Garagnani, G. L. (2009). Impact behaviour of A356 alloy for low-pressure die casting automotive wheels. *Journal of materials processing technology*, 209(2), 1060-1073.

- [14] Lalpoor, M., Eskin, D. G., & Katgerman, L. (2010). Investigation of fracture behavior of high strength aluminum alloys in the as-cast condition. In Proceedings of the 11th International Conference on Aluminium Alloys, 22-26 September 2008, Aachen, Germany. DGM & Wiley-VCH.
- [15] Callister, W. D., & Rethwisch, D. G. (2018). Materials science and engineering: an introduction (Vol. 9). New York: Wiley.
- [16] Osman, T.M. and Rigney, J. D., Introduction to the Mechanical Behavior of Metals, Mechanical Testing and Evaluation, Vol. 8, ASM Handbook, p. 35. 2000
- [17] Cobden, R., Alcan, Banbury, (1994). Aluminium: Physical Properties, Characteristics and Alloys, Training in Aluminium Application Technologies, Lec. 1501, Sf. 20–21.
- [18] Erdoğan, A. (2008). Aluminyum ve Alaşımları. Yıldız Teknik Üniversitesi, İstanbul.
- [19] Hernandez, F. C. R., Ramírez, J. M. H., & Mackay, R. (2017). Erratum to: Al-Si Alloys: Automotive, Aeronautical, and Aerospace Applications. In Al-Si Alloys (pp. E1-E1). Springer, Cham.
- [20] Götz G, (2002) The Aluminium Automotive Manual. Products–Cast alloys and products, European Aluminium Association, 25 – 30, <https://www.european-aluminium.eu/resource-hub/aluminium-automotive-manual/> (05.02.2021)
- [21] Polmear, P., StJohn, D., Nie, J. F., & Qian, M. (2017). *Light alloys: metallurgy of the light metals*. Butterworth-Heinemann.
- [22] Götz G, (2002) The Aluminium Automotive Manual. Manufacturing – Casting methods, European Aluminium Association, 25 – 30, <https://www.european-aluminium.eu/resource-hub/aluminium-automotive-manual/> (05.02.2021)
- [23] Radhakrishna, K., Seshan, S. and Seshadri, M.R., (1980). Dendrite Arm Spacing in Aluminium Alloy Casting, *AFS Transactions*, 88, 695-702.
- [24] Kılıç, E. (2018) AlSi7MgCu0.5 Alaşımı Silindir Kapaklarında Isıl İşlem Süreçlerinin İyileştirilmesi. Yüksek Lisans Tezi, Dokuz Eylül Üniversitesi Fen Bilimleri Enstitüsü, İzmir, Türkiye.
- [25] Barresi, J., Kerr, M.J., Wang H., Couper, M.J. (2000). Effect of Magnesium, Iron and Cooling Rate on the Mechanical Properties of AlSi7Mg Foundry Alloys, *Transactions of American Foundryman Society*, Pittsburgh.
- [26] Topçuoğlu, Ö., Çe, Ö.B., Aybarç, U. ve Keskiç, M. (2014). Alçak Basınç Döküm Prosesinde Kullanılan Kalıp Kaplama Malzemesinin Metal Akışkanlığına Etkisi, 7. Uluslararası Ankıros Döküm Kongresi, İstanbul, Türkiye.
- [27] Tarkun, D. (2015). AlSi7Mg T6, AlSi7Mg ve AlSi11Mg Alaşımlarının Binek Araç Jant Malzemesi Olarak Kullanılabilirliklerinin Araştırılması. Yüksek Lisans Tezi, İstanbul Teknik Üniversitesi Fen Bilimleri Enstitüsü, İstanbul, Türkiye.

- [28] Karakaş, H.E. (2020) Binek Araç Jantlarının Yorulma Ömrü Test Süresinin Optimizasyonu. Yüksek Lisans Tezi, Dokuz Eylül Üniversitesi Fen Bilimleri Enstitüsü, İzmir, Türkiye.
- [29] Erdoğdu, M.B. (2019) Flow Forming Yöntemi İle Alüminyum Jant Üretiminin İncelenmesi ve Sonlu Elemanlar Yöntemi İle Jant Analizlerinin Yapılması. Yüksek Lisans Tezi, Ege Üniversitesi Fen Bilimleri Enstitüsü, İzmir, Türkiye.
- [30] Karagöz, O. (2017). Sıvama Operasyonunun Malzemenin Mekanik ve Mikroyapı Özelliklerine Etkisinin İncelenmesi. Yüksek Lisans Tezi, Adnan Menderes Üniversitesi Fen Bilimleri Enstitüsü, Aydın, Türkiye.
- [31] Çolak, M. (2015) Alüminyum Döküm Alaşımının Katılılaşması Sırasında Yarı-Katı Bölge Sıvı Geçirgenliğinin Modellenmesi. Sakarya Üniversitesi Fen Bilimleri Enstitüsü, Sakarya, Türkiye.
- [32] Callister Jr, W. D., & Rethwisch, D. G. (2013). Materials science and engineering. An introduction; Materialwissenschaften und Werkstofftechnik. Eine Einführung.
- [33] Yaşa, S. (2018) Alüminyum A356 Alaşımının Titreşimli Dökümü. Yıldız Teknik Üniversitesi Fen Bilimleri Enstitüsü, İstanbul, Türkiye.
- [34] Leis, B. N. (2013). The Charpy impact test and its applications. *Journal of Pipeline Engineering*, 12(3), 183-198.
- [35] Nanstad, R. K., Swain, R. L., & Berggren, R. G. (1990). Influence of thermal conditioning media on Charpy specimen test temperature. In *Charpy Impact Test: Factors and Variables*. ASTM International.